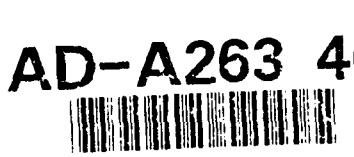

Final Report
on
Geoscience Center Research

ARO Grant DAAL03-86-K-0175

from

The Center for Geosciences at the
Cooperative Institute for Research in the Atmosphere
Colorado State University
Fort Collins, CO 80523

Jan L. Behunek and Thomas H. Vonder Haar, Editors

with

Principal Investigators:

Viswanathan N. Bringi
Thomas A. Brubaker
Pierre Y. Julien
Thomas B. McKee
Roger A. Pielke
Thomas H. Vonder Haar

Co-Investigators:

William R. Cotton
Stephen K. Cox
David A. Krueger
Ross J. Loomis
Chiao-Yao She
Daryl B. Simons
Graeme L. Stephens
Stanley A. Schumm
Gerald D. Taylor

to

Army Research Office, Geosciences
4300 S. Miami Blvd.
Research Triangle Park, NC 27709

Walter D. Bach Jr., Technical Representative

Period Covered: September 1, 1986 - June 15, 1992

November 1992

DISCLAIMER NOTICE

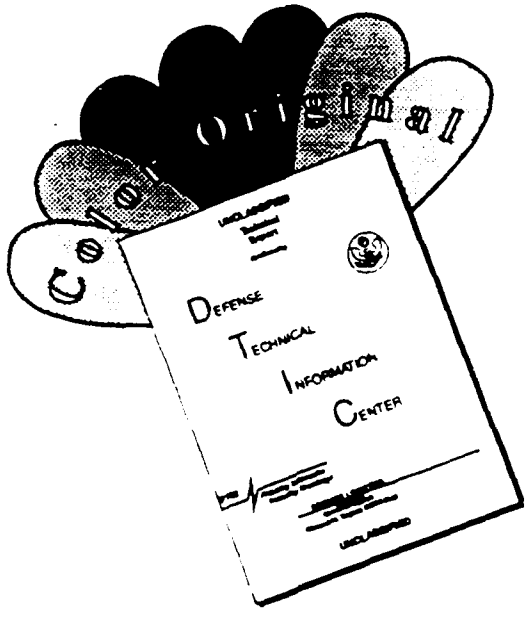

THIS DOCUMENT IS BEST QUALITY AVAILABLE. THE COPY FURNISHED TO DTIC CONTAINED A SIGNIFICANT NUMBER OF COLOR PAGES WHICH DO NOT REPRODUCE LEGIBLY ON BLACK AND WHITE MICROFICHE.

REPORT DOCUMENTATION PAGE

Form Approved
OMB No. 0704-0188

1. AGENCY USE ONLY (Leave blank)	2. REPORT DATE	3. REPORT TYPE AND DATES COVERED
	11/92	Final (9/1/86 - 6/15/92)

4. TITLE AND SUBTITLE

ARO Geoscience Center Research

5. FUNDING NUMBERS

DAAL03-86-K-0175

6. AUTHOR(S)

Dr. Thomas H. Vonder Haar
Mr. Jan L. Behunek

7. PERFORMING ORGANIZATION NAME(S) AND ADDRESS(ES)

Cooperative Institute for Research in the Atmosphere (CIRA)
Colorado State University
Fort Collins, CO 80523

8. PERFORMING ORGANIZATION REPORT NUMBER

9. SPONSORING / MONITORING AGENCY NAME(S) AND ADDRESS(ES)

U.S. Army Research Office
ATTN: SLCRO-URI-86
Research Triangle Park, NC 27709-2211

10. SPONSORING / MONITORING AGENCY REPORT NUMBER

ARO 24608.15-GS-UIR

11. SUPPLEMENTARY NOTES

12a. DISTRIBUTION / AVAILABILITY STATEMENT

Distribution and availability per DODD 5230.24, "Distribution Statements on Technical Documents."

12b. DISTRIBUTION CODE

13. ABSTRACT *(Maximum 200 words)*

The research grant was supported by the ARO Center for Geosciences located at the Foothills Campus at Colorado State University under the auspices of the Cooperative Institute for Research in the Atmosphere (CIRA). The Center for Geoscience at Colorado State University was established in collaboration with the Army Research Office on October 1, 1986.

The Center brought together a wide range of expertise into one focused multi-disciplinary research framework. Under the administrative structure of CIRA, the Center involved investigators from the University's Departments of Atmospheric Science, Civil Engineering, Electrical Engineering, Earth Resources, Forest and Wood Science, Physics and Psychology.

The technical components of the Center are in Atmospheric and Surface Remote and In-Situ Sensing; Atmospheric Modeling; Hydrologic Modeling; and Geoscience Information Extraction.

14. SUBJECT TERMS

Research Grant, Geosciences

15. NUMBER OF PAGES

195

16. PRICE CODE

17. SECURITY CLASSIFICATION OF REPORT	18. SECURITY CLASSIFICATION OF THIS PAGE	19. SECURITY CLASSIFICATION OF ABSTRACT	20. LIMITATION OF ABSTRACT
Unclassified	Unclassified	Unclassified	Unlimited

Preface

This final report summarizes the accomplishments of the Army Center for Geosciences at Colorado State University, under support from the federal University Research Initiative. The Center for Geosciences has been very productive during the six years of its existence. Positive effects of the research accomplished continue to be realized at Army, DoD and research laboratories. In this report we concentrate on brief discussions of the most important results and their scientific impact from each of the research projects supported by the Center. Detailed discussions can be found in the peer-reviewed journal articles for which abstracts are included in Section 3 of this report.

We have demonstrated that multi-disciplinary team research can be successfully applied to complex geoscience problems. We developed a strong cadre of PhD. students supported by Center research. As they matured scientifically, they joined our faculty and often lead the cross-disciplinary discussions and research work. Most of them finished their PhD. studies and graduated under Geoscience Center auspices.

We learned about the need for almost daily research coordination on the major science objectives of the Center, while also maintaining open lines of scientific inquiry. Colorado State University has a history and system of multi-disciplinary cooperation that allows the Center for Geosciences to be highly productive. Of course, the six faculty co-principal investigators, the other participating faculty, and the ARO and Army Lab scientists, who provided regular review and advice to us, were the nucleus of individuals who provided key scientific and technical guidance to the Center. We thank all of them, the students and the CSU staff who participated in the first phase of the Center for Geosciences at Colorado State University.

Thomas H. Vonder Haar
Professor of Atmospheric Science and
Director of the Cooperative Institute for
Research in the Atmosphere

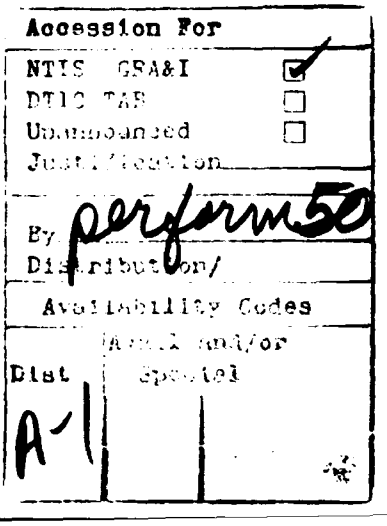

Table of Contents

	Page
Preface	ii
1.0 Introduction	1
2.0 Research Summaries	3
2.1 Satellite Remote Sensing	4
2.2 Radar Remote Sensing	14
2.3 Lidar Remote Sensing	18
2.3.1 HSRL	19
2.3.2 Doppler	23
2.4 Atmospheric Modeling	27
2.5 Boundary Layer	39
2.6 Hydrology	48
2.7 Climatic Geomorphology	55
2.8 Four-Dimensional Data Assimilation	61
2.9 Information Extraction & Visualization	64
3.0 Publications	69
3.1 Journal Articles	70
3.2 Ph.D. Dissertations	122
3.3 M.S. Theses	154
4.0 Fellows and Graduate Students	173
5.0 Technical Transfers	177
6.0 Conclusion	189
7.0 References	191
8.0 Acknowledgements	194

1. INTRODUCTION

The Center for Geosciences was established at Colorado State University in 1986 as a center for basic, interdisciplinary research in the geosciences. The focus of the work accomplished at the Center has been on basic research and development of tools for exploring geosciences, and the investigation of interactions between terrestrial and atmospheric processes. Research at the Center for Geosciences was distinguished by the synergism which existed between the disciplines represented in the center. These disciplines included:

satellite, radar and lidar remote sensing,

atmospheric modeling,

hydrologic modeling,

boundary layer studies,

climatic geomorphology,

information extraction and visualization.

This Center was funded through the Army Research Office (ARO) under the University Research Initiative (URI) for nearly six years. During that period, the Center was a peer-reviewed focal point for high quality geosciences research. A measure of the research accomplishments of the Center is the more than 200 scientific publications (more than 65 are refereed journal articles) generated from that research.

The research center concept has been utilized in order to emphasize an interdisciplinary approach to basic research in the geosciences. For example, The Regional Atmospheric Modeling System (RAMS) developed by the atmospheric modeling group was used by the boundary layer studies group for the simulation of boundary layer processes. Members of the radar remote sensing group have worked with the hydrologic modeling group on utilizing radar data as input to the hydrologic model, and with the satellite group on the interpretation of passive microwave signals from precipitating clouds. The scientists and research projects of the Center also have had considerable interaction with scientists at Federal research laboratories, primarily those supported by the DoD. These interactions included visits to the labs by Center scientists, visits by Center scientists to the labs, the conduct of collaborative and contract research with lab scientists on applied spinoffs from Center research, participation by Center scientists in DoD-sponsored scientific conferences and advisory panels, and the publication of jointly authored scientific articles with lab scientists. The majority of these interactions were with the Army Atmospheric Sciences Laboratory, the Army Waterways Experiment Station, various district offices of the Army Corps of Engineers, the Army Engineering Topographic Laboratory, and the Army Cold Regions Research and Engineering Laboratory.

The Center for Geosciences administered other programs and grants in addition to its research program. A series of geosciences workshops was conducted with support from the research grant. The topics of these workshops were:

Precipitation Measurement and Modeling,

Hydrology,

Large Eddy Simulation,

Geoscience Information Extraction,

4-Dimensional Data Assimilation.

Workshop participants were from DoD labs and science offices and from throughout the scientific community. Programs funded separately from the research program were the ARO Graduate Fellowships in Geosciences and the ARO Grant for Geosciences Equipment Purchase. The Fellowship and equipment grant programs have been summarized in separate final reports to ARO. The Fellowship program provided financial support for Masters and Ph.D. candidates working with the Geosciences research projects. The equipment grant developed or enhanced scientific facilities at the Center, including:

High Spectral Resolution Lidar,

Doppler lidar,

Atmospheric modeling computer system,

Satellite receiving earthstation,

Multiparameter Doppler radar,

Atmospheric vertical wind profiling system,

Computer hardware and software for 3-D visualization of geosciences data and output.

The availability of these and other facilities was an invaluable asset to the Center for Geosciences.

This Final Report of the research and related activities of the Center for Geosciences summarizes the most significant results of those activities and explores the impact of the results on the state of the science. Those summaries are organized by research project topic and subtopic in the following section. Next, the significant publications of the Center for Geosciences are documented by the inclusion of abstracts from peer-reviewed articles, Ph.D. dissertations, and M.S. theses. We incorporate lists of Geosciences Fellows and other graduate students supported under the various programs. We also list technical transfers to Army and DoD laboratories resulting from research at the Center.

2. RESEARCH SUMMARIES

2.1 Satellite Remote Sensing
2.2 Radar Remote Sensing
2.3 Lidar Remote Sensing
2.3.1 HSRL
2.3.2 Doppler
2.4 Atmospheric Modeling
2.5 Boundary Layer
2.6 Hydrology
2.7 Climatic Geomorphology
2.8 Four-Dimensional Data Assimilation
2.9 Information Extraction & Visualization

2.1 SATELLITE REMOTE SENSING

Satellite Remote Sensing of Tropospheric Moisture

A significant part of the research effort on Satellite Remote Sensing was devoted to the mesoscale diagnosis and characterization of water substance from space. This focus was based on the importance of moisture for driving the energetics of convective clouds and weather systems that can have a large impact on battlefield scale weather. Satellite data provide unique moisture information because of their current ability and further potential to estimate moisture parameters where no other data sources are available.

Studies using multispectral sounding data from geostationary and polar orbiting satellites showed the large spatial variability of lower tropospheric water vapor over mesoscale regions (Hillger and Vonder Haar, 1988; Hillger et al., 1988). These studies applied spatial and temporal structure and auto-correlation function analyses to raw single channel radiances and to products retrieved from multiple channels. For example, the analyses showed that moisture gradients are detectable on spatial scales of approximately 20 km from Geostationary Operational Environmental Satellite (GOES) sounder data. It also was possible to diagnose the orientation of moisture gradients and the velocity of features within the moisture field using this technique. These results provide some quantitative measures of the capabilities and limitations of satellite data for mesoscale moisture analysis and model input.

The influence of water substance behavior on convective storm dynamics was investigated further using dual-polarization Doppler radar data in an interdisciplinary approach to examine latent heating and cooling in one such storm. This case study investigated a microburst-producing thunderstorm observed on 20 July 1986 during the COoperative Huntsville Meteorological Experiment (COHMEX) in Alabama. Liquid and ice water contents and rainfall rate within that storm were quantified from the radar horizontal and vertical reflectivity, the differential reflectivity, and the differential phase reflectivity. The time rate of change of liquid, ice, and rainfall rate then were used to calculate the latent heating rate. Results showed that net latent heating rate increased nearly steadily from the early stages of the storm until about 10 minutes before the microburst occurred, at which point it began to decrease. The net latent heating rate went from positive to negative less than five minutes before the microburst impacted the ground. Net latent heating approached zero near the end of the decaying stage of the storm. The results emphasized the usefulness of differential phase reflectivity for computing ice fraction and latent heating amounts. The ability to diagnose latent heating also is significant for mesoscale numerical model initialization and validation. Henry (1991) has investigated the impact of radar-derived latent heating (from rainfall) rates on the initialization and reinitialization of mesoscale model convective simulations. That work was accomplished at CSU under separate funding. She found that simulations were greatly improved by inclusion of the radar-derived heating rates.

Other topics related to tropospheric moisture sensing also were investigated as part of the Satellite Remote Sensing project. Studies of cloud liquid water and precipitation estimation from satellite data are treated as separate subtopics within this section. The Abstract of Dissertation from Alan Lipton contained in Section 3 discusses the impact of satellite temperature and humidity analyses on mesoscale atmospheric simulations.

Satellite Remote Sensing of Cloud Liquid Water and Surface Wetness

Studies of cloud liquid water content and surface wetness were conducted using data from the Defense Meteorological Satellite Program (DMSP) and from GOES (Jones and Vonder Haar, 1990). Data from the 85.5 GHz channel collected by the Special Sensor Microwave/Imager on DMSP are sensitive to cloud liquid water in the form of small cloud droplets and larger raindrops, and also to water contained in the surface soil and in water bodies. Radiation in the 85.5 GHz channel is more strongly attenuated by cloud water than that in the lower frequencies (<40 GHz) previously used for satellite cloud liquid water studies. Therefore, it was possible to estimate cloud liquid water amounts over land from satellite for the first time. The method was based on detecting the brightness temperature depression caused by attenuation and emission of microwave radiation within clouds where the temperature is colder than that of the earth background. Atmospheric attenuation in the microwave due to oxygen and water vapor was diagnosed using a millimeter-wave propagation model. Raining areas were eliminated by a brightness temperature threshold. Figure 1 depicts a cloud liquid water field estimated by this method.

Greater effort was required to account for variations in the background microwave emission caused by variations in surface soil moisture, and therefore in surface emittance. The surface emittance retrieval method employed infrared window channel measurements from GOES collocated with the SSM/I data. A special software package called the Polar Orbiter Remapping and Transformation Application Library (PORTAL) was created to manipulate the different data formats and natural (satellite) coordinate systems represented by the geostationary and polar-orbiting (DMSP) satellite data sets. PORTAL is a very general tool which can be used for the fusion of many different types of satellite data. Cloud-free conditions were selected for the cloud liquid water analysis to allow the surface skin temperature to be calculated from the IR data. The surface temperature obtained in this way then was substituted in the radiative transfer equation along with a microwave brightness temperature to calculate the value of surface emittance. Efforts to use the satellite-derived surface emittance/soil moisture estimates in conjunction with mesoscale simulation and prediction studies also were begun. This work investigates methods for using the satellite soil moisture information to initialize and make subsequent corrections to the surface characteristics module in the RAMS model (see section 2.4 for further details on RAMS). The use of satellite-derived soil moisture estimates as model input will provide an excellent test of the data assimilation capabilities of the model. The potential improvements in soil moisture analysis and model initialization could lead to a better understanding of and ability to simulate boundary layer processes.

It was impossible to obtain cloud liquid water truth data from aircraft for the cases studied. An error sensitivity analysis indicated an average uncertainty of 0.15 kg/m^2 in retrieved cloud liquid

water for data collected during the first week of August, 1987 over northeastern Colorado. The cloud liquid water estimates obtained from satellite data also were in good qualitative agreement with values derived from ground-based microwave radiometers. Preliminary results from a winter case study were considerably less encouraging due to difficulty with separating the background emission from cloud emission. There was little brightness temperature contrast between cloud and ground for the wintertime case.

This investigation of cloud liquid water suggests that satellite remote sensing techniques can provide estimates of this quantity over land. This result is quite significant because cloud liquid water measurements typically are extremely sparse. The ability to analyze cloud liquid water could be valuable for the diagnosis and prognosis of mesoscale circulation and convective development. The satellite estimates also could be used to initialize mesoscale numerical models and to evaluate their simulations. Estimation of aircraft icing potential is another task that could benefit from application of this method.

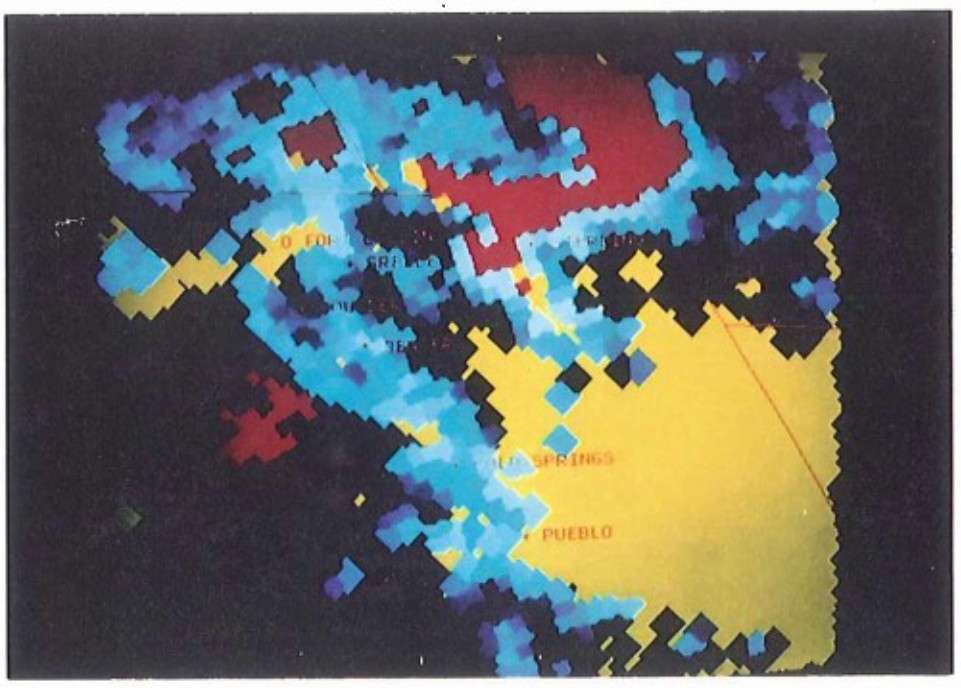

Figure 1. Cloud liquid water analysis over eastern Colorado based on Special Sensor Microwave/Imager data taken by the Defense Meteorological Satellite Program. Gray shades denote liquid water concentrations, red areas contain rain, and yellow is cloud free.

Precipitation Volume Estimates From Satellite Data Using Area-Time Integrals

Precipitation estimates from satellite data were pursued in conjunction with the emphasis on analysis of tropospheric moisture. A technique called the Area-Time Integral (ATI) method was investigated to generate estimates of convective precipitation volume over mesoscale regions. The ATI method had been developed and tested previously using radar data (Doneaud et al., 1984). The Area-Time Integral is defined by

$$P(x,y,t) = \int_t \int_A \; FNR(N)\, dA\, dt, \qquad (1)$$

where F is the frequency of occurrence of a number (N) of rain events with rainrate R. Radar data were utilized in conjunction with satellite data in order to develop the satellite ATI method. The radar data were used initially to determine the satellite infrared cloud top brightness temperature threshold which defined the raining area indicated by the radar. That threshold then was used for the lifetime of the storm to obtain precipitation volume from equation 1. This method was applied to data collected during several research field experiments located in different geographical regions of the U.S. Each of these particular regions yielded a characteristic satellite temperature threshold. This difficulty led to the search for a more general method of determining the appropriate threshold from satellite data alone. The method which was discovered and utilized establishes a correlation between the coldest cloud top temperature observed by satellite over the lifetime of a convective cell or complex and the required temperature threshold. This discovery allows the satellite ATI method to be applied over a range of geographical areas without the need for calibration to radar measurements.

The investigation and use of the satellite ATI technique is a significant development because it generates meteorologically and hydrologically useful estimates of precipitation in the absence of ground-based sensors. The success of the method is partly due its suitability for use with satellite data, which are excellent for surveying the areal coverage and duration of convective clouds. It does not attempt to produce estimates of point rainfall, in contrast to methods such as those of Scofield and Oliver (1977), and Griffith and Woodley (1978). Instead, it estimates precipitation volume over mesoscale regions having areas of order 1000 km^2 or more. The ATI method based on equation 1 assumes a characteristic rainrate for the precipitating cloud or system, and the success of the method implies the validity of that assumption. Additional study will be required to determine the relationship between the dynamics and microphysics of convective systems and the ability of the ATI method to diagnose their precipitation volume. Such studies also may explain the existence of the characteristic rainrate.

Cloud Detection and Characterization

Studies of several cloud detection methods and of specific cloud field characteristics were completed. Boundary layer clouds were of particular interest to these investigations. Theoretical studies of cloud detection analysis techniques sought improved methods of extracting cloud information from satellite data. These techniques then were tested and applied to the examination of observed cloud fields in order to improve our ability to determine the impact of clouds on Army operational concerns and the interaction of clouds with other meteorological phenomena and events. The most common cloud analysis technique was the creation of composite images from a time sequence of instantaneous views over a region of interest. Composite images allow climatological cloud characteristics such as cloud frequency to be diagnosed as a function of location and time of day. Theoretical work provided automated cloud/no-cloud determinations for each image of which the composite was made up.

The most basic cloud detection method consisted of a digital count threshold applied to a satellite image from a single spectral channel. That threshold defined the boundaries between clouds and background in images from that channel. Gibson and Vonder Haar (1990) used a brightness threshold selected by a human analyst. Kelly et al. (1989) chose a threshold by an automated method based on the spatial variation of digital counts surrounding each image pixel. That spatial variation is maximized where object (eg. cloud) boundaries exist. Spatial variations were measured in three different ways, based on the absolute deviation of a pixel count from that of its neighbors, its deviation from the median of the surrounding pixels, and the variance of the local digital count field. The cloud detection analyses resulting from the application of those three operators were evaluated objectively using a nonparametric statistical technique called Imagery Randomized Block Analysis (IRBA). The absolute deviation operator was found to be the most reliable of the methods tested on three case studies. Applications of these cloud detection methods are discussed below. One additional study of cloud field characterization methods quantified cloud-free regions in terms of interval length probabilities. That method was applied to very high resolution cloud field images taken from the Space Shuttle. These techniques for objective cloud detection and for evaluation of cloud detectors are significant because they allow rapid, fully-computerized cloud analysis.

Composite cloud image construction was based partly on the cloud detection methods discussed above. Gibson and Vonder Haar (1990) built their regional cloud composites from individual digital satellite images in which cloudy regions were determined manually. These composites revealed significant mesoscale cloud field variations over the southeastern U.S. study area. The maximum cloud frequency over that region was 45 percent, occurring at approximately 1400 Local Time. Convective clouds were analyzed separately, showing that well-developed

convective cloud coverage peaked at about 1500 Local Time. Geographical features such as terrain variations and water/land distributions were found to have a significant impact on the overlying cloud field. For example, afternoon cloud frequency maxima were discovered over high or steep terrain and over peninsulas on the Gulf of Mexico. Many lakes and reservoirs had cloud minima during the afternoon. Total cloudiness and convection over the Gulf of Mexico peaked at night. The results of this particular cloud composite study could be used in conjunction with other data analyses or simulations to study the interaction of terrain or sea breeze circulations with cloud formation processes. The relationship of cloud pattern to the divergence field and to mesoscale or synoptic regime also could be analyzed. Kelly (1988) applied automated cloud detection techniques to the creation of cloud composite images over and surrounding Cuba. These composites then were combined with real-time satellite images to estimate future cloud cover in the form of an Estimated Cloud Image (ECI). The ECI is essentially a statistically based short term forecast of cloud cover which could be used operationally or for comparison with numerical model output.

Fog Detection, Prediction, Characterization From Satellite Data

Fog is among the more important weather phenomena that can have an effect on Army operations because of its potential impact on transport and intelligence gathering activities. Fog was one of the topics of research within the Satellite Remote Sensing group at the Army Center for Geosciences. The specific subtopics that we addressed within available resources were: (a) the detection of radiation fog at night; (b) the anticipation of fog formation through the analysis of both satellite data and related meteorological parameters; (c) the analysis of the physical and microphysical characteristics of fog.

Nighttime radiation fog detection was based on the brightness temperature difference between satellite images of fog taken in the 3.9 μm and 11 μm spectral bands. Data in those channels are available from the GOES and NOAA satellites. The method relied on the greater transparency of water clouds at 3.9 μm than at 11 μm. This resulted in colder brightness temperatures at 3.9 μm than at 11 μm over fog because the surface temperature generally was colder than the fog top temperature in the case of radiation fog. The brightness temperature difference was much smaller where fog was absent. This nighttime fog detection method was tested in case study mode, and fog reported by surface observing stations was detected by the satellite method with a very high rate of success. The capability to remotely detect fog potentially could be very important to the Army in regions where no friendly human observers or automated surface stations are available.

Our study of the potential to predict fog formation also focused on radiation fog. Of the meteorological factors that would affect fog formation, including atmospheric moisture, surface wind speed, presence of overlying clouds, and microphysical effects, we investigated overlying clouds and lower tropospheric moisture availability from satellite. Overlying clouds were diagnosed by their colder radiating temperature in the infrared than that of the fog or earth's surface. A brightness temperature threshold was used to separate cloudy regions from clear or foggy areas. Lower tropospheric moisture analysis was attempted using the bispectral split window technique developed by Chesters et al. (1983). That technique relies on the stronger water vapor absorption at 12 μm than at 10.7 μm. The split window technique was found to be relatively insensitive to moisture variations very close to the ground under the temperature inversion conditions conducive to radiation fog formation. This failure to detect moisture gradients was caused by the shallow depth of the temperature inversions and the rather deep layer of the atmosphere contributing to the split window signal. We conclude that the split window technique is unsuitable for fog prediction.

The diagnosis of fog optical and microphysical characteristics such as optical depth and drop size distribution was investigated using radiometric data from aircraft and satellite-borne sensors. Detection of these quantities is important for a number of reasons, including their impacts on aircraft icing, visibility, and multispectral extinction coefficient within the fog layer, and their

potential as input for prognostic modeling of fog evolution. *In situ* microphysical measurements within fog layers rarely are available. Therefore, reliable remote sensing estimates of those quantities would be quite valuable. The first question we examined was whether the optical depth of fog layers is sufficient to allow estimation of the remaining parameters. This question was studied using reflected radiation in the 0.85 μm spectral band compared to theoretical Mie scattering calculations for cloud layers of varying optical depths in that band. Preliminary results from aircraft data collected near San Diego, California during June, 1986 indicated fog optical depths in the range from two to four. These optical depths are in the marginal range for determination of droplet size distribution from the combination of 0.85 μm and 1.6 μm radiometric measurements (Wetzel and Vonder Haar, 1991). Doubts regarding the accuracy of radiometer and pyranometer calibration suggest that further study of this data set is needed. After the calibration issues have been addressed, it will be possible to estimate a droplet size distribution index by comparing theoretical scattering calculations in the 1.6 μm channel with observed reflectance values at that wavelength.

2.2 RADAR REMOTE SENSING

Multiparameter Radar Rainfall Intensity Measurements

Significant advances were made in the application of multiparameter radar techniques for measuring rainfall intensity. The specific differential phase (K_{DP}) parameter (Golestani et al., 1989) was studied in detail using data from the NCAR CP-2 radar and via statistical simulations. Two different estimators were proposed for rainrate measurements with radar, i.e., one estimator using reflectivity (Z) and differential reflectivity (Z_{DR}) for light-to-moderate rainrates (less than 70 mm/hr), and one estimator using specific differential phase for moderate-to-intense rainrates (greater than 70 mm/hr). In the presence of hail, the second estimator was found to be very robust. These rainfall estimators provide greater accuracy under a range of rainfall intensities and with a variety of hydrometeor species than available from the conventional Z-R relationship. Their discovery will become increasingly beneficial as advanced radar technology becomes more frequently available in the field.

Multiparameter Radar Measurement of Cloud Microphysics

Significant advances were made in the radar remote sensing of storm microphysical structure at 3 and 5 GHz using multiparameter radar observables such as differential reflectivity, specific differential phase, backscatter differential phase (δ) and copolar correlation coefficient (ρ_{HV}). The measurement of δ was accomplished for the first time using data from the German DLR (5 GHz) and NSSL Cimarron (3 GHz) radars. The ρ_{HV} parameter was found to be a good indicator of hail mixed with rainfall. Propagation effects at C-band (5 GHz) were documented and methods to correct for these based on propagation differential phase were developed. It was demonstrated that variations in raindrop size distribution parameters could be measured by radar. The evolution of the water and ice precipitation fields are particularly amenable to remote sensing by multiparameter radar. Simulation of multiparameter radar parameters using numerical cloud model microphysical outputs is imminent. The CSU RAMS model output is being coupled to a multiparameter radar module permitting further understanding of the radar parameters, especially under conditions of a mixture of precipitation types.

Microwave Remote Sensing of Cloud Ice Water Path

Theoretical calculation of the upwelling microwave radiances from storms containing layers of rain, melting ice, and ice were performed at 18, 37, and 92 GHz. A highly accurate plane-parallel microwave radiative transfer model with Mie phase matrices was used to solve the equation of transfer in a scattering atmosphere over a land surface. Unlike many schemes which link observed microwave brightness temperature to the liquid water content, this study emphasized the use of scattering-based channels to infer the ice water content. The high altitude ice region remains fairly unobscured to a space-borne sensor, suggesting the implementation of the scattering-based channels in a top-down methodology for retrieval of the cloud vertical structure.

Aircraft radiometer measurements at the frequencies of interest were compared with the output of the multiparameter radar-initialized radiative transfer model. Deviations at 92 GHz were attributed to uncertainties in the bulk density and size distribution of the ice region. Using both multiparameter radar observations and cloud model output, the 37-85 GHz T_B difference (ΔT_B) was found to be sensitive to the amount of integrated ice water path (IWP) lying above the rain, independent of ice density. Presence of coexisting cloud water and ice had the net effect of compressing the ΔT_B for a given IWP. Over convective regions, 85 GHz T_B depressions < 200°K were noted to be relatively insensitive to the amount of underlying liquid water content, and mainly dependent upon the optical thickness of the ice layer. The results demonstrate the potential usefulness of scattering-based channels to characterize the ice phase. These measurements also are important for latent heat calculations.

2.3 LIDAR REMOTE SENSING

2.3.1 HIGH SPECTRAL RESOLUTION LIDAR

High Spectral Resolution Lidar Theory

The concept for a high spectral resolution Rayleigh-Mie lidar was developed at the Center for Geosciences for measuring atmospheric backscatter ratio and temperature profiles. This technique requires comparison of Rayleigh scattering calculations for molecular scattering with measurements of actual scattering of the lidar beam. The returned signal was filtered to eliminate on-resonance interference. Backscatter ratio, r, and atmospheric temperature, T, were determined from

$$r = (N_1/N_2)f_m \quad (1)$$

$$N_2/N_2' = f_m/f_m' \quad (2)$$

$$f_m = \int R(v,P,T)F(v)\,dv \quad (3)$$

where N_1/N_2 and N_2/N_2' are the measured ratios of the total scattering signal to the filtered signal and the molecular scattering signal passed through two different filters, respectively. The factors f_m and f_m' are normalized molecular scattering signals after filtration, and F(v) and F'(v) are their measured spectral transmission functions. The function R is the theoretical normalized molecular scattering spectrum, which partly depends on atmospheric temperature. The inversion of eq. 3 requires knowledge of the atmospheric pressure at one height to deduce the temperature, pressure, and air density throughout the entire profile. Parameterization of the theoretical Rayleigh/Brillouin scattering function has made the inversion process simple and fast. Inclusion of rotational Raman scattering calculations removes a large temperature bias found in our early experiments.

The High Spectral Resolution Lidar (HSRL) developed at CSU is unique in terms of its ability to measure aerosol backscatter and atmospheric temperature with high range resolution. The temperature sensing capabilities of the system were enhanced by the utilization of high spectral resolution and by the development of atomic vapor filters to separate the aerosol and temperature signals. The atomic vapor filter concept and application is discussed further in the next subsection.

High Spectral Resolution Lidar Experimental Setup

The HSRL system was created by assembling equipment designed to operate on the theory outlined in the previous subsection. The resulting HSRL was tested in the laboratory and field. The HSRL signal was generated by a tunable, narrowband pulsed laser transmitter. That transmitter started from a Continuous Wave (CW) single-mode dye laser tuned to the wavelength of interest. Its output was amplified by a pulsed dye amplifier pumped by a doubled Nd:YAG laser. Figure 1 shows a schematic of the HSRL configuration.

The measurement of optical properties by means of Rayleigh-Mie scattering required the separation of molecular and aerosol contributions to the lidar return. A narrowband barium vapor blocking filter was designed and implemented for that purpose. The bandwidth of that filter was adjusted by varying its temperature. The barium vapor filter successfully attenuated the return from aerosol scattering, which made temperature profile measurements possible. The laser was tuned to the center of the barium filter at 553.7 nm for that purpose. Aerosol backscatter ratio was obtained from an unfiltered return given knowledge of the temperature profile. Development of the vapor filter technology is important because it can be used with other existing narrowband lidar systems that currently do not separate molecular and aerosol scattering.

The HSRL receiver began with a Cassegrain telescope aligned with the coaxial transmitter beam. The lidar return was split into two channels, each passing through a barium vapor filter and detected by a photomultiplier. The analog outputs of both photomultipliers were digitized by a dual-channel digitizing scope for computer processing. The tuning of the transmitter frequency on and off the barium resonance was monitored by observing the transmission of a third barium filter set at roughly 50 percent peak absorption. A photon counting detection system also was installed in order to extend the range of HSRL to approximately 10 km.

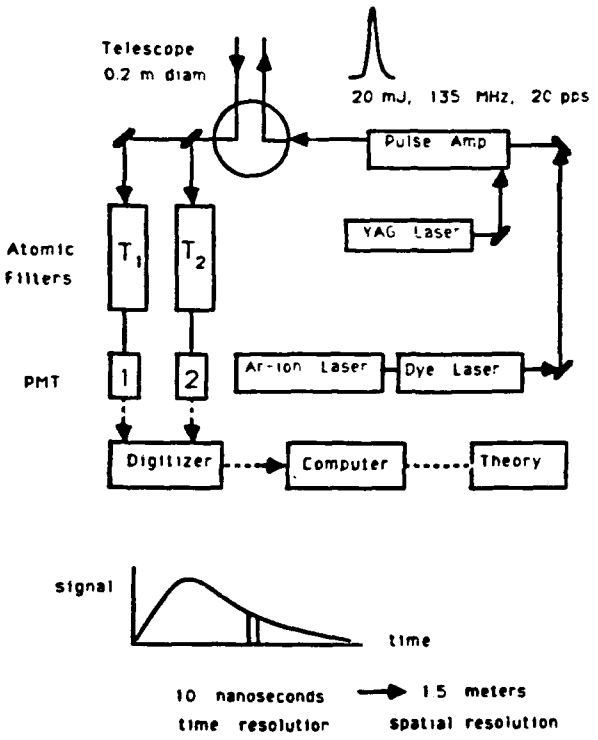

Figure 1. Schematic of experiment showing both the properties of the transmitter an receiver.

High Spectral Resolution Lidar Experimental Results

HSRL field tests were conducted on several occasions in order to verify the theory and system design. We have deduced profiles from about 1 km up to 5 km with a spatial resolution of about 0.4 km after averaging over 20 minutes. Figure 2 shows results for aerosol attenuation coefficient and vertical temperature profile. A nearly simultaneous radiosonde profile is plotted on Figure 2b for comparison. The uncertainties in the temperature are about 8° K and 14° K, respectively, at heights of 1 km and 5 km. Values of the aerosol backscatter ratio, extinction coefficient, and phase function are within the ranges of values reported by other workers in other experiments.

We believe that the CSU HSRL is the first lidar instrument of its kind to be able to measure atmospheric aerosol, temperature, pressure, and density. This unique capability has demonstrated the usefulness of much theoretical work, while suggesting further improvements for the design and use of this boundary layer instrument. An error analysis of our experiment shows that improvements of the atomic vapor filter would reduce the temperature uncertainty to about 2° K. Our results suggest that use of a lower temperature (350° K vs 750° K) iodine cell would eliminate significant variations in the filter width. It is also anticipated that use of the iodine filter would facilitate gross simplification of the transmitting laser system. This would make the system easier to use and less costly.

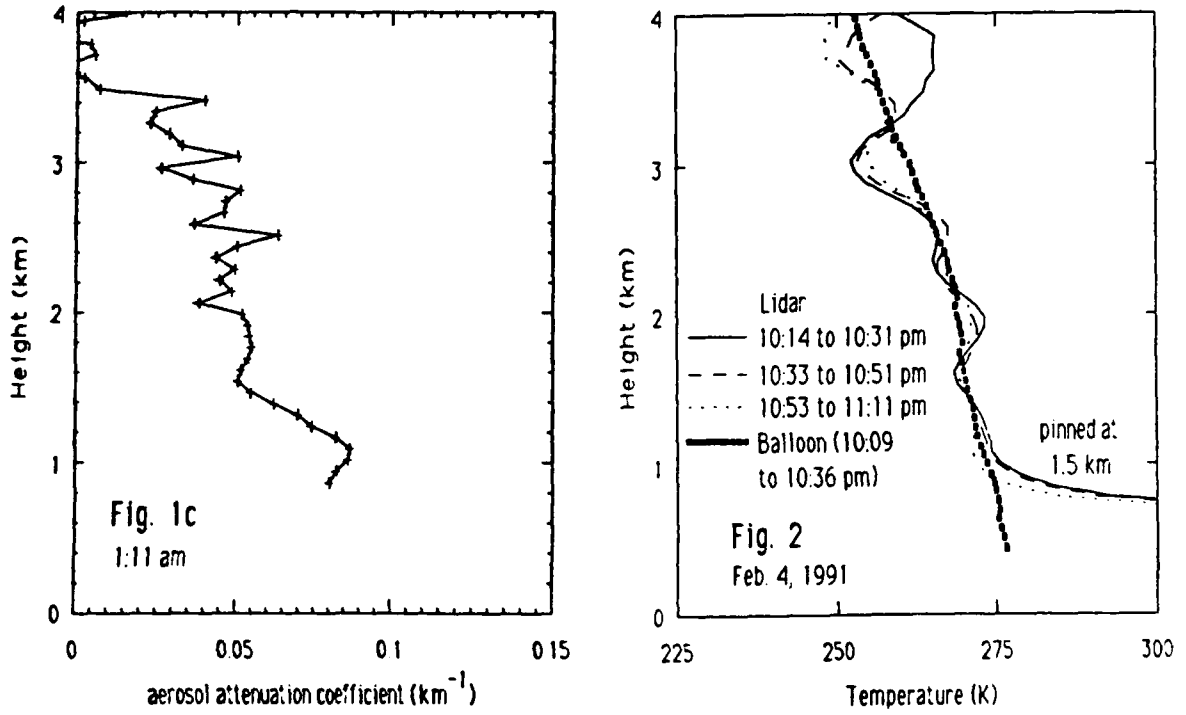

Figure 2. (a) Aerosol extinction coefficient vs. height from the HSRL at 0811 UTC on 15 August 1990; (b) Temperature vs. height from HSRL (thin line) and radiosonde (thick line) taken near 1730 UTC on 4 February 1991.

2.3.2 DOPPLER LIDAR

Doppler Lidar Design

The Colorado State University Doppler lidar was designed and developed with support from the Center for Geosciences in order to take atmospheric boundary layer measurements of wind. The behavior of the atmospheric boundary layer is of greatest interest to the Army. The Doppler lidar concept makes use of the Doppler shift of a beam of light emitted by a laser and backscattered by aerosol particles moving with the atmospheric flow. The Doppler shift is proportional to the radial component of the aerosol velocity. Design specifications for the Doppler lidar included a range of 10 km, range resolution of 150 - 300 meters, and wind speed accuracy of ±1 m/s. The CSU lidar also has the potential to measure boundary layer temperature and humidity using the DIfferential Absorption Lidar (DIAL) technique (Mason, 1975).

The CSU Doppler lidar has built upon experience gained from the design, development, and use of a similar lidar system at the NOAA Wave Propagation Laboratory in Boulder, Colorado (Hardesty, 1984). The CSU system incorporated several differences in design which were intended to make that lidar more compact, portable, and automated. Laser control and data collection were accomplished by IBM-compatible personal computers utilizing the Intel 80x86 CPU. This choice minimized the physical size of the system, which will allow it to be mounted in a van for use in field experiments. It also kept the cost of the system down. The use of PCs made system maintenance and expansion easier because of the ready availability of replacement parts and add-on boards. Automation of the lidar control and data collection was accomplished by the computers for functions such as system startup, tuning the lasers, and processing the returned signal. The computers were assisted with the laser control task by a single board computer communicating through the computers' RS232C port.

The Doppler lidar utilized a pulsed infrared carbon dioxide laser as the transmitter. The primary laser within the system was a hybrid cavity composed of a Continuous-wave (CW) laser and a Transverse Excited Atmospheric pressure (TEA) laser. The original glass tube CW CO_2 laser, which belonged to NOAA, failed during construction and testing of the CSU Doppler lidar. The replacement laser was custom designed and built at CSU. The new CW laser was built with ceramic, rather than glass, tubes. This laser was smaller than the original, which aided the compactness of design for field tests. It also allowed the entire hybrid laser to be housed in an invar structure, which minimized frequency modulation effects caused by thermal expansion. The TEA laser used in the CSU system was commercially built by Laser Science, Inc. It is unusual to find commercial lasers in research lidar systems. Although commercial lasers are much less expensive than custom-built lasers, they may have undesirable characteristics such as noise. In this case, the commercial TEA laser exhibited a frequency variation called a chirp. The magnitude and

effects of that frequency chirp on wind velocity measurements were investigated, along with means for minimizing its effect on the measurements. These topics are discussed separately in the next subsection.

Frequency Chirp in the Doppler Lidar

The CSU Doppler lidar exhibits frequency variations because it is a gas laser. These variations, called frequency chirping, are caused by changes in the density of emitting carbon dioxide in the TEA laser. The frequency chirp broadens the spectrum of the lidar return signal, increasing the error in wind velocity estimates. Two main processes are involved in creating the frequency chirp. The first of these processes is known as the plasma effect. It is caused by the lingering partial ionization of the laser plasma at the beginning of a laser pulse. The resulting abundance of free electrons changes the refractive index of the gas, and therefore the output pulse frequency. The second process is caused by heating of the gas during the laser pulse, which changes the density of the gas, as well as its refractive index and emitting frequency.

Several experiments were performed to characterize the frequency chirp of the TEA laser, namely: heterodyne detection of dual CO_2 laser beat frequencies, a Mach-Zender interferometer experiment, and a heterodyne HeNe interferometer experiment. The two heterodyne detection experiments were the most successful for quantifying the frequency chirp. The initial experiments accomplished with no laser modifications and no extra signal processing indicated a frequency chirp of approximately 60 MHz. Much of this chirp was eliminated by shock mounting the TEA laser on the optical table. Other hardware modifications included increasing the laser beam diameter, increasing laser cavity size, shortening the pulse duration, and increasing the output energy. These changes reduced the frequency chirp to 1.5 MHz, which corresponds to a velocity error of ± 3.5 m/s. This error exceeds the Army's requirement for ± 1 m/s wind measurement accuracy for boundary layer experiments and operations. The remaining error reduction was accomplished during the signal processing portion of the wind retrieval.

The Doppler lidar signal processor has four main elements: the detector and preamplifier, a demodulator, a high speed analog to digital converter, and the computer. The actual velocity estimate was generated by a computerized poly-pulse pair algorithm applied to the digital signal. That algorithm located the peak of the lidar return spectrum. The frequency of the maximum was not affected by the spectrum-broadening frequency chirp. Therefore, the poly-pulse pair algorithm can find wind velocity with less than ± 1 m/s error. The velocity estimate also was improved by averaging the return frequency spectrum from multiple laser pulses. This increased the signal-to-noise ratio, which improved the probability of obtaining a velocity within acceptable error limits.

2.4 ATMOSPHERIC MODELING

RAMS Overview

The Regional Atmospheric Modeling System (RAMS) was developed at Colorado State University in order to merge several numerical weather simulation codes being used side by side at the same site (i.e., Pielke, 1974; Tripoli and Cotton, 1982; Tremback et al., 1985). By merging the capabilities of the different models, a range of specific enhancements were introduced to RAMS, of which the telescoping, interactive nested-grid capability is one of the most significant. Based on the two-way grid interactive procedures of Clark and Farley (1984), RAMS has the ability to represent a large-scale area (e.g., the Northern Hemisphere) and then to nest progressively to smaller scales (e.g., a 10 km^3 volume of the atmosphere). More than one set of telescoping nests can be specified within a larger-scale grid and user-specified, and movable, grids can be activated. RAMS has a non-hydrostatic option so that all meteorologically relevant spatial scales can be represented. The concept of "plug-compatible" modules is used in RAMS in order to assist developers of parameterizations to interface into RAMS. Current RAMS features and options are shown in Table 1.

Table 1
RAMS Characteristics and Options

Category	Available Options
Basic equations	• Nonhydrostatic; compressible • Hydrostatic, anelastic or incompressible
Dimensionality	• 1D • 2D • 3D
Vertical coordinates	• Cartesian • Terrain-following σ_s
Horizontal coordinates	• Stereographic tangent plane
Grid stagger and structure	• Arakawa C grid, single grid (fixed) • Arakawa C grid, multiple nested grids (fixed) • Arakawa C grid, multiple nested grids (movable)
Time differencing	• Leapfrog; time split; 2nd or 4th order spatial accuracy • Forward; 2nd or 6th order spatial accuracy
Turbulence closure	• Smagorinsky deformation K • O'Brien K/Blackadar K • Deardorff level 2.5 K
Stable precipitation	• No condensation • Condensation
Cumulus parameterization	• None • Modified Kuo
Explicit microphysics	• None • Warm microphysics • Ice microphysics - specified nucleation • Ice microphysics - predicted nucleation
Radiation	• No radiation • Shortwave I • Shortwave II • Longwave I • Longwave II
Surface layer	• Louis (1979)
Lower boundary	• Specified air-surface temperature and moisture differences • Diagnosed surface temperature and moisture fluxes based on a prognostic soil model • Vegetation parameterization

Category	Available Options
Upper boundary	• Rigid lid • Prognostic surface pressure • Material surface • Gravity-wave radiation condition • Optional Rayleigh friction layer
Lateral boundaries	• Radiative boundary condition I • Radiative boundary condition II • Radiative boundary condition III • Radiative boundary condition and MCR • Large-scale sponge boundary conditions • Large-scale nudging boundary conditions
Initialization	• Horizontally homogeneous (HHI) • HHI plus variations to force cloud initiation • Variable initialization I • Variable initialization II
Transport and diffusion	• Lagrangian particle dispersion module

Large Eddy Simulations of the Convective Boundary Layer

The structure and statistical properties of large eddies in a convective boundary layer of inhomogeneously heated surfaces and over terrain consisting of a series of parallel, sinusoidal ridges and valleys has been investigated. The central result of this work was that the inhomogeneously heated surface and heated terrain induces thermally-driven, stationary circulations upon the background eddy motions, with convection over the hot spots and ridges, and subsidence over the cool spots and valleys. Even relatively low hills cause significant circulations which are readily extracted from the motion field by time averaging. The properties of the eddies and mean circulations were investigated in three phases of this research:

The LESs showed that stationary, thermally-driven circulations induced by inhomogeneities in surface heating and hilly terrain comprise a significant fraction of the total kinetic energy in the boundary layer. Many statistical properties of the boundary layer are altered locally. For example, in one experiment the probability of upward eddy motion was found to exceed 70 percent, while the probability of downward motion exceeds 80 percent over a valley. However, in spite of these circulations, a vertical profile of nearly all eddy statistics horizontally-averaged over the entire domain was found to have no significant differences from profiles over flat terrain. Small differences in horizontal velocity variances were noted.

The influence of the eddy motions on passive tracers emitted at various locations over heated surfaces and near hilly terrain surfaces has been studied; Figure 1 shows an example. The thermally-driven circulations were found to have a significant effect on the dispersion patterns of the tracers, causing them to develop asymmetric shapes. For example, surface concentrations were found to spread more rapidly perpendicular to the ridges and valleys than parallel to them. The propagation in the perpendicular direction was not entirely continuous, but partially discrete.

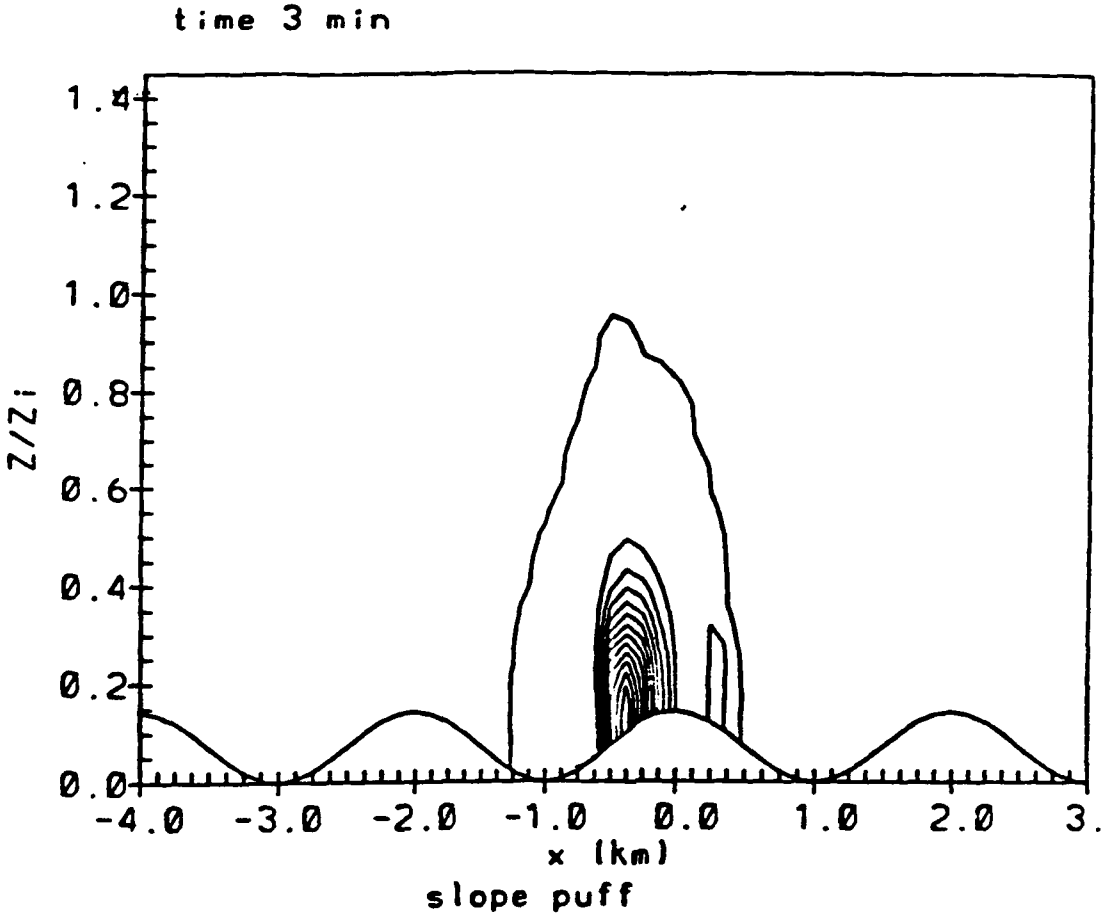

Figure 1. Example of passive tracer released as a single puff along a slope midway between the valley and hill (at location x = -1 km).

Large Eddy Simulations of the Convective Boundary Layer East of the Colorado Rockies

This research provided base-line simulations of the impacts of small-scale variations in physiographic features on the convective boundary layer and on transport and dispersion. It also demonstrated how a model such as RAMS can be useful in furthering our understanding of the behavior of the convective boundary layer over inhomogeneous terrain.

This research used a large eddy simulation (LES) nested within a mesoscale simulation to study the development and characteristics of the large eddies of the daytime boundary layer in an area where the convective boundary layer can be influenced by larger scale circulations. The application of a LES in this way was unique and was possible because of the interactive nested grid capabilities of the RAMS model. This allowed a much wider use of LES, including the applications of the LES to a case study. The case study in this research was taken from the Phoenix II observational program on the Colorado Great Plains, 25 km from the Front Range of the Colorado Rockies. The case day was 22 June 1984, which was analyzed by Schneider (1991).

Results of the two dimensional simulation indicate that the boundary layer over the plains develops separately from the boundary layer over the elevated terrain. The elevated boundary layer begins to advect eastward with the mean wind, above the plains boundary layer, and the circulations within it weaken as they move away from the higher terrain. Eventually, the plains boundary layer grows deep enough to interact with the elevated boundary layer. Also, gravity waves, triggered by the convection in the elevated boundary layer, may be influencing the character of the large eddies in the boundary layer over the plains. This is consistent with LeMone (1990), who speculated that gravity waves interacting with the observed convective boundary layer explain the differences found in vertical velocity skewness between LES and observations, and Clark et. al. (1986), who have suggested that gravity waves influence the character of boundary layer eddies. Figure 2 shows an example of the separate generation of turbulent kinetic energy (TKE) over the mountains and plains.

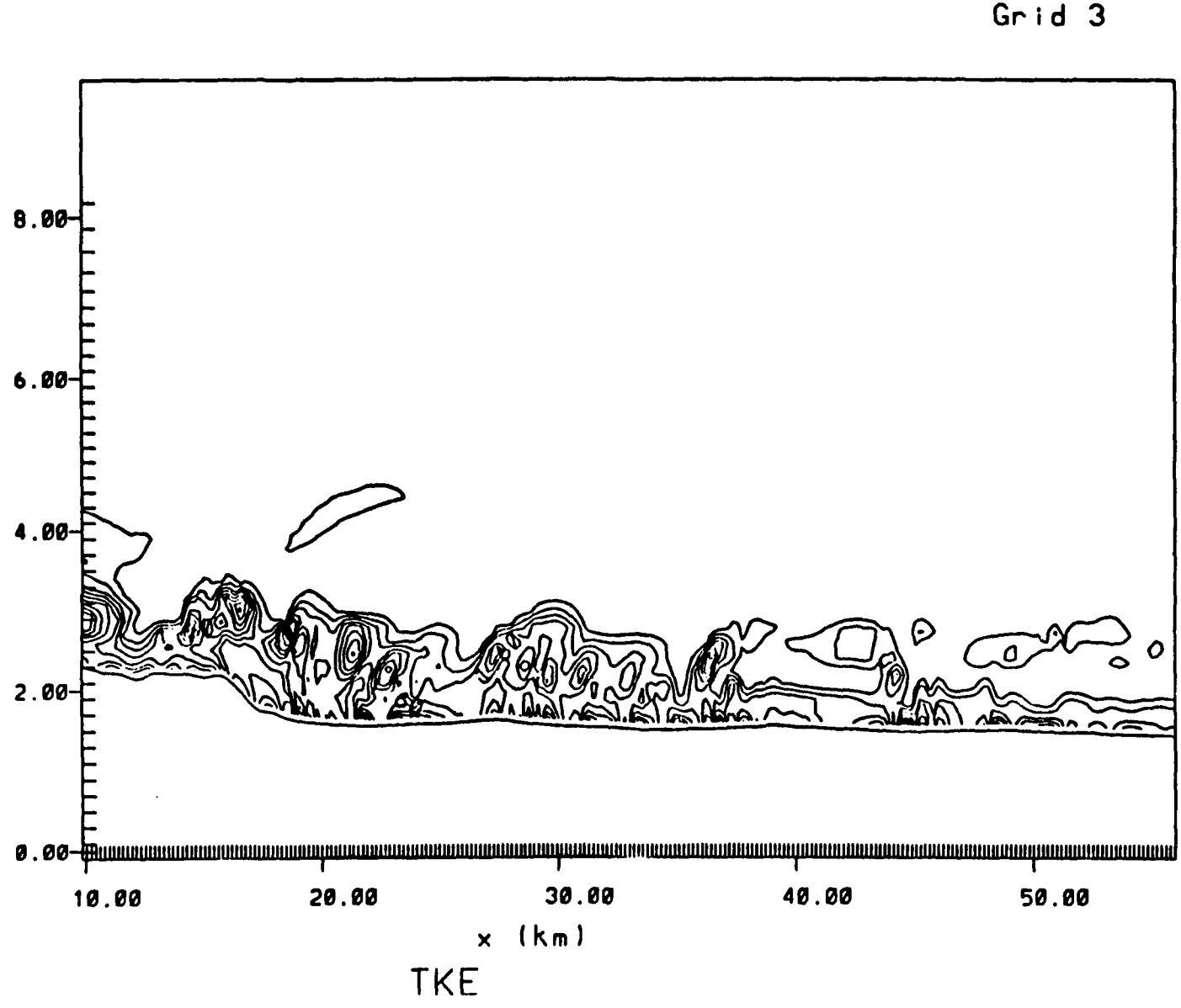

Figure 2. Turbulent kinetic energy field simulated by RAMS for 1520 UTC on 22 June 1984 for the Phoenix II region.

Quantitative Precipitation Forecasting (QPF) of Wintertime Orographic Snowfall

As part of the ARO research, Meyers and Cotton have evaluated the usefulness of a non-hydrostatic cloud model with explicit ice phase physics (the RAMS) for QPF of snow and rainfall in an orographic precipitation case study. They also ran sensitivity tests to determine the physical controls on clouds and precipitation. By examining the physical controls and performing sensitivity tests on the microphysics, dynamics, and resolution, one can determine an optimal computational setup for future versions of forecast models. Preliminary two-dimensional, cross barrier simulations produced flow fields and microphysical structures which compared well with observations (Meyers and Cotton, 1992). A significant challenge found in the preliminary runs was that kinematic and microphysical structure and the resultant QPF exhibited a profound sensitivity to the input sounding. Obtaining a representative upstream environment is quite difficult when using a homogeneous initialization, especially where the soundings across the region of interest are modified by the local topography. The model simulations compared much better with the observations with a modified sounding inferred from the geostrophic winds.

Another characteristic of the two-dimensional runs was the evidence of convective bands, which initiated in the Central Valley and propagated downstream with the ambient flow. Potential instability was the mechanism responsible for the cellular convective bands, which were triggered by the orographic blocking and lifting that extended westward across the Central Valley. A fine resolution model is needed to resolve these and similar convective-type responses, which are prevalent in many orographic precipitation events. (Our grid increment is 1.5 km).

A major advantage of using an explicit cloud model is that the precipitation type (frozen or liquid) can be predicted. This parameter would be extremely useful for a hydrologist, enabling more accurate runoff calculations. In the three-dimensional simulations, the model was initialized with an inhomogeneous objective analysis. A difficulty with the three-dimensional simulations was that the convective scale processes found in the 2-D simulations (1.5 km grid increment) were not resolved by the 3-D simulations (50 km grid increment). Therefore, numerical experiments were conducted with the 3-D version of RAMS which employed finer grid nests (12 km and 3 km grid increments). These results showed that with finer grid nests, the overall model structure and resultant QPF compared much better with the observations.

Like other bulk microphysical models, RAMS previously had approximated the number of ice crystals at a given degree of supercooling based on the Fletcher curve (Fletcher, 1962), and used a simple contact nucleation scheme following Young (1974a,b). Predictions of pristine ice crystal concentrations by these schemes were very inaccurate. Using new data from continuous flow diffusion chambers which combined the effects of deposition and condensation-freezing nucleation, a new formula for the exponential variation of ice nuclei concentration with ice

supersaturation was derived. Predicted ice concentrations from these measurements exceeded values predicted by the widely used temperature-dependent Fletcher approximation by as much as one order of magnitude at temperatures warmer than -20°C. A contact-freezing nucleation model was also formulated based on laboratory data gathered by various authors using techniques which isolated this nucleation mode. Predicted contact nuclei concentrations based on the newer measurements were as much as three orders of magnitude less than values estimated by Young (1974a). These schemes predicted pristine ice crystal concentrations which compared much better with the observations. In addition, the amount of surface precipitation is more sensitive to variations in microphysics than with the old scheme.

Orographic Influences on Snowfall in the Front Range of the Rocky Mountains

This study utilized detailed observational data to document and describe several aspects of the topographical effects on snowstorms in the Front Range of the Rocky Mountains. Specifically, the processes contributing to enhanced snowfall along the foothills and adjacent plains were emphasized, using primarily a special spotter network and three-hourly radiosonde releases at Fort Collins. Several mesoscale model experiments complemented the analysis of observational data.

Through analysis of data from special radiosondes, surface meso-network, volunteer spotters, geostationary satellite, profilers, Doppler radars, and standard NMC gridded files, a series of storms were analyzed in detail in order to isolate the various topographical influences. A series of RAMS simulations also was completed, some including full microphysics, to further evaluate terrain-forced regions of ascent in the lower troposphere.

The findings of this investigation benefit the scientific knowledge of winter storms occurring throughout the United States and the rest of the world, especially in complex terrain. Both cold-air damming and arctic air mass overrunning occur not only along the entire lee side of the Rocky Mountain barrier, but also near mountain ranges in other parts of the world. Overrunning of arctic air not associated with mountains also exhibits some similar features.

The focus of this investigation dealt directly with a more general problem evident in atmospheric science at this time: the understanding of physical processes involved in mesoscale precipitating systems. Snowfall distributions in complex terrain consistently exhibit significant variations on spatial scales of a few to 50 km, and much more research is required to quantitatively assess the underlying causes of this variability. The present study furthers the fundamental understanding of snowstorm microphysical and dynamical processes both in Colorado and any other region of complex terrain. WISP, centered in Boulder, Colorado is currently applying the findings of this study to the analysis of two years of field data.

Regional-Scale Flows in Complex Terrain: An Observational and Numerical Investigation

Observations have shown the development of recurrent "regional-scale" circulation system across the Colorado mountain barrier, operating on a diurnal time scale. During the nocturnal phase, the winds are particularly strong and from a southeasterly direction, which is generally counter to the upper-level winds, with an abrupt onset in early evening and steady flow thereafter. Soundings have shown this nocturnal current to be shallow and within a distinctly stable air mass.

Idealized three-dimensional experiments with RAMS showed that thermal forcing over realistic topography in conditions of negligible, or weak ambient flow, is capable of producing many of the flow features observed throughout the diurnal cycle. This experiment further showed how the deep mountain-plains solenoid along and above the Front Range crest evolves in late afternoon into a shallower density current, which then propagates westward over the mountains of the western slope. This unexpected flow phenomenon is the primary process responsible for the strong nocturnal southeasterly winds found in observations. As a result of the numerical experiments, four phases of the thermally forced regional-scale diurnal circulation system have been identified. These consist of a daytime mountain boundary layer development phase, a late afternoon transitional phase, an evening propagating density current phase, and a late night adjustment phase.

The findings of this study will benefit our understanding of atmospheric flows over complex terrain providing a motivation for others to seek similar flow features in other regions. The work also demonstrates the usefulness of a mesoscale model such as RAMS in defining low-level wind fluctuations that are important to transport and diffusion studies.

2.5 BOUNDARY LAYER STUDIES

The Daytime Evolution of the Atmosphere East of a Large North-South Mountain Barrier

The west-east nature of the daytime evolution is examined for conditions of clear skies, little spatial or temporal change in synoptic-scale wind and thermal fields, and light ambient winds with a westerly component around 5ms^{-1}. This study uses computer simulations and observations. Many two-dimensional, non-hydrostatic simulations are run using the CSU RAMS, and the simulations have a nighttime phase before the daytime phase is simulated. The observations mainly consist of deep airsonde launches which are taken from near sunrise until late in the afternoon.

The daytime evolution in northeast Colorado results from a complicated interaction between the ambient and thermally driven flows. From the simulations and observations a conceptual model of the daytime evolution is developed. The conceptual model consists of a sunrise state, which is substantially different from a horizontally homogeneous state, and three phases during the daytime. The phases describe periods of the day in which different features dominate the evolution. The main features of the sunrise state include a jet down the east side of the barrier and a deep layer of cold, stable air to the east of the barrier. Phase 1 lasts until 3-4 hours after sunrise and results from the weakening nocturnal flows interacting with the daytime heating. The main features are the weakening of the nocturnal flows and warming within 20km of the eastern base of the barrier associated with the weakening nocturnal jet. Phase 2 has a developing solenoid with upslope flow on the eastern plains, a region of strong rising motion on the eastern slope of the barrier, westerly return flow above the upslope flow, and sinking motion on the eastern plains. The solenoid is not horizontally and vertically symmetric, and it does not develop uniformly with time. Phase 3 is characterized by a migrating solenoid. The migrating solenoid is a perturbation - which can substantially influence the atmosphere on the eastern plains - in the main daytime circulation. This conceptual model is an excellent basis for future examinations of the daytime evolution.

The constantly evolving daytime circulation influences the thermal and wind structure on the eastern plains. On the eastern plains the depth of the convective boundary layer (CBL) is suppressed. Upslope winds occur in and above the CBL, and the winds rapidly change to westerly component flow above the upslope flow. When the migrating solenoid passes over a site, the CBL often explosively grows 600 to 1200m in one hour, and the depth of the upslope flow rapidly increases. After the solenoid passes a site the CBL is capped by a layer of weak stability and strong vertical wind shear, and the CBL depth is near the height of barrier top. The constantly evolving thermal and wind structure has profound influences on the dispersion of air pollutants, potentially hazardous aerosols, moisture, and other airborne gases and particles.

This study improves upon the past studies of the daytime mountain-plains circulation east of large north-south mountain barriers, including the Front Range of the Colorado Rockies, in four ways. First, the simulations include a nighttime phase before the daytime phase is simulated, and the simulations have a grid spacing of 100 to 200m in the lower part of the domain to accurately simulate many of the features of the nocturnal and sunrise states. Second, the simulations have improved parameterizations for longwave and shortwave radiation, a soil module which predicts a surface sensible heat flux at each point, and realistic topography. Previous observational studies do not include frequent airsonde launches near sunrise and in the morning. Finally, many simulations are run with different initial conditions to show the universality of the features of the daytime evolution. A journal article on the daytime evolution is being prepared, and it will be submitted to the *Journal of the Atmospheric Sciences*.

Sensitivity of the Daytime Evolution East of a Large North-South Mountain Barrier to Different Initial Conditions

A variety of two-dimensional, non-hydrostatic simulations using the CSU RAMS are run to examine how the daytime evolution qualitatively and quantitatively changes for different conditions. The sensitivity runs have differing time of year, patterns of surface moisture which influence the patterns of surface sensible heat flux, ambient winds, ambient thermal structure, or barrier height. One simulation is run without a nighttime phase. The summary entitled "The Daytime Evolution of the Atmosphere East of a Large North-South Mountain Barrier"describes the daytime evolution east of a large north-south barrier.

Plots of the various model fields are used to qualitatively ascertain how the evolution changes for the different conditions. The quantitative comparison uses parameters describing the strength and depth of the wind field and the influence of the circulation on the thermal field. The parameters used to quantify the wind field include the mass flux in the upslope flow, maximum u-component of the return flow, depth of the upslope flow, and the height where the mass flux towards the barrier equals the mass flux away from the barrier. The thermal field is quantified by the CBL depth, horizontal cold air advection in the CBL, and amount of warming above the CBL.

The sensitivity runs show the following changes in the daytime evolution for different conditions. At sunrise the jet down the east side of the barrier is weaker when no ambient winds are present compared to simulations with ambient u-component of 5 to 10ms^{-1}. The vertical wavelength of the hydrostatic mountain wave above the barrier appears to influence the sunrise structure of the atmosphere. Phase 1 warming does not occur if no ambient winds are present. If the surface sensible heat flux on the eastern slope of the barrier does not significantly increase within the first several hours after sunrise, phase 1 warming does not occur.

The circulations in phases 2 and 3 are generally weaker and shallower for days closer to the winter solstice, moister soil on the eastern plains, moister soil west of barrier crest, stronger ambient winds, and a lower CBL on the previous day. The circulations are generally deeper and stronger for less ambient stability and times closer to the summer solstice. Similarly, the CBL depth on the eastern plains is shallower for moister soil on the eastern plains, days closer to the winter solstice, stronger ambient winds, and lower CBL the previous day. The migrating solenoid may be absent on some days because of lack of heating due to the time of year or because of increased stability in the afternoon above the CBL on the eastern plains. The no nighttime phase simulation shows that the nighttime phase is essential for properly simulating the daytime evolution, especially early in the day.

Some examples of quantitative differences in the simulation resulting from various initial conditions include the mass flux in the upslope flow in a simulation run for December 21 heating being only 18% as large as in a simulation with September 21 heating. Similarly, the CBL in the

December 21 run is only 1/3 as deep as in the September 21 heating run. Moister soil on the eastern plains can reduce the amount of upslope flow by 1/3 compared to dry soil on the eastern plains. The moister soil also reduces the CBL depth on the eastern plains to 1/2 its depth compared to when dry soil is present. Increasing the ambient u-component of the winds above barrier top from 5 to 10ms^{-1} reduces the amount of upslope flow by up to 60%.

Different ambient winds, ambient thermal fields, time of year, patterns of soil moisture, and barrier height can drastically influence the strength of the daytime circulations, and they can sometimes result in the absence of some of the features of the daytime evolution. Having these correct conditions is very important to accurately simulate the wind and thermal fields at sunrise and during the day.

The Usefulness of Frequent Airsonde Launches as an Observing Tool

The atmosphere varies in four dimensions. Horizontal and vertical gradients in the atmosphere are almost always present, and the atmosphere is constantly evolving, changing the horizontal and vertical structure of the atmosphere. Observing methodologies cannot simultaneously observe the atmosphere in four dimensions. For example, aircraft can measure horizontal gradients in the atmosphere very well at one level. However, the atmosphere can change significantly in the time between flights at different altitudes resulting in the aircraft not providing an accurate view of the variations of the atmosphere with height. Surface data can provide a good horizontal and temporal understanding of the atmosphere but without any indication of the vertical variations.

The usefulness of frequent airsonde launches as an observing methodology is examined. With the rapid rise rate ($5ms^{-1}$) the vertical profile of the atmosphere is measured nearly instantaneously. Launches every two to three hours show how the atmosphere over the site varies vertically with time. Several observing sites show how the evolution varies horizontally providing an indication of horizontal changes in the atmosphere. Wind profilers and RASS take nearly instantaneous deep profiles of the wind and thermal fields, and the results of the examination of the frequent airsonde launches as an observing tool can be applied to these automated observing devices.

In the study of the daytime evolution east of the crest of the Colorado Rockies, frequent airsonde launches were the main observing tool. The summary entitled "The Daytime Evolution of the Atmosphere East of a Large North-South Mountain Barrier" describes the daytime evolution east of a large north-south barrier. The frequent airsonde launches were very useful for identifying the changing features of the daytime evolution above the surface including the nocturnal jet down the east side of the barrier, stable core, phase 1 warming, and the developing solenoid. The frequent airsonde observations also allowed for the quantitative comparison between computer simulations and observations. The depth of the upslope flow, the mass flux towards the barrier, and the CBL depth were used to show how well computer simulations quantitatively agree with the observations. Frequent airsonde launches at two sites showed how well the simulations replicate the horizontal changes in the atmosphere during the daytime evolution.

The frequent observations of the thermal profiles measured the amount of heating which occurs above a site. On several days surface energy budget stations were located at the sites where the frequent airsonde launches occurred. The comparison of the heating observed in the launches and the local surface sensible heat flux show the usefulness of the heating observed in the frequent airsonde launches as an areal average of the surface sensible heat flux. Throughout the day at the Fort Collins site, the amount of heating observed in and above the CBL was much greater than the surface sensible heat flux. The soundings showed a complex vertical profile of temperature and wind for a large depth of the atmosphere. Frequent airsonde launches were also performed at

Carpenter, Wyoming in cooperation with a NCAR field project. This NCAR field project measured the surface sensible heat flux over a nearly flat field without any significant terrain variations in the region. The amount of heating observed in the CBL was several times larger than the surface sensible heat flux measured by the eddy correlation and Bowen ratio method. The Carpenter site appeared to be influenced by mesoscale circulations, which is not very surprising since the site is located near the crest of the 600m high Cheyenne Ridge. The use of sounding data to obtain an areal average of the surface sensible heat flux likely requires very minimal influence from mesoscale circulations of little horizontal variability in the surface sensible heat flux. The observations indicate that the atmosphere often is disturbed, and the amount of heating differs vertically from the locally measured surface sensible heat flux.

Development of Radio-Acoustic Sounding System for Boundary Layer Studies

A Radio-Acoustic Sounding System (RASS) research program has been established to pursue improved methodology for remotely sensing the vertical temperature structure in the atmospheric boundary layer. RASS utilizes a UHF wind profiler to measure the speed of vertically propagating acoustic waves. Their speed depends on the temperature of the atmosphere in a simple manner. The RASS technique allows an almost constant monitoring of the vertical temperature structure, whereas conventional soundes may be launched at periods of an hour or more. The focus of the program is twofold; first to improve the technological approach in order to improve the system capability, and second, to utilize the rapid temperature sensing to better understand boundary layer processes. Thus, RASS is a very useful tool for investigations of the mountain-plains boundary layer discussed earlier in this section.

The RASS capability developed to date is unique in that it is being used with a five beam wind profiler, allowing a greater flexibility of directional probing of the acoustic wave front, rather than more conventional three beam systems. A diagnostic model has been developed to be used in conjunction with the RASS to enable more precise placement of the acoustic sources to maximize vertical coverage with the RASS. The need for this model arises because horizontal winds typically advect the acoustic wave through and out of the RF antenna beam. Since the profiler can observe the wind structure, actual observations may be used in the model to predict the best acoustic source - profiler beam configuration to yield RASS temperature information for a specific height. The system has been used during major field projects, such as FIRE (the First ISCCP (International Satellite Cloud Climatology Project) Regional Experiment), to improve our understanding of the coupling between cloud and boundary layer processes. Preliminary results from FIRE indicate that profiles obtained from RASS compare reasonably well with those measured by rawinsonde. The ability of RASS to resolve a low level temperature inversion was especially encouraging.

Inference of Horizontal Temperature Gradients Using Passive Radiometric Methods

The sensitivity of infrared radiances to horizontal temperature gradients has been established in an effort to use passive radiometric measurements to infer temperature inhomogeneities in the boundary layer. The investigation established the radiometric precision required for deducing temperature gradients of various magnitudes. A means of detecting the gradients was developed in which absolute calibration of radiometers is not required. The method utilizes radiances normalized by the radiance measured in a direction perpendicular to the horizontal temperature gradient. This method greatly simplifies actual field measurements where precise calibrations may not be practical. The work identified the portion of the radiometric spectrum between 500 cm^{-1} and 800 cm^{-1} as best suited to such remote sensing activities. This research has established the groundwork for field testing of the method and feasibility of acquiring temperature structure in the boundary layer. Such a capability would enhance the performance of other boundary layer modeling requiring a more detailed knowledge of boundary layer characteristics.

2.6 HYDROLOGY

Effect of Temporal and Spatial Variability of Rainfall and Watershed Geometry on Surface Runoff

A detailed examination of the effect of rainfall rate temporal variability was performed in both one- and two-dimensional simulations. Factors considered were the temporal sampling interval of the rainfall data δt, the duration of rainfall t_r, and the time to equilibrium t_e. Results show that the relative sensitivity R_s increases with δt. As t_r exceeds t_e an asymptotic R_s value is reached which is proportional to $\sqrt{\delta t}$. One-dimensional simulations with combined temporal and spatial variability show that R_s is highly dependent on t_r. When $t_r < t_e$, R_s is predominantly caused by spatial variability, while as t_r increases beyond t_e, temporal variability becomes dominant. Relative sensitivity data from all forms of watershed spatial variability tested show that R_s is independent of runoff geometry.

Results from this study provide new scientific insight into the role of rainfall spatial and temporal characteristics on outflow. The duration of rainfall is found to completely dictate the relative importance of spatial or temporal rainfall variability on runoff. These factors outweigh watershed geometric impacts on runoff. The design of physically based runoff models which minimize runoff prediction error by proper spatial and temporal sampling is made possible as never before.

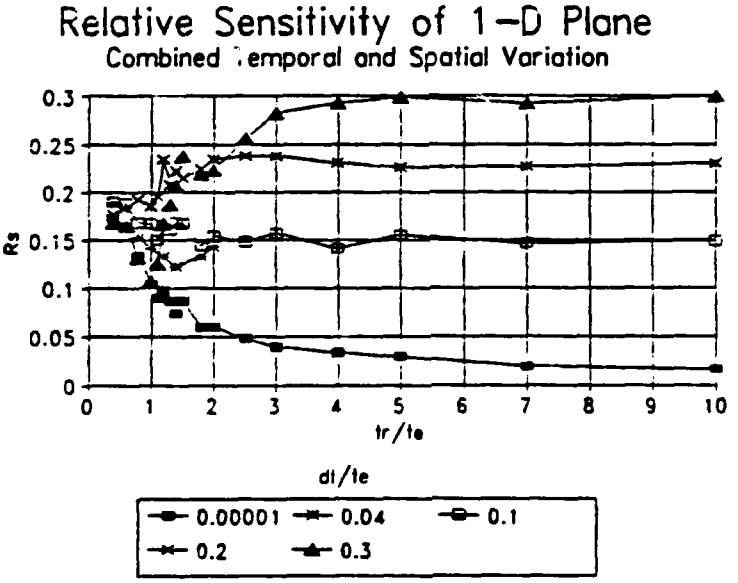

Figure 1. Relative Sensitivity of 1-D Plane to Combined Temporal and Spatial Variability in Precipitation Intensity.

Effects of Spatially Varied Infiltration on Surface Runoff

A two-dimensional Monte-Carlo analysis of spatially varied saturated hydraulic conductivity has been conducted (Saghafian, 1992). As suggested by some reported field data, hydraulic conductivity was assumed to follow a lognormal spatial distribution over watersheds. The main soil infiltration parameters were K_m, C_v, and S denoting mean hydraulic conductivity, spatial coefficient of variation of hydraulic conductivity, and degree of initial soil moisture, respectively. The storm parameters were i and T_r, respectively denoting rainfall intensity and duration. Based on the result of simulations by CASC2D, the following figure illustrates the variation of normalized relative sensitivity versus two major dimensionless parameters $T^* = T_r/T_{he}$ and $K^* = K_m/i$ where $T_{he} = T_p + T_e$, T_p = ponding time corresponding to a system with uniform distribution of hydraulic conductivity, T_e = wave travel time for a very long storm with the steady state excess rainfall intensity equal to $(i-K_m)$. The hypothetical equilibrium time (T_{he}) accounts for both the initial soil condition and hydraulics of the watershed. Also the curve associated with the behavior of two-dimensional spatially varied overland roughness on impervious watersheds has been included for comparison.

The results confirm that the relative spatial sensitivity for pervious areas demonstrates a similar trend to that of impervious basins when K^* is small and the rainfall duration is sufficiently long to produce surface runoff. For large values of K^*, however, normalized R_s reaches a constant value for long storm durations. This occurs because the runon generated in the upstream area of some given spatial distributions of hydraulic conductivity may infiltrate as it travels downstream. Therefore the location of elements of hydraulic conductivity is more important for long storms when K^* is large and for short storms when K^* is small. This study has yielded a quantitative method for determining when these hydraulic conductivity elements must be properly placed. It also has confirmed the conditions under which hydraulic conductivity is an important parameter for simulating surface runoff.

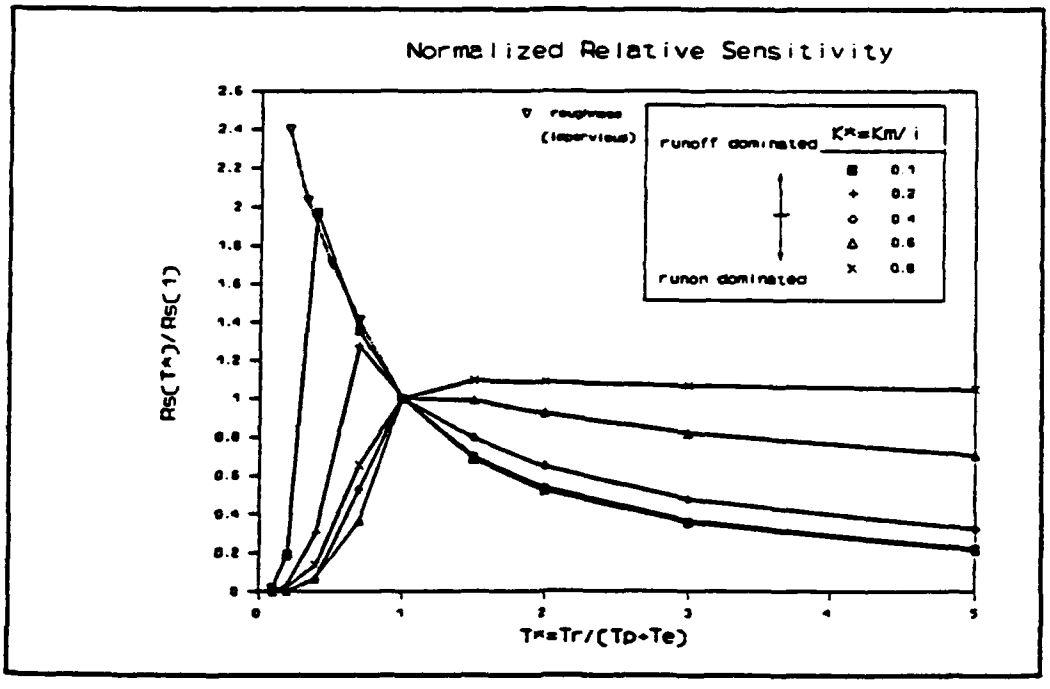
Normalized Relative Sensitivity
roughness
(impervious)
runoff dominated
K*=Km/i
0.1
0.2
0.4
0.6
0.8
runon dominated
Rs(T*)/Rs(1)
T*=Tr/(Tp+Te)

Figure 2

Effect of Storm Motion on Surface Runoff

The importance of closely simulating storm motion in runoff simulations was examined. Storm motion effects on peak discharge were determined in both one- and two-dimensional simulations. Parameters considered included the length of block storms in the direction of motion L_s, the length of the runoff plane L_p, the storm speed U, and the runoff surface time to equilibrium t_e. Results show that storm motion effects are pronounced at dimensionless storm speeds Ut_e/L_p between 0.5 and 1.0, when the storm moves in the drainage direction.

These simulations indicate that the detailed simulation of storm motion with physically based runoff models is important only when storms move near a speed of L_p/t_e. In reality, this is much less than typical storm speeds on basins of mild slope. This new discovery indicates that the detailed simulation of storm motion is necessary for accurate runoff simulations only in limited cases.

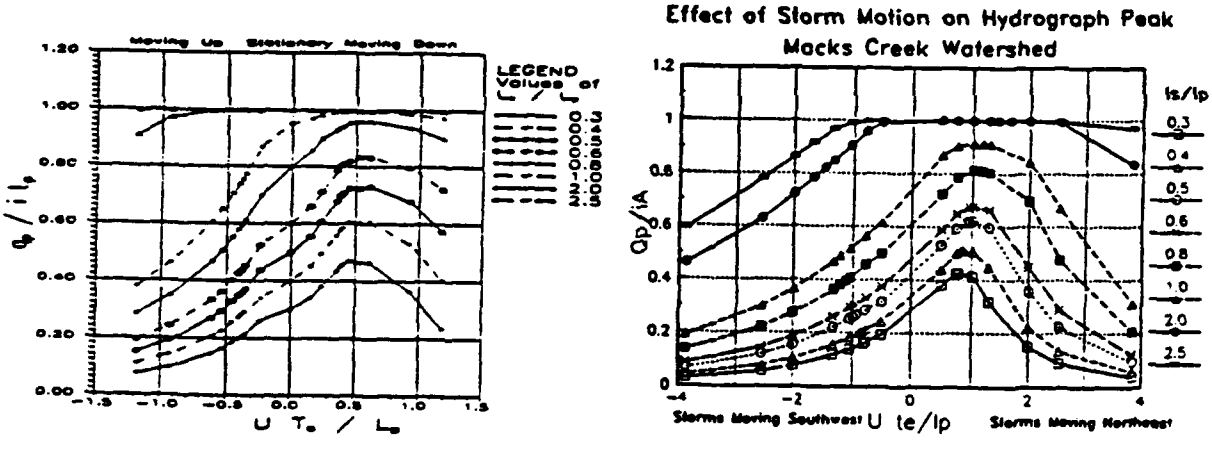

Figure 3. (a) Effect of Storm Motion on Hydrograph Peak on One-Dimensional Runoff Plane (Richardson, 1989); (b) Effect of Storm Motion on Hydrograph Peak on Two-Dimensional Macks Creek Watershed (Ogden, 1992).

Hydrologic Simulations Using Radar Rainfall Data

Rainfall estimates from a polarimetric weather radar were linked with the CASC2D runoff model to examine the effect of radar data resolution on runoff. Radar parameters used to estimate rainfall include the reflectivity factor Z, the differential reflectivity Z_{DR}, and the specific differential propagation phase K_{DP}. Rainfall rate estimates within mixed phase precipitation require measurements of K_{DP} because it is relatively insensitive to hail.

Results of simulations without infiltration on two watersheds with surface areas of 32 and 121 km^2 show that an input data resolution of 2 km is sufficient for accurately describing the spatial variability of continental convective rainstorms. Simulations with infiltration show that watershed response is highly dependent on input data resolution, because of a decrease in excess rainfall rates. These real-time radar data simulations represent the most detailed study to-date of the effect of precipitation data resolution on runoff model performance. Results provide sufficient information for the analysis of resolution induced runoff calculation errors from physically based runoff models.

Effects of Army Maneuvers on Watershed Response

The land use impacts of large scale mechanized military maneuvers on Army training lands is a critical natural resources management issue. LTC William Doe, a U.S. Army officer, used the CASC-2D rainfall-runoff model with a Geographic Information System (GIS) to illustrate how technology integration could enhance the scientific understanding of maneuver effects on hydrologic processes.

A 50-square mile watershed within the U.S. Army Pinon Canyon Maneuver Site in southeastern Colorado was selected to demonstrate the potential application of the integrated model-GIS system. LTC Doe performed extensive field investigations at the Maneuver Site to quantify the critical hydrologic parameters. The field data were combined with spatial map layer information in the Geographical Resources Analysis Support System (GRASS) to characterize the spatial components of the watershed. The raster data from GRASS were exported directly to the CASC-2D model. Computer simulations of rainfall-runoff events were performed to assess how various maneuver scenarios might impact the internal watershed dynamics. The spatial outputs from the model, including infiltration depth and overland flow depth, were imported back to GRASS for spatial analysis and display.

The integration of GRASS and the CASC-2D model proved very useful in analyzing the hydrologic perturbations caused by maneuvers on the watershed. The extraction of decision information, such as the location of hydrologically sensitive areas, provides the land manager with critical spatial information which can be used to mitigate future environmental impacts.

This research has integrated state-of-the-art hydrologic modeling with GIS technology to examine the spatial and temporal impacts of Army maneuvers on the hydrology of an Army training area. The research represents the first effort to provide a comprehensive understanding of how maneuvers effect watershed response using computer simulation. The visualization capabilities of the model and GIS greatly enhance the non-technical person's understanding of the maneuver-land-hydrology interface.

2.7 CLIMATIC GEOMORPHOLOGY

Geomorphic and Climatic Controls on Streamflow, Sediment, and Salt Loads, Upper Colorado River Basin

Suspended-sediment discharge and dissolved-solids discharge in the Upper Colorado River Basin decreased after the early 1940s, while streamflow in the three principal rivers - the Colorado, Green, and San Juan - did not change significantly. This decline followed a period of high sediment yield caused by extensive arroyo incision around the turn of the century. Field investigation of 57 incised channels in the Upper Colorado River Basin reveals that significant amounts of sediment and salt are being stored in the lower and middle reaches of many of these channels, as they evolve toward a new condition of relative stability. Large-scale atmospheric circulation patterns significantly control streamflow within the basin, and anomalously high and low flows can be spatially correlated over hundreds of kilometers.

The amount of soluble minerals (salt) stored within the valley alluvium primarily reflects the surrounding drainage basin geology and soil types; concentrations were especially high in areas underlain by marine shales in Utah and Western Colorado. Soluble mineral concentrations (SMC) for 429 samples average 1.2 percent and range between 0 to 23 percent by weight. Concentrations greater than 3 percent can be found immediately above impermeable boundaries such as silty-clay layers within the floodplain sediments or the alluvium/bedrock interface. Individually, the salt concentrations may appear low. However, when integrated over the volume of sediment within the incised-channel networks, the total quantity of salt stored in the alluvium is at least 10 to 20 times the annual dissolved-solids load in the Colorado River at Hoover Dam.

The stability of the channel networks governs the response of the fluvial system to large-scale climatic events, thereby controlling the long-term sediment and salt yields of the drainage basins in the southwestern United States. In the major sediment-producing regions of the Colorado River Basins, the valleys are efficiently storing sediment and salt within their middle and lower reaches. The external (climatic) factors of precipitation and runoff control the input into the hydrologic system and thereby influence the seasonal and year-to-year variability of sediment and salt loads in rivers. However, internal (geomorphic) factors have caused the most significant changes in sediment and dissolved-solids yield. These internal factors are primarily the decreased size and stabilized condition of the incised channel network.

These conclusions have significant implications for land management within the semiarid western U.S., especially in view of the potential for climate change. Appropriate management practices in the middle reaches of western drainage basins, where sediment and salt storage is large, are very important. This study indicates that current efforts to manage salt and sediment within entire drainage basins may be misdirected.

Drainage Density

Drainage density (the ratio of total channel length to drainage area) is clearly an important geomorphic variable that has been related to climatic conditions, flood peaks, mean annual discharge, and sediment yields. It has long been used to detect variations of rock type and structure by photogeologists and to document the stage of erosional evolution of a drainage system. Drainage density is also a significant factor for the reclamation of mined land in the U.S. Therefore, there is a great need to improve the understanding of drainage density and to predict how altered conditions will affect it.

Drainage basins developed on shale in Texas and on granite in California were selected through a large range of annual precipitation in order to investigate the relationships among drainage density, climate, and lithology. These examples represent humid and arid conditions, respectively.

The results from the two areas were markedly different. Drainage density on shale increased from low values in arid areas to a maximum in semiarid areas, and then decreased under humid climatic conditions. However, drainage density on granite increased to a maximum in the arid regions. These results were unexpected because it was assumed that the results would be similar, but that drainage density would be lower on granite.

One explanation is that the shale drainage basins represent dominant overland flow conditions, whereas on granite throughflow is dominant because of the deeply weathered soil mantle that covers bedrock, except in the most arid areas. Another explanation is that the granite drainage basins reflect the influence of past climate change. Obviously, the shale basins will more readily reflect current climatic conditions than the granite basins because shale is much more responsive to change. For example, if the arid shale basins experienced an increase of precipitation and runoff, drainage density would increase accordingly. When the climate became drier, hillslope erosion would continue to deliver sediment to the low-order stream channels, and they would be obliterated by creep and dry ravel. However, the channels would remain incised in the granite basins as the climate became drier because of the resistance of the rock. Hence, we assume that a large part of the drainage pattern of the arid granite basins survives from a wetter climate. Therefore, the very different relations between drainage density and climate in the Texas and California studies suggests that perhaps past climatic conditions exert an important influence on lithologies that are resistant, where the drainage network cannot adjust readily to climate change.

This research has established that drainage density is a function not only of climate, but also of lithology, relief, and past climate conditions. Past geomorphic processes that differ from the present, such as relative rates of surface versus subsurface runoff also may have an effect.

Sediment Movement Through Meanders

The results of the Fall River research into flow dynamics, sediment transport and sorting in meander bends increase our understanding of the dynamics of channel adjustment, especially adjustments at the reach scale. This research has helped to define some of the ways that a channel with adequate mobile bedload adjusts to changing discharge levels, and can also help to predict river response to other stimuli. Some specific examples of practical applications include the following:

1) Structures such as bridges which cross rivers are usually supported by piles; when piles are installed, scour occurs around their base. The model developed during this research would predict the size of the bedload moving past each pile, and the undisturbed shear stresses acting on that bedload. This information would improve the estimates of scour at each point, and possibly avoid bridge failure.
2) When channels are actively eroding their outer banks, many different methods are employed to stabilize them: rip-rap; jetty fields; dikes. A better understanding of the shear forces acting on the bedload moving through the thalweg and the grain sizes dominant in the thalweg would help in estimating the size of rip-rap or the placement of other structures.
3) Local zones of scour and deposition often occur in active channels. Given the grain size distribution, channel configuration, and discharge characteristics of the reach, the model developed in this research could help to predict the future exacerbation or stabilization of these channels.
4) Local changes to a channel reach, such as gravel mining, can upset the dynamics of the channel. Given the channel characteristics mentioned in 3), a prediction of the channel response to these stimuli may be ascertained.
5) A more complete understanding of sediment transport of different grain sizes through meander bends can also be of importance in sedimentology. The Fall River research indicates that ancient point bar deposits not only fine upward (i.e., the grain size decreases vertically), they also fine laterally, in a downstream direction. This may increase the understanding of the geometry, and changes in porosity and permeability of point bar deposits and thus help improve recovery of gas and oil from these deposits.

Dynamics of Sandy Bedforms in Meandering Channels: Examples from the Lower Mississippi River

In contrast to recent statements concerning the uniformity or similarity of sandy bedforms, two types of bedforms are observed in the Mississippi River: single bedforms and compound bedforms. Single bedforms are clearly related to flow characteristics such as discharge, mean velocity, and flow resistance, whereas compound bedforms are less demonstrably a function of flow properties. The former are hydrodynamically-created dunes, whereas the latter are likely produced by nonuniform and unsteady sediment transport or by the irregular movement of dunes themselves and may best be termed sand waves.

Much of the progress in understanding the dynamics of sandy bedforms has taken place in experimental flumes, where flow depth is limited, and flow is uniform for the length of the channel. Predictors of bedform size, shape and hydraulic resistance produced from these studies do not predict bedform dimension and shape for the Mississippi River. For example, nonuniformity of flow in a given reach produces a variety of forms. In an expanding reach, the decrease in average depth and average velocity coincident with increasing bedform size suggests that dune height for given mean conditions is locally controlled by downstream change in rate of suspended load and bedload transport.

Hydraulic roughness for 500-m segments of an individual profile cannot successfully be related to size of bedforms. The roughness effects of bedforms may be controlled by the hydraulic geometry variation of contrasting stream segments. In a pool-riffle transition, increasing discharge and dune size are accompanied by decreasing resistance. In a pool, increasing discharge and dune size are accompanied by an increase in roughness even though dunes become less "steep". Thus bedform size and shape combine with velocity and slope to determine roughness for a given discharge.

The depth and velocity conditions at different positions within the channel, as well as the temporal and spatial change in sediment transport control the shape and size of bedforms. However, a temporal shift in the locus of maximum velocity or sediment transport may cause variable response even within a single cross section.

The results of this study have been gleaned from voluminous and costly data sets collected by organizations such as the U.S. Army Corps of Engineers. The results illuminate processes by which river reaches are differentiated, and they contribute to the following description of the characteristics of large alluvial rivers.

Variability of Large Alluvial Rivers

In order to manage large alluvial rivers, an understanding of their complexity in space and through time is necessary. Large alluvial rivers differ in three ways: 1) there is a spectrum of river types that are dependent upon hydrology, sediment loads and geologic history; they differ among themselves; 2) rivers change naturally through time and as a result of climatic and hydrologic change; 3) there can be considerable variability of channel morphology along any one river, as a result of geologic and geomorphic controls. Information on these differences, especially the last two, will aid in predicting future river behavior and response to human activities.

One could assume that great alluvial rivers should have a relatively uniform morphology because the controlling factors of water discharge and sediment load should not vary greatly. However, other factors intervene to cause considerable variability. For example, a glance at even a coarse scale map of the pre-cutoff Mississippi River reveals great variability. In fact, 24 reaches were identified between Cairo, Illinois and Old River, a distance of 768 valley kilometers. The reaches were identified by changes of valley slope, channel variability through time and the pre-cutoff (1930) river pattern.

The Mississippi has been a very dynamic river characterized by a lack of uniformity in its morphology and dynamics, which has made the job of the river engineer difficult. The great variability is largely the result of geomorphic and geologic controls. Uplift, faulting and tributaries have an impressive influence on this great alluvial river. As a result of the dynamic character of this river, the density of population along its banks is low.

Another great alluvial river, the Nile, is found to be much less variable and dynamic when studied using the same geomorphic techniques. Because of the great population density along its course, even minor changes are of importance, however. There appears to have been little change of the pattern of the River Nile since mapping in the 18th century.

The differences between these two rivers dispel the assumption that all large alluvial rivers respond to change in the same way. For example, the steeper Mississippi River responded dramatically to cutoffs and sediment reduction, whereas the gentler Nile responded less dramatically to the effects of the High Aswan Dam. Also, if the morphology and behavior of large alluvial rivers are determined primarily by hydrology and hydraulics, long reaches of alluvial rivers should maintain a characteristic and relatively uniform morphology. In fact, this is not the case, and the variability of large alluvial rivers is an indication that hydraulics and hydrology are not always the dominant controls.

2.8 FOUR-DIMENSIONAL DATA ASSIMILATION

Adjoint Technique Assimilation in RAMS

We have investigated the various assimilation schemes, both 3-D and 4-D, available to limited area mesoscale models. The result of this investigation has been the decision to pursue the development of a version of RAMS and its adjoint to be used for 4-D assimilation. This decision is based on the potential of using the adjoint method to obtain an initial condition which minimizes the difference between the model and the observations over the observing period.

The adjoint method is a variational assimilation technique which includes the dynamical constraints of the prognostic model's equations. One defines a cost function based upon the difference between model and observational values. The adjoint model is used to obtain the gradient of the cost function. The value of the cost function and its gradient are used to minimize the cost function to obtain an "optimal" initial state. During the data assimilation there is potential for retrieval of non-measured variables and parameters which are unavailable in the observations. The iteration procedure used in assimilation is computationally expensive: Perhaps more useful is the potential for sensitivity studies with the adjoint method. Instead of minimizing the cost function, its gradient can be used to show the sensitivity of a forecast with respect to other atmospheric variables at prior times and at different geographical locations.

The adjoint technique was pursued with the following results:

- successful test of adjoint-based assimilation for 1-D shallow water model. Results in preprints of 9th Conference on Numerical Weather Prediction;
- qualitatively discovered the importance of cost function scaling in attaining minimization convergence;
- determined setup of RAMS that will be the basis for an adjoint based four-dimensional data assimilation scheme;
- developed a two-dimensional shallow water model for development and testing of the adjoint method with particular emphasis on data density in time and space, and length of assimilation;
- coded the linear tangent model of the 2-D shallow water equations. This is a prognostic model that forecasts the evolution of perturbations on the forward model. The adjoint model is derived from the adjoint of the linear tangent model.

The Adjoint Technique in Air Pollution Modeling and Sensitivity Studies

The adjoint technique has been applied in two other areas: (1) sensitivity analysis of meteorological mesoscale models in order to study model predictability related to uncertainty in input parameters; and (2) air pollution dispersion modeling.

The adjoint code was derived and implemented for a 3-D mesoscale meteorological model developed at the Warsaw University of Technology. In the present version of the adjoint 3-D code, perturbations in physical parameterizations (land surface representation, turbulence closure) are neglected for simplicity. The adjoint code was used to perform some preliminary experiments on model sensitivity to initial fields and eddy diffusivities using a case of a sea breeze circulation as an example. Since there are difficulties with deriving an adjoint code for complicated physical parameterizations, efforts were made to combine the sensitivity analysis based on the adjoint technique with another type of sensitivity analysis provided by the FAST method (Fourier Amplitude Sensitivity Test). This method is well-suited for the analysis of simple mathematical models or particular parameterizations in complex mesoscale models when it is possible to obtain multiple model solutions. Probability distributions of input parameters must be specified by a user and the FAST analysis provides the following results: (1) mean value of model output (2) variance of model output, and (3) partial variances of model output related to the uncertainty in particular input parameters. There is no limit to the size of input parameter uncertainties, and the method can be easily applied to any mathematical model. The computer package developed also includes the WASP method (Walsh Amplitude Sensitivity Procedure), which is similar to the FAST, but can be used for bivariate distributions of input parameters only (each input parameter can assume one of two values).

The adjoint technique applied to dispersion models governed by linear partial differential equations allows us to use two complementary approaches in chemical and biological dispersion studies:

- A traditional source-oriented modeling to calculate concentration fields forward in time for given emission sources;
- A receptor-oriented modeling to calculate the influence function backward in time for a given receptor.

The influence function obtained as a solution of adjoint equations depends on the meteorology and chemical transformations of effluent in the atmosphere, but is independent of emission sources. It characterizes transport and dispersion conditions in the atmosphere for the receptor under consideration. With the aid of the influence function, the concentration at the receptor can be expressed as a sum of contributions from emission sources within a modeling domain, distant emission sources outside the modeling domain and initial concentration fields.

2.9 INFORMATION EXTRACTION

Scientific Visualization Using 3-D Polygon Techniques

The Information Extraction and Visualization project has examined various visualization techniques for scientific data, analyses, and model output. The investigation of visualization methods began with 3-D polygon techniques, which are widely used within the computer graphics and other scientific communities. We succeeded in separately representing cloud surfaces from satellite data, precipitation volumes from radar data, and contours of constant pressure surfaces from global upper air data. One of our visualization requirements was for fused depictions of data products from multiple sensor types. For example, we wished to display a radar precipitation echo along with a satellite-derived representation of the cloud generating that precipitation. We discovered that theoretical difficulties exist with the algorithms utilized for polygonal representations when the data fusion issue is considered. Polygon depictions of fused data sets require the merger of those data sets as a separate step prior to their visualization. We abandoned the polygon visualization method for this reason.

Information Extraction and Visualization by Octree Encoding

The investigation of geosciences information extraction and visualization techniques focused on a method called octree encoding. We concentrated on this method after concluding that the polygon technique did not meet our needs. Octree encoding involves subdividing a Cartesian representation of a 3-dimensional data field until each cube within this volumetric depiction represents a uniform characteristic or data value. Octree encoding essentially results in a transformation of the original data field into a (frequently) more compact form. Certain spatial structure relationships within the field also may be more readily observed in the octree encoded version. Thus, octree encoding can aid the process of obtaining information from the data. This technique also allows the data volume to be graphically rendered in 3 dimensions.

We have applied octree encoding to the 3-D depiction of cloud boundaries derived from satellite data and to radar observations of precipitation volumes. We also have fused the radar and satellite octrees into a unified depiction of precipitation within the cloud. Figure 1 shows an example of such a fused product. The data fusion task is much more tractable via the octree method than by polygon techniques. The most significant difficulties that we have encountered with the data fusion task concern the spatial and temporal alignment of the data fields being fused. The octree visualization method has been enhanced by the addition of graphical clipping capabilities in all three of the dimensions displayed, allowing the inside of the data volume to be viewed, and by the creation of a unique rotation algorithm for changing the spatial orientation of the volume.

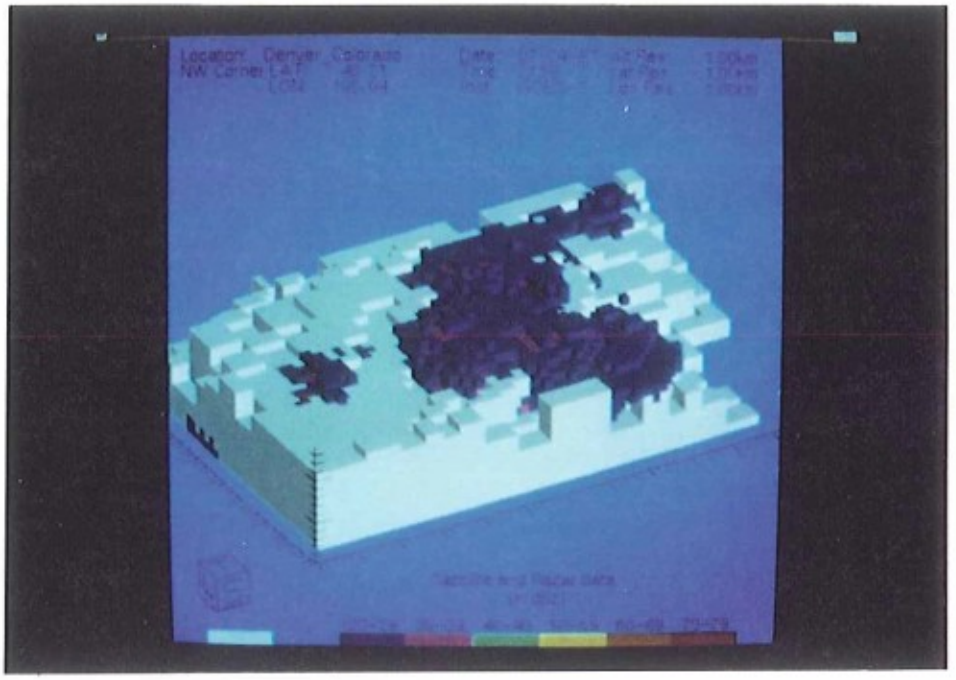

Figure 1. Graphics product created by fusion of satellite and radar data, followed by octree encoding of the result. GOES satellite data allow the cloud surface to be depicted, in white. Doppler radar data show rain (echo) intensity, which is color-coded. Data are from 24 July 1987 during the Convection Initiation and Downburst Experiment.

Human Factors Effects On Information Extraction and Visualization

Human factors effects on information extraction and interpretation were studied with the help of a prototype weather analysis computer workstation developed by NOAA / Forecast Systems Laboratory (formerly PROFS). This study examined the influence of user interface format on the accessibility of the system and the ability to interpret output from the system as a function of the number of output fields displayed and the use of color. The single, full-screen window user interface employed by that system was found to be quite effective for providing access to the system with minimal training. The ability of users to interpret the information displayed as output sometimes was degraded by the sheer volume of information that could be displayed on the workstation terminal. Appropriate use of color tended to mitigate that problem.

3. PUBLICATIONS

3.1 Journal Articles

3.2 Ph.D. Dissertations

3.3 M.S. Theses

3.1 JOURNAL ARTICLES

876 JOURNAL OF ATMOSPHERIC AND OCEANIC TECHNOLOGY VOLUME 7

High-Spectral Resolution Lidar Measurement of Tropospheric Backscatter Ratio Using Barium Atomic Blocking Filters

R. J. ALVAREZ II, L. M. CALDWELL, Y. H. LI, D. A. KRUEGER AND C. Y. SHE

Physics Department, Colorado State University, Fort Collins, Colorado

(Manuscript received 21 February 1990, in final form 13 July 1990)

ABSTRACT

Initial measurements of the aerosol backscatter ratio using a new atomic barium filter (FWHM from 2.0–3.0 GHz at 553.7 nm) in conjunction with a narrowband-pulsed dye laser system are reported. Using analog detection and a 0.2 m diameter receiving telescope, variations of about 10 percent are obtained over a range of 0.25–2.0 km with 30 m resolution within two minutes. Dense regions of aerosols (e.g., clouds) as thin as 10 m and at ranges of up to 6.5 km have been observed in the backscattered signal. Under appropriate climate conditions, sequential measurements of backscatter ratio profiles can be used to follow cloud dispersal dynamics. Techniques for improving accuracy and the potential of using this technique for measuring temperatures throughout the troposphere are discussed.

1. Introduction

Measurement of aerosol optical properties is of considerable importance to the study of atmosphere. For example, the distribution of the optical extinction coefficient is needed for assessing the earth's radiation budget as well as for monitoring air pollution. To measure the vertical distribution of aerosol optical properties by means of Rayleigh–Mie scattering, molecular and aerosol contributions to the lidar return must be disentangled and determined separately. Both Rayleigh (molecular) and Mie (aerosol) scattering are quasi-elastic and are contained, respectively, within a band of approximately 2 GHz and 10 MHz. To sort out, spectrally, aerosol scattering from molecular scattering requires the use of a high-spectral-resolution lidar (HSRL) consisting of a narrowband laser system and a narrowband blocking filter. When this is done, a profile of atmospheric backscatter ratio can be measured by Rayleigh–Mie lidar and the optical properties of atmospheric aerosols can be assessed quantitatively. Using a Fabry–Perot polyetalon interferometer, Eloranta and his colleagues (Shipley et al. 1983; Sroga et al. 1983) have successfully separated scattered light from the atmosphere into a Doppler-broadened molecular channel and an elastically scattered aerosol channel for the determination of backscatter ratio profiles. The performance of a Fabry–Perot polyetalon interferometer depends upon optical alignment, which is difficult, as well as on the optical quality of the interferometer. Because a Fabry–Perot interferometer is a linear device, the molecular channel of their instrument can reject aerosol scattering only partially and the cross talk between the two channels must be dealt with by an inversion analysis. Despite these difficulties and complications, they have continued to perform exciting studies on the optical properties of aerosols and cirrus clouds (Grund and Eloranta 1988).

In order to reject aerosol scattering more effectively, the use of atomic resonance blocking filters for HSRL applications is proposed (Shimizu et al. 1983). The proposed system is expected to improve the backscatter ratio measurements and may allow the much more demanding atmospheric temperature measurements (Schwiesow and Lading 1981). We have developed a barium vapor filter whose blocking bandwidth may be varied by adjusting its temperature. Using such a filter in a recent laboratory experiment with a single-frequency cw laser, the feasibility for measuring atmospheric backscatter ratio and atmospheric temperature (Lehmann et al. 1986) was demonstrated. In this article, the first HSRL measurement of atmospheric backscatter ratio profiles using barium atomic resonance blocking filters is reported.

2. Background

Since the backscatter ratio, r, is defined as the ratio of total backscattering to molecular backscattering (Shimizu et al. 1983; Kobayashi 1987), it can be determined by comparing the total scattering return to the molecular scattering return passing through the blocking filter as:

$$r(z) = [N_t(z)/N_m(z)][\xi_m(z)/\xi_t(z)][f_m/f_0] \quad (1)$$

Corresponding author address: Dr. David A. Krueger, Department of Physics, Colorado State University, Fort Collins, CO 80523.

Reprinted from JOURNAL OF ATMOSPHERIC AND OCEANIC TECHNOLOGY, Vol. 8, No. 5, October 1991
American Meteorological Society

Octree Encoding for Visualization of Atmospheric Conditions and Processes

THOMAS A. BRUBAKER

Department of Electrical Engineering, Colorado State University, Fort Collins, Colorado

RUSSELL J. HUONDER

United States Army Center for Geosciences, Colorado State University, Fort Collins, Colorado

THOMAS H. VONDER HAAR

Department of Atmospheric Science and Cooperative Institute for Research in the Atmosphere, Colorado State University, Fort Collins, Colorado

19 July 1990 and 10 March 1991

ABSTRACT

Meteorological sensors with digital image output have created a need to generate rapid three-dimensional renderings for visualization of atmospheric conditions and processes. This paper describes the use of octree encoding to produce three-dimensional scenes using a digital image as input. The three-dimensional or four-dimensional digital input is composed of pixels with each pixel value represented as a numerical number. The concept is demonstrated using infrared images from the GOES geosynchronous satellite. By relating observed radiance values with atmospheric sounding information, each pixel value is transformed to a height of the cloud in the atmosphere. Subsequent octree encoding and display, with simulated illumination, yields a three-dimensional cloud image. Examples are provided from photographs taken from a DEC VAXStation 8000 image processing system. The octree methodology is suggested as a contribution both to scientific–operational visualization and four-dimensional data assimilation (4DDA).

1. Introduction

The rapid evolution of the graphics-based engineering workstation has resulted in systems that can efficiently produce three-dimensional scenes via computation on geometric models. The models are generated using geometry to approximate actual physical objects or physical phenomena. The geometry engine is the computational heart of the workstation and is programmed to generate model output that is subsequently displayed. The three-dimensional effect is accomplished by using illumination and shading algorithms that are described in graphics textbooks, for example Foley and Van Dam (1984).

The current engineering workstation systems can also be programmed to operate on image data generated by meteorological sensors. The sensors may be active or passive, remote or in situ. Here the image is composed of pixels whose magnitude represents a value of the parameter or process being observed. The pixel resolution is dependent on the sensor. Given the image, one method for generating a three-dimensional surface is to rotate the pixel and use a polygon fit to the surface. Depending on the pixel resolution, the result may or may not provide a smooth three-dimensional rendering. However, smoothness can be enhanced by filtering at the expense of increased computation. The polygon method is again described in computer graphics texts with meteorological examples illustrated by Vonder Haar et al. (1988), Hasler et al. (1985), and others. Carefully note that the polygon approach fits the surface of objects with a loss of internal information unless additional polygon fits are undertaken. An example of a polygon fit and a comparison with octree encoding is given later.

An interesting and useful alternative to the polygon fit is octree encoding of images. Like the polygon method, the octree approach allows the surface of an object to be visualized and, in addition, the octree approach allows the interior of an object to be viewed by peeling and/or slicing layers. This is due to the fact that octree encoding maintains all of the internal organization of three-dimensional datasets.

Corresponding author address: Dr. Thomas A. Brubaker, Cooperative Institute for Research in the Atmosphere, Colorado State University, Foothills Campus, Fort Collins, CO 80523.

Reprinted from JOURNAL OF APPLIED METEOROLOGY, Vol. 30, No. 6, June 1991
American Meteorological Society

Multiparameter Radar and Aircraft Study of Raindrop Spectral Evolution in Warm-based Clouds

V. N. BRINGI

Colorado State University, Fort Collins, Colorado

D. A. BURROWS

University of North Dakota, Grand Forks, North Dakota

S. M. MENON

Colorado State University, Fort Collins, Colorado

(Manuscript received 17 July 1990, in final form 5 December 1990)

ABSTRACT

Radar measurements of reflectivity, differential reflectivity, and X-band (3-cm wavelength) specific attenuation are used to infer some microphysical characteristics of warm-based convective clouds with emphasis on raindrop spectral evolution. The case study of 22 July 1986, during the Cooperative Huntsville Meteorological Experiment, was chosen for analysis. This day was characterized by multicellular storm types; one such multicell configuration was repeatedly penetrated by the University of North Dakota Citation aircraft equipped with cloud physics instrumentation. Radar data acquisition was coordinated with aircraft penetrations made at a constant pressure altitude of 2.7 km enabling a detailed interpretation of differential reflectivity in terms of mean raindrop size. The evolution of several radar reflectivity cells was studied and certain key microphysical features were identified, notably the evolution of raindrop spectra from a "growth" type to an equilibrium type. Further evidence that positive differential reflectivity columns are centered on regions of updraft is provided. A small hail melting model is used to show that the large observed differential reflectivities near cloud base may be due to substantial raindrop growth occurring during continuous collection of cloud water as the particle melts and descends in moderate updrafts.

1. Introduction

This paper presents an observational study of multiparameter radar and aircraft measurements obtained on 22 July 1986 of the Cooperative Huntsville Meteorological Experiment (COHMEX, see Dodge et al. 1986). The evolution of warm-based clouds forced by a weak convergence boundary were studied using the National Center for Atmospheric Research (NCAR) CP-2 multiparameter radar and the University of North Dakota (UND) Citation aircraft, which was operated at an altitude of 2.7 km MSL or about 10°C. The principal radar measurements analyzed were reflectivity at horizontal polarization (Z_H, dBZ), differential reflectivity (Z_{DR}, dB), and X-band specific attenuation (Ax, dB km^{-1}). The principal aircraft measurements analyzed were vertical air motion, cloud water, and precipitation sizes obtained with two PMS (Particle Measuring Systems, Inc.) probes; i.e., the 1D-precipitation (P) probe and the 2D-cloud (C) probe. The evolution of two radar reflectivity "cells" were studied for a period of about 25 min. The two cells typically evolved according to the Byers and Braham (1949) model of air-mass-type storms. However, the added capability of Z_{DR} and Ax data enabled the determination of microphysical detail that hitherto has been unavailable.

COHMEX provided the first opportunity to use the CP-2 radar in an environment outside of the High Plains region. A number of studies already conducted with the CP-2 radar during COHMEX clearly show the application of Z_{DR} and Ax data to storm evolution, (Wakimoto and Bringi 1988; Tuttle et al. 1989; Illingworth 1988; Goodman et al. 1988). For example, early echoes (at temperatures warmer than 0°C) with low reflectivity and unusually large Z_{DR} values were interpreted as precipitation developing via the "warm" rain process, (Caylor and Illingworth 1987). With increased updrafts the formation of the so-called positive Z_{DR} columns have been frequently noted. Such columns are regions of positive Z_{DR} (typically 1 dB or larger), which extend 1 to 2 km above the 0°C level. Near the top of this column—i.e., in the transition region between liquid and ice hydrometeors—an Ax core (>1

Corresponding author address: Dr. V. N. Bringi, Dept. of Electrical Engineering, Colorado State University, Fort Collins, CO 80523.

Reprinted from JOURNAL OF ATMOSPHERIC AND OCEANIC TECHNOLOGY, Vol. 7, No. 6, December 1990
American Meteorological Society

An Examination of Propagation Effects in Rainfall on Radar Measurements at Microwave Frequencies

V. N. BRINGI

Colorado State University, Fort Collins, Colorado

V. CHANDRASEKAR

University of Alabama in Huntsville, Huntsville, Alabama

N. BALAKRISHNAN* AND D. S. ZRNIĆ

NOAA/ERL, National Severe Storms Laboratory, Norman, Oklahoma

(Manuscript received 10 January 1990, in final form 19 June 1990)

ABSTRACT

Propagation effects in rainfall are examined at three microwave frequencies corresponding to S (3.0 GHz), C (5.5 GHz), and X (10.0 GHz) bands. Attenuation at horizontal polarization, as well as differential attenuation and differential propagation phase between horizontal (H) and vertical (V) polarizations are considered. It is shown that at the three frequencies both attenuation and differential attenuation are nearly linearly related to differential propagation phase (ϕ_{DP}). This is shown through simulation using (a) gamma raindrop size distributions (RSD) with three parameters (N_0, D_0, m) that are varied over a very wide range representing a variety of rainfall types, and (b) measured raindrop size distributions at a single location using a disdrometer. Measurements of X-band specific attenuation and S-band specific differential phase in convective rainshafts using the National Center for Atmospheric Research CP-2 radar are presented in order to experimentally demonstrate the linear relationship between attenuation and differential propagation phase. Correction procedures for reflectivity and differential reflectivity (Z_{DR}) are developed assuming that differential propagation phase is measured using a radar that alternately transmits H and V polarized waves with copolar reception through the same receiver and processor system. The correction procedures are not dependent on the actual rainrate profile between the radar and the range location of interest. The accuracy of the procedure depends on, (a) RSD fluctuations, (b) variability in the estimate of differential propagation phase due to measurement fluctuations, and (c) nonzero values of the backscatter differential phase (δ) between H and V polarizations. Simulations are used to gauge the accuracy of correction procedures at S- and C-bands assuming δ is negligible. The correction accuracy for attentuation at S-band is estimated to be $\sim$0.05 dB while at C-band it is estimated to be within 1 dB if $\phi_{DP} \leq 60°$. Simulations further indicate that C-band differential attenuations effects can be corrected to within $\sim$35% of the mean value.

1. Introduction

Radars that operate at higher frequencies such as C- or X-band offer the advantage of lower cost resulting from smaller antenna size compared to S-band radars having the same spatial resolution. Also, higher frequencies are preferred, since the power returned by atmospheric scatterers is inversely proportional to the fourth power of the wavelength (Doviak and Zrnić 1984). However, the resulting gain in sensitivity and spatial resolution is vastly offset by attenuating precipitation. Quantitative interpretation of echo powers at higher frequencies requires correction for this attenuation.

Hitschfeld and Bordan (1954) showed that an indirect estimate of the specific attenuation A (attenuation in dB over 1 km distance), due to the scatterers can be obtained using empirical relationships such as Z–R (between the reflectivity factor Z and rain rate R) and A–R (between attenuation constant, A and R). In their scheme, the correction for the attenuation of the power received from the nth range location is done using the reflectivity measurements made at all the preceding $(n-1)$ range locations. The attenuation correction is first invoked for the range location nearest to the radar and then at successive range locations. Hitschfeld and Bordan also demonstrated that at 3 cm

* NRC/NOAA Research Associate.
Permanent affiliation: Department of Aerospace Engineering, Indian Institute of Science, Bangalore 560012, India.

Corresponding author address: Dr. V. N. Bringi, Department of Electrical Engineering, Colorado State University, Fort Collins, CO 80523.

POLARIMETRIC RADAR MEASUREMENTS IN CONVECTIVE STORMS

V. N. Bringi, V. Chandrasekar and Y. Golestani
Department of Electrical Engineering
Colorado State University
Fort Collins, CO 80523, USA

ABSTRACT. The National Center for Atmospheric Research (NCAR) CP-2 radar is capable of simultaneously measuring dual-polarized, dual-frequency (S/X bands) and Doppler parameters. From these measurements it is possible to deduce differential reflectivity (Z_{DR}), one-way X-band specific attenuation (dB km^{-1}) and X-band linear depolarization ratio (LDR). The evolution of these parameters is depicted as a time sequence of vertical cross sections through a severe storm during its early, mature and strong downdraft stages. In 1987, a time series collection capability was added to the CP-2 radar permitting calculations of the differential propagation phase and the cross-correlation between H and V-polarized signals. Examples of range profiles of these variables are shown through convective rainshafts, and also as vertical cross sections through convective rain shafts.

1. INTRODUCTION

Polarimetric techniques are currently at the forefront of radar remote sensing of storm microphysics. The technology and techniques of radar polarimetry have recently been reviewed by Bringi and Hendry (1990) who also provide a detailed listing of the characteristics of 21 meteorological radars which have varying degrees of polarimetric capability. A history of radar polarimetry in meteorology is provided by Seliga and Humphries (1990) while applications to cloud physics, and precipitation measurement have been provided by Jameson and Johnson (1990), and Joss and Waldvogel (1990), respectively.

Polarimetric techniques are based on the following microphysical characteristics of the hydrometeors which fill the radar resolution volume, (i) the particle size distribution which includes parameters such as concentration, mean size, and maximum size, (ii) the particle shape distribution which includes parameters such as mean and variance of shapes, as well as any relation between mean shape and size (as exists for raindrops), (iii) the particle orientation (canting angle) distribution, and (iv) the particle refractive index which depends on temperature, radar frequency, density and particle composition (if inhomogeneous). Except for raindrops, the important microphysical characteristics listed above are not known with any degree of certainty

W.-M. Boerner et al. (eds.), Direct and Inverse Methods in Radar Polarimetry, Part 2, 1749–1778.

'olarimetric radar signatures of precipitation t S- and C-bands

of. V.N. Bringi, PhD
Chandrasekar, PhD
Meischner, PhD
Hubbert, MS
Golestani, PhD

lexing terms: Radar, Polarimetry, Propagation

Abstr:ct: Polarimetric radar measurements in precipitation at S- and C-band frequencies are considered. Time series data were obtained from three advanced radars: the National Center for Atmospheric Research (NCAR) CP-2 radar, the National Severe Storms Laboratory's (NSSL) Cimarron radar, and the C-band Poldirad radar operated by the German Aerospace Research Establishment (DLR). Measurements of radar reflectivity, differential reflectivity Z_{DR}, differential propagation phase ϕ_{DP}, and the crosscorrelation between horizontal and vertical polarised waves are derived from time series data in rain, rain mixed with ice, and in the stratiform ice phase of convective storms. Raindrops are modelled as oblate in shape with a gamma form for their size distribution. The gamma parameters (N_o, D_o, m) are varied over an entire range encompassing a wide variety of rainfall types. The radar rain measurements are shown to be in good general agreement with the model rain simulations. By combining Z_{DR} and ϕ_{DP} it is possible to identify regions of mixed particle types, e.g. raindrops and hail, or ice crystals and snowflakes. The differential phase upon backscatter may be identified by examining the range profile of ϕ_{DP}, giving additional clues as to the type and size of particles responsible for the backscatter.

Introduction

th the recent advent of sophisticated, polarimetric-ed clutter characterisation methods, it is important to asure and model effectively the polarimetric back-tter and propagation effects of rainfall at typical crowave frequencies [1]. The raindrop size distribution SD) is governed by microphysical, thermodynamic and amical factors present in cloud systems. The RSD ically varies over orders of magnitudes both temporally and spatially; for example, spatial variability is found in the interior of cumulo-nimbus clouds and the stratiform anvil regions of large storm systems. It is also well known that microwave/millimetre waves are significantly affected by rainfall, and the extent of attenuation, for example, suffered by electromagnetic waves depends on the RSD and its variability in space and time. The rain medium also introduces significant differential attenuation and differential phase shift between the principal polarisation states (namely, horizontal (H) and vertical (V) polarisations) because the raindrops are oblate spheroidal in shape with a high degree of preferred orientation of their symmetry axis along the vertical direction. Additionally, the larger raindrops are uniformly more oblate than the smaller ones. A good review of these properties can be found in Reference 2. While a substantial body of literature exists on the propagation aspects of microwave/millimetre waves through rainfaill, detailed modelling and experiments for different polarisation states is currently not available.

The use of advanced meteorological radars to characterise precipitation has reached a rather high level of sophistication only recently. The pioneering studies of McCormick, Hendry and their associates at the National Research Council of Canada have established the basis of polarimetric techniques, both for backscatter as well as forward scatter (propagation), using circular polarisation [3–6]. They have reported measurements of differential attenuaton and differential phase shift in rain at K-, X- and S-bands, using the range profile of W/W_2 were W is the complex crosscovariance between the co- and cross-polar (simultaneously) received signals and W_2 is the conventional reflectivity. These studies have been extended [7–9] principally at S-band where differential phase shift is dominant with both absolute and differential attenuation being negligible.

The advent of pulse-to-pulse switching between H and V states and reception of copolar received signals through a single receiver system have advanced the accuracy to which the rain medium can be characterised [10, 11]. In additon, polarimetric techniques have found wide application in the detection of targets in clutter [12–14]. The technology of such polarimetric radar systems for meteorology has been reviewed by Bringi and Hendry [15], who also describe the main characteristics of 21 such radars existing worldwide. In this paper we present data from three advanced radars: the National Center for Atmospheric Research (NCAR) CP-2 radar located in Boulder, Colorado, USA, the National Severe Storm Laboratory's Cimarron radar located in Cimarron, Okla-

er 7822F (E15), first received 3rd July 1989 and in final revised form September 1990

. Bringi, Mr. Hubbert and Dr. Golestani are with the Department lectrical Engineering, Colorado State University, Fort Collins, CO 3, USA

Chandrasekar is with the Department of Electrical Engineering, ersity of Alabama in Huntsville, Huntsville, Alabama 35899, USA

Meischner is with the Institute of Atmospheric Physics, DLR PA, Oberpfaffenhofen, D-8031 Wessling, Federal Republic of nany

Appeared in Radar In Meteorology, Ed. D. Atlas, AMS.

apter 19a

chnology of Polarization Diversity Radars for Meteorology

'. Bringi, Colorado State University
Hendry, National Research Council of Canada*

NTRODUCTION

nventional radars for meteorological measurements te and receive waves of a single fixed polarization. ost invariably, linear polarization is used. Generally, nt-day conventional systems have Doppler capability thus they measure the first three moments of the pler spectrum, the zeroth moment being the usual ra- eflectivity which depends upon the sixth moment of article size distribution (for Rayleigh scatterers) and lesser extent on the thermodynamic phase state (via lielectric constant). Thus three target characteristics, ely the reflectivity and the mean and the spectral width e Doppler spectrum, are measured for each resolution n the volume covered by such a radar. The science technology of Doppler radar measurements are de- ed in the book by Doviak and Zrnić (1984), while l processing techniques are reviewed in this book sarelli and Keeler, Chapter 20a).

contrast to conventional radars, polarization diversity ms provide either for the variation of one or both of ansmitted and received wave polarizations, or provide dual-channel reception of orthogonally polarized s. These radar polarimetric techniques, the subject of review, thus permit the measurement of additional t echo characteristics. For precipitation, these polar- on characteristics are related to the mean values and ibutions of size, shape, and spatial orientation of the cles filling the radar resolution volume, and also to thermodynamic phase state.

e use of circular polarization as a means of suppress- ain clutter in primary detection radars has been widely gnized; see White (1954). Evidence of particle shape ts had been obtained experimentally in the years -53 from observations with a linear depolarization (LDR) radar (Browne and Robinson, 1952) and with -channel circularly polarized radars (Hunter, 1954; et al., 1963). A notable early contribution was that ewell et al. (1957). For a review of the early history olarimetric radar techniques, see Seliga et al., Chapter These early results were limited by the relatively poor rization characteristics of the radar used. With the ication of numerous theoretical papers on scattering, such as those of Atlas et al. (1953) and Stevenson (1953), the necessity of constructing CDR and LDR radars with significantly better performance was evident if microphysical shape effects were to be determined without the contaminating effects of polarization impurities. This need for high performance was the factor that initiated the design of improved polarization diversity radar systems by the National Research Council of Canada for use in Alberta and at Ottawa.

While the initial goal was to obtain improved measurements of CDR from which drop oblateness could be determined, provision for measurements of relative phase and coherency in dual-channel circularly polarized systems were also incorporated into the 1.8-cm NRC radar at Ottawa and the Alberta Research Council 10-cm radar in the late 1960s. These additional capabilities were for the purposes of determining the extent to which precipitation particles have a common alignment, and for measuring their mean orientation angle.

Using the fact that raindrop oblateness is related to size, and that the drops are highly oriented, Seliga and Bringi (1976) showed on theoretical grounds that the median volume diameter (of an assumed exponential drop-size distribution) could be related to Z_{DR}. They also proposed a scheme whereby Z_{DR} could be measured by switching the transmitted polarization state between horizontal (H) and vertical (V) states on a pulse-to-pulse basis and receiving the copolar signal via the same receiver and processor chain. The fact that Z_{DR} could be measured in rainfall and in the range predicted by theory was first shown conclusively using data from the Illinois State Water Survey's CHILL radar (Seliga et al., 1979), which used sequential block switching between H and V states rather than pulse-to-pulse switching.

Following the theoretical work of Seliga and Bringi (1976), the group at the Appleton Laboratory (now called the Rutherford Appleton Laboratory) in the United Kingdom went forward with building a fast polarization switch which could switch the polarization state of the transmitted wave on a pulse-to-pulse basis. Time series data analysis showed that the standard error in Z_{DR} could be reduced to the 0.1–0.2 dB level (Bringi et al., 1978). In fact, this level of accuracy was assumed by Seliga and Bringi (1976) to predict the level of improvement in rainfall estimates that could be achieved by combining Z_H and Z_{DR}. Further mea

tired.

Reprinted from JOURNAL OF ATMOSPHERIC AND OCEANIC TECHNOLOGY, Vol. 8, No. 5, October 1991
American Meteorological Society

Octree Encoding for Visualization of Atmospheric Conditions and Processes

THOMAS A. BRUBAKER

Department of Electrical Engineering, Colorado State University, Fort Collins, Colorado

RUSSELL J. HUONDER

United States Army Center for Geosciences, Colorado State University, Fort Collins, Colorado

THOMAS H. VONDER HAAR

Department of Atmospheric Science and Cooperative Institute for Research in the Atmosphere, Colorado State University, Fort Collins, Colorado

19 July 1990 and 10 March 1991

ABSTRACT

Meteorological sensors with digital image output have created a need to generate rapid three-dimensional renderings for visualization of atmospheric conditions and processes. This paper describes the use of octree encoding to produce three-dimensional scenes using a digital image as input. The three-dimensional or four-dimensional digital input is composed of pixels with each pixel value represented as a numerical number. The concept is demonstrated using infrared images from the GOES geosynchronous satellite. By relating observed radiance values with atmospheric sounding information, each pixel value is transformed to a height of the cloud in the atmosphere. Subsequent octree encoding and display, with simulated illumination, yields a three-dimensional cloud image. Examples are provided from photographs taken from a DEC VAXStation 8000 image processing system. The octree methodology is suggested as a contribution both to scientific–operational visualization and four-dimensional data assimilation (4DDA).

1. Introduction

The rapid evolution of the graphics-based engineering workstation has resulted in systems that can efficiently produce three-dimensional scenes via computation on geometric models. The models are generated using geometry to approximate actual physical objects or physical phenomena. The geometry engine is the computational heart of the workstation and is programmed to generate model output that is subsequently displayed. The three-dimensional effect is accomplished by using illumination and shading algorithms that are described in graphics textbooks, for example Foley and Van Dam (1984).

The current engineering workstation systems can also be programmed to operate on image data generated by meteorological sensors. The sensors may be active or passive, remote or in situ. Here the image is composed of pixels whose magnitude represents a value of the parameter or process being observed. The pixel resolution is dependent on the sensor. Given the image, one method for generating a three-dimensional surface is to rotate the pixel and use a polygon fit to the surface. Depending on the pixel resolution, the result may or may not provide a smooth three-dimensional rendering. However, smoothness can be enhanced by filtering at the expense of increased computation. The polygon method is again described in computer graphics texts with meteorological examples illustrated by Vonder Haar et al. (1988), Hasler et al. (1985), and others. Carefully note that the polygon approach fits the surface of objects with a loss of internal information unless additional polygon fits are undertaken. An example of a polygon fit and a comparison with octree encoding is given later.

An interesting and useful alternative to the polygon fit is octree encoding of images. Like the polygon method, the octree approach allows the surface of an object to be visualized and, in addition, the octree approach allows the interior of an object to be viewed by peeling and/or slicing layers. This is due to the fact that octree encoding maintains all of the internal organization of three-dimensional datasets.

Corresponding author address: Dr. Thomas A. Brubaker, Cooperative Institute for Research in the Atmosphere, Colorado State University, Foothills Campus, Fort Collins, CO 80523.

Reprinted from JOURNAL OF ATMOSPHERIC AND OCEANIC TECHNOLOGY, Vol. 5, No. 6, December 1988
American Meteorological Society

Error Structure of Multiparameter Radar and Surface Measurements of Rainfall Part I: Differential Reflectivity

V. CHANDRASEKAR AND V. N. BRINGI

Department of Electrical Engineering, Colorado State University, Ft. Collins, Colorado

(Manuscript received 26 June 1987, in final form 4 April 1988)

ABSTRACT

Fluctuations in the radar measurements of Z_{DR} are due to both signal power fluctuations and the cross-correlation between the horizontal and vertical polarized signals. In Part I of this study, these signals are simulated for an S-band radar for backscatter from rain media, which is characterized by a gamma model of the raindrop size distribution (RSD). The parameters N_0, D_0, m of the gamma RSD are then varied over the entire range found in natural rainfall. Thus, the radar simulations contain the effects of both statistical fluctuations and physical variations. We also simulate sampling of raindrops by disdrometer. The sampling errors are related to the Poisson statistics of the total number of drops in the fixed sample volume and to the statistics that govern the gamma distribution of drops as a function of size. We simulate disdrometer RSD samples over the entire range of N_0, D_0, m values found in rainfall, so that the effects of statistical fluctuations and physical variations are introduced.

It is shown that Z_{DR}, computed from disdrometer RSD samples, is correlated with Z and with other moments of the RSD when the same disdrometer data is used. This correlation is purely statistical and is independent of the physical correlation. We use the radar and disdrometer simulations to intercompare the rain rate as derived by the radar Z_{DR}-method with the rain rate estimated by the disdrometer. Our simulation results are used to explain the correlation and error structure of radar/disdrometer-derived rain rate intercomparison data reported in the literature.

1. Introduction

The differential reflectivity (Z_{DR}) technique was first introduced by Seliga and Bringi (1976) to improve the accuracy of radar estimates of rainfall rate over conventional Z–R methods. This improvement is achieved by making two nearly simultaneous measurements of horizontally and vertically polarized reflectivities (Z_H, Z_V) of the rain medium from which differential reflectivity (in decibels) is derived as $Z_{DR} = 10 \log(Z_H/Z_V)$. From Z_H and Z_{DR} two parameters of the raindrop size distribution (RSD) are estimated (Ulbrich and Atlas 1984). Considerable progress has been made by researchers in this respect, and comparative case studies of rainfall rate (R) measurements with Z_{DR} radars and ground-based disdrometers or rain gauges have produced very encouraging results (Bringi et al. 1982; Seliga et al. 1986; Goddard et al. 1982; Goddard and Cherry 1984; and Direskeneli et al. 1986).

Even though researchers have achieved improvements by using Z_{DR}-based rain rate estimates rather than estimates using reflectivity (Z) alone, however, the actual degree of improvement is not conclusive and is still being debated. Goddard and Cherry (1984), for example, concluded that they obtained an improvement using the Z_{DR}-method rather than Z–R relations. Based on disdrometer data, they obtained a reduction in the standard error of R using the Z_{DR} method to 14% from the 33% obtained using the Z–R relationship. Similar results using radar measurements of Z and Z_{DR} resulted in a reduction in the standard deviation to only 32% from the 40% obtained using Z–R relations. Ulbrich and Atlas (1984) analyzed a large number of disdrometer-based RSD samples (moderate-to-high rain rates) and showed that Z_{DR} methods could theoretically decrease the standard error in rain rate estimates to 14% from the 30% to 50% standard error associated with Z–R relations. Direskeneli et al. (1986) used radar data to show that the Z_{DR}-method improved rain rate estimates by reducing the standard error to 31% from the 40% obtained using a local Z–R relationship. A cursory inspection of these results would appear to imply that the Z_{DR} method did not perform significantly "better" than Z–R relations, at least not to the extent shown by Ulbrich and Atlas (1984). Since fluctuations in the radar and surface (e.g., disdrometer) observations of rainfall are governed by two totally different stochastic processes, the fluctuations and mutual correlations in these processes must be considered before firm conclusions can be drawn.

Corresponding author address: Dr. V. N. Bringi, Dept. of Electrical Engineering, Colorado State University, Ft. Collins, CO 80523.

Error Structure of Multiparameter Radar and Surface Measurements of Rainfall Part II: X-Band Attenuation

V. CHANDRASEKAR AND V. N. BRINGI

Department of Electrical Engineering, Colorado State University, Ft. Collins, Colorado

(Manuscript received 26 June 1987, in final form 4 April 1988)

ABSTRACT

In Part II of this study, simulations of multiparameter radar observables to include X-band specific attenuation (A) are performed in order to study the relationship between A, Z, and Z_{DR}. We also compute the triplet (A, Z, Z_{DR}) from simulations of disdrometer raindrop spectra. As in Part I, our simulations include the fluctuations due to both measurement errors and physical variations of the gamma raindrop spectra parameters (N_0, D_0, m). We examine the correlation between (A/Z) and Z_{DR} derived from both disdrometer and radar simulations, and show that the disdrometer-based data yields a negative correlation (~ -0.9) between (A/Z) and Z_{DR}, whereas for radar data the correlation ≈ 0. We emphasize that these correlations are due only to measurement fluctuations and not to physical variations. The large magnitude for the negative correlation compresses the scatter in plots of (A/Z) versus Z_{DR} based on disdrometer RSD samples, whereas the same scatter plots using multiparameter radar data show very large scatter. We also simulate A, Z and Z_{DR} from three separate disdrometers (all sampling the same gamma RSD) and show that the scatter is more realistic and much larger than when using a single disdrometer.

1. Introduction

Part I of this two-part paper dealt with the error structure of differential reflectivity and surface measurements of rainfall. In this part we continue these studies by focusing on X-band attenuation due to rain and consider the triplet of measurements (A, Z, Z_{DR}) corresponding to specific attenuation (dB km^{-1}), radar reflectivity and differential reflectivity, respectively. The physical basis for attenuation-rainfall relationships has been extensively studied; see, for example, Atlas and Ulbrich (1974, 1977), and the review article by Oguchi (1983), which includes an extensive reference list. More recently, radar measurements of Z and Z_{DR} have been used to predict rain attenuation in the 10–30 GHz range (Goddard and Cherry 1984; Leitao and Watson 1984), while Bringi et al. (1986) have directly intercompared path-averaged X-band attenuation predicted by Z and Z_{DR} (and a gamma raindrop size distribution model) with path averaged X-band attenuation measured by the dual-frequency ratio technique (Eccles and Mueller 1973; Aydin et al. 1983; Tuttle and Rinehart 1983). However, there are only two radars capable of making the triplet of measurements (A, Z, Z_{DR}): the National Center for Atmospheric Research CP-2 radar and the Illinois State Water Survey CHILL radar.

Atlas et al. (1984) have computed the triplet (A, Z, Z_{DR}) from raindrop size distribution (RSD) samples obtained from momentum disdrometers (Joss and Waldvogel 1969), and show scatter plots of rain rates derived using multiparameter methods, e.g., (Z, A), (Z, Z_{DR}) or (A, Z, Z_{DR}) versus disdrometer measured rain rates. Their "simulations" of radar observables showed that the absolute average deviation (AAD) between multiparameter-deduced rain rates and "actual" rain rates could be made extremely small ($\leq 5\%$) and much less than single-parameter methods (e.g., $Z-R$ relations) that gave AADs of $\sim 30\%$. In this paper, using analytical techniques and simulations, we examine the relationship between A, Z, and Z_{DR} as measured by radar and as computed from disdrometer RSD samples. As explained in Part I, it is our intent to simulate the fluctuations in the observables so that both statistical and physical variations can be included.

Figure 1a shows a scatter plot of A/Z versus Z_{DR} computed from disdrometer RSD samples by Aydin et al. (1983). The scatter in Fig. 1a is very small and clearly shows the mean relationship between A/Z and Z_{DR}. Figure 1b shows CP-2 radar measurements from convective rainshafts taken on 13 June 1984 near Boulder, Colorado; see Bringi et al. (1986) for details regarding these measurements. In Fig. 1b, the dual-frequency algorithm developed by Tuttle and Rinehart (1983) is used to estimate path-averaged X-band specific attenuation. Figure 1b shows the scatter plot of A/Z versus Z_{DR}, where each observable is obtained from radar data. Clearly the scatter in Fig. 1b is much larger than in Fig. 1a, and it is desirable to understand

Corresponding author address: Dr. V. N. Bringi, Dept. of Electrical Engineering, Colorado State University, Ft. Collins, CO 80523.

Reprinted from JOURNAL OF ATMOSPHERIC AND OCEANIC TECHNOLOGY, Vol. 7, No. 5, October 1990
American Meteorological Society

Error Structure of Multiparameter Radar and Surface Measurements of Rainfall. Part III: Specific Differential Phase

V. CHANDRASEKAR

University of Alabama in Huntsville, Huntsville, Alabama

V. N. BRINGI

Colorado State University, Fort Collins, Colorado

N. BALAKRISHNAN* AND D. S. ZRNIĆ

NOAA/ERL, National Severe Storms Laboratory, Norman, Oklahoma

(Manuscript received 18 September 1989, in final form 21 February 1990)

ABSTRACT

Parts I and II of this three part paper dealt with the error structure of differential reflectivity and X-band specific attenuation in rainfall as estimated by radar and surface disdrometers. In this Part III paper we focus on the error structure of the specific differential phase (K_{DP}, °km^{-1}) measurement in rainfall. This allows us to analyze three estimators of rainfall rate, the first based on the reflectivity factor Z_H, the second based on combining reflectivity and Z_{DR}, $[R(Z_H, Z_{DR})]$, and the third based on K_{DP} alone, $R(K_{DP})$. Simulations are used to model random errors in Z_H, Z_{DR} and K_{DP}. Physical variations in the raindrop size distribution (RSD) are modeled by varying the gamma parameters (N_0, D_0, m) over a range typically found in natural rainfall. Thus, our simulations incorporate physical fluctuations onto which random measurement errors have been superimposed. Radar-derived estimates of $R(Z_H, Z_{DR})$ and $R(K_{DP})$ have been intercompared using data obtained in convective rainfall with the NSSL Cimarron radar and the NCAR/CP-2 radar. As practical application of the analysis presented here, we have determined the range of applicability of the three rainfall rate estimators: $R(Z_H)$, $R(Z_H, Z_{DR})$ and $R(K_{DP})$. Our simulations show that when the rainfall rate exceeds about 70 mm h^{-1}, $R(K_{DP})$ performs better than $R(Z_H, Z_{DR})$. This result is valid over a 1 km propagation path. At intermediate rainfall rates around $20 \leq R \leq 70$ mm h^{-1}, our simulations show that $R(Z_H, Z_{DR})$ gives the least error. However, there are other reasons which make $R(K_{DP})$ useful; i.e., (i) its stability with respect to mixed phase precipitation, and (ii) the fact that it is a differential phase measurement and thus insensitive to system gain calibration. This last premise suggests an accurate method of system gain calibration based on the rain medium.

I. Introduction

Application of polarimetric techniques to the remote measurement of rainfall rate (R) is an area of continuing importance. Conventional techniques based on Z–R relations are known to introduce considerable errors when small time (~3 min) and space scales (~1 km) are considered, e.g., convective rainfall scales. In this Part III paper we discuss errors in the estimation of R using the specific differential phase measurement, i.e., the measurement that is proportional to the real part of the difference in the complex forward scatter amplitudes at horizontal (H) and vertical (V) polarizations. Seliga and Bringi (1978) first proposed that the differential propagation phase measurement could be used to determine rainfall rate, in a manner similar to that using differential reflectivity (Z_{DR}). They assumed that the differential propagation phase (ϕ_{DP}) could be measured using "fast" pulse-to-pulse switching between H and V states with corresponding copolar reception through the same receiver and processor. Mueller (1984) proposed algorithms for estimating ϕ_{DP}, one of which was analyzed by Sachidananda and Zrnić (1986) and shown to yield standard errors of about 1°–2° using 64 H and 64 V samples. Furthermore, Sachidananda and Zrnić (1989) devised a scheme to correct the ambiguities inherent in this measurement and developed formulas for simultaneously estimating Doppler spectral moments with minimum error. Jameson (1985) and Jameson and Mueller (1985) discussed the microphysical interpretation of ϕ_{DP} in rainfall assuming Rayleigh scattering (S-band

* NRC/NOAA Research Associate; permanent affiliation with Department of Aerospace Engineering, Indian Institute of Science, Bangalore 560012, India.

Corresponding author address: Dr. V. N. Bringi, Department of Electrical Engineering, Colorado State University, Fort Collins, CO 80523.

Reprinted from JOURNAL OF ATMOSPHERIC AND OCEANIC TECHNOLOGY, Vol. 6, No. 4, August 1989
American Meteorological Society

Efficient Differential Reflectivity Processing Using Logarithmic Receivers

V. CHANDRASEKAR AND V. N. BRINGI

Department of Electrical Engineering, Colorado State University, Fort Collins, Colorado

G. R. GRAY AND R. J. KEELER

National Center for Atmospheric Research, Field Observing Facility, Boulder, Colorado*

(Manuscript received 19 February 1988, in final form 2 January 1989)

ABSTRACT

The differential reflectivity (Z_{DR}) measurement introduced by Seliga and Bringi has shown potential for extending cloud microphysical studies and improving rainfall rate measurement. The sensitivity of Z_{DR} measurement requires it to be estimated with a high degree of accuracy. Our theoretical analysis and experimental observations show that the estimates of Z_{DR} using log ratio estimators typically have twice the standard error compared to those from square law estimators. A "lookup table technique" which converts the log value to the equivalent square law value prior to integration is proposed to improve the accuracy of Z_{DR} estimates from logarithmic receivers. The size of the lookup table dictates the accuracy of the resulting Z_{DR} estimate. Experimental observations demonstrate that the log receiver lookup table technique estimates Z_{DR} to an accuracy nearly the same as that from a square law receiver. We present the implementation of this technique in integer arithmetic applied to the NCAR CP-2 radar.

1. Introduction

The differential reflectivity (Z_{DR}) measurement proposed by Seliga and Bringi (1976) has shown great potential in improving the accuracy of rain rate estimation and remote hydrometeor identification, such as hail detection. Many meteorological radars with dual linear polarization capability have been operated since the introduction of Z_{DR}. Because of the sensitivity of the Z_{DR} signal for rainfall rate measurement and other related observations, it is desirable to estimate Z_{DR} with accuracy of about 0.2 dB. This accuracy is dictated by the statistical properties of Z_{DR} signal that are controlled by Doppler spectra, length of integration time, cross-correlation between the horizontally and vertically polarized signals, and the type of processing algorithm used, among other things. Two different estimators are typically used. The square law estimator of Z_{DR} is given by $10 \log(\langle P_H \rangle / \langle P_V \rangle)$ and the log ratio estimator of Z_{DR} is given by $\langle 10 \log P_H \rangle - \langle 10 \log P_V \rangle$. P_H and P_V are the received powers at horizontal (H) and vertical (V) polarizations respectively, and the angle brackets denote sample averages. Bringi et al. (1983) discuss the statistical properties of differential reflectivity and compare these two estimators of Z_{DR}. Their analysis is based on independent samples and shows that both the log ratio and the square law are two useful estimators with the square law estimator having the smallest standard error for Z_{DR} measurements. The log ratio estimator is more easily implemented with a conventional logarithmic receiver. In practice the successive copolar measurements of H and V pairs are not independent but have significant correlation between them.

Bringi et al. (1983) show for independent samples that the standard deviation of Z_{DR} from a log ratio estimator is roughly twice that obtained from the square law estimator. Sachidananda and Zrnić (1985) have analyzed correlated samples from a square law receiver and show that Z_{DR} can be estimated to an accuracy of typically 0.15 dB. In appendix A we obtain a similar value for correlated samples from a log receiver.

Appendix A and the included figures show the standard deviation in Z_{DR} (dB) obtained from the log ratio estimator as a function of number of sample pairs. Comparing these data with similar results from Sachidananda and Zrnić (1985) shows that the standard deviation in Z_{DR} obtained from the log ratio estimator is approximately twice that obtained using the square law estimator. Figure 1 shows the measured standard deviation of Z_{DR} estimates obtained using the square law and log ratio estimator on time series data from the NCAR CP-2 radar observing rain. The standard deviation of Z_{DR} estimates from the log ratio estimator

* NCAR is sponsored by the National Science Foundation.

Corresponding author address: Dr. R. Jeffrey Keeler, National Center for Atmospheric Research, P.O. Box 3000, Boulder, CO 80307-3000.

Reprinted from JOURNAL OF ATMOSPHERIC AND OCEANIC TECHNOLOGY, Vol. 7, No. 2, April 1990
American Meteorological Society

Fourier and Moment Methods Applied to Two-Dimensional Raindrop Images

V. CHANDRASEKAR

University of Alabama in Huntsville, Huntsville, Alabama

Y. GOLESTANI, J. TURK AND V. N. BRINGI

Colorado State University, Fort Collins, Colorado

(Manuscript received 13 February 1989, in final form 4 September 1989)

ABSTRACT

Two-dimensional PMS precipitation probes mounted with horizontal optical axis have been previously used to study the shapes of hydrometeors such as raindrops and graupel. Fourier and moment descriptors have been applied to such images for the purposes of parameter estimation (axis ratio, canting angle) of raindrops, and for classifying raindrops in a raindrop/graupel mixture. Simulations have been used to evaluate these techniques. Our results show that axis ratios of raindrops can be accurately estimated using both Fourier and moment methods. We also show that the canting angle of the raindrop image can be accurately estimated using the moment method. Two image classification techniques were applied to data from below the melting level in a convective storm for classifying raindrops and graupel. The potential usefulness of such techniques is demonstrated in this paper.

1. Introduction

Two-dimensional PMS (Particle Measuring Systems, Inc.) probes are widely used in cloud physics research (Knollenberg 1981). However, the application of advanced image processing techniques for hydrometeor feature extraction and image classification has not found widespread use in the context of 2D-PMS images. Duroure (1982) used the method of Fourier descriptors (FD) to extract shape discrimination parameters of an image. Rahman et al. (1981a,b) developed classification methods for hydrometeors using statistical pattern recognition techniques. They found that incomplete images were difficult to classify. Chandrasekar et al. (1988, henceforth referred to as CCB) used FD methods to accurately compute axis ratios of raindrops imaged by a 2D probe with optical axis mounted horizontally rather than the conventional vertical orientation. Thus, raindrop images are elliptical rather than circular; the conventional circular images are frequently sized using the "circle-fit" algorithm developed by Cooper (1980). Harris-Hobbs and Cooper (1987) classified raindrops and graupel particles using the circle-fit method; i.e., a circle was fitted to the image perimeter and the variance of the measured data about the fitted circle was used for classification. Cooper et al. (1983) used a variant of this technique on elliptical raindrop images to estimate the canting angle of the image. This was determined by a fit procedure in which an ellipse of fixed axis ratio was allowed to rotate about the image center. The canting angle was taken to be that which led to the minimum sum of squared deviations. Chandrasekar et al. used Fourier descriptors for filtering purposes in order to reduce the quantization noise and other systematic errors in the images. They showed that raindrop axis ratios could be determined with a precision of 0.5%–3% for drops with volume-equivalent spherical diameters (Deq) in the range 2–6 mm. Since raindrops can be modeled as oblate spheroids to high accuracy, estimates of Deq can be obtained from vertically oriented probes (which give circular images) by accounting for the axis ratio of the oblates (Beard et al. 1986).

The advent of polarimetric radar techniques for the classification of hydrometeors using their shape and orientation information is giving new impetus for the application of sophisticated image processing techniques to data obtained with 2D-PMS probes (Bringi and Hendry 1989; Jameson and Johnson 1989). Polarimetric radar techniques need considerable evaluation using in situ measurements, especially in cases where the resolution volume contains mixtures of different particle types; e.g., raindrops and melting ice, ice crystals, and aggregates (Bader et al. 1987). Even though the general image classification problem as shown by Rahman (1981a,b) is difficult, it may be useful at times to narrow the scope of the problem in known meteorological conditions. Indeed, this paper addresses the specific problem of raindrop parameter

Corresponding author address: Dr. V. N. Bringi, Dept. of Electrical Engineering, Colorado State University, Fort Collins, CO 80523.

Multiple Disdrometer Observations of Rainfall

V. CHANDRASEKAR

Colorado State University, Fort Collins, Colorado

ENRICO G. GORI

Institute of Atmospheric Physics, CNR, Rome, Italy

(Manuscript received 17 December 1990, in final form 29 April 1991)

ABSTRACT

Raindrop sampling instruments, such as disdrometers and optical array probes, have been used by researchers to observe raindrop-size distributions. Estimates of raindrop-size distribution (RSD) can be made from these instruments, which can subsequently be used to study several derived parameters such as liquid-water content, rainfall rate, and radar reflectivity. These instruments have limited sampling volume, which affects the estimates of raindrop-size distribution and the derived integral parameters. Although fluctuations in the derived parameters obtained from the same disdrometer samples are correlated, estimates from independent disdrometers are not. This paper addresses the issues involved in comparing data from disdrometers. Data from four disdrometers sampling the same rain volume are analyzed to study the measurement fluctuations in a single disdrometer with time and between disdrometers at the same time interval. Theoretical analysis and data show that the correlation between derived parameters of sampled RSD helps in observing the mean feature between the parameters with much less scatter. It is also shown that the scatter between the derived parameters of a single disdrometer, or between different disdrometers, is a function of the correlation between the estimates.

1. Introduction

Raindrop-size distributions (RSD) can be estimated by using surface instruments like the disdrometer (Joss and Waldvogel 1967) or using probes mounted on instrumented aircraft (Knollenberg 1981). Joss and Gori (1978) have conducted studies combining RSD estimates from many disdrometers in order to observe the influence on mean shape with averaging. Observations of single disdrometer or multiple disdrometer measurements have also been used to study the natural variability of RSD (Gori and Joss 1980; Ulbrich 1983). Comparison of data from different RSD sampling instruments is controlled by several factors, including spatial, temporal, and measurement fluctuations. In this paper we address the issues involved in comparing data between different disdrometers. We consider the mean feature common to the disdrometers as well as the difference between the measurements. We extend this principle of analysis to comparison of derived parameters such as reflectivity Z and rainfall R between disdrometers, in order to interpret the variability between measurements.

The paper is organized as follows. Section 2 describes the RSD model and computation of integral parameters from the RSD estimate. Section 3 provides the theoretical basis for analyzing multiple disdrometer observations. Data collected using four disdrometers sampling the same rainfall are presented in section 4. Section 5 summarizes the results of this paper.

2. Raindrop-size distribution

The space–time variability of raindrop-size distribution (RSD) is typically due to a variety of physical processes, for example, evaporation, collision–coalescence, collisional breakup, inhomogeneities produced by turbulent fluctuations, drop sorting, etc. The RSDs are important in determining characteristics of rain medium such as reflectivity Z, liquid water content W, and rainfall rate R. Ulbrich (1983) showed that a gamma RSD can describe many of the natural variabilities in the RSD. The gamma form of the RSD can be written as

$$N(D) = N_0 D^m \exp(-\Lambda D), \qquad (1)$$

where $N(D)$ is the number of raindrops per unit volume per unit size interval (D to $D + \Delta D$). This distribution can be written in terms of the total number of drops per unit volume (N_T) as

$$N(D) = \frac{N_T}{\Gamma(\alpha)\beta^\alpha} D^{\alpha-1} \exp(-D/\beta), \qquad (2)$$

where $\alpha > 0$, $\beta > 0$, $D \geq 0$. Note that $m = \alpha - 1$,

Corresponding author address: Dr. V. Chandrasekar, Dept. of Electrical Engineering, Colorado State University, Fort Collins, CO 80523.

WATER RESOURCES BULLETIN
VOL. 25, NO. 3 AMERICAN WATER RESOURCES ASSOCIATION JUNE 1989

AN AUTO-CAD-BASED WATERSHED INFORMATION SYSTEM FOR THE HYDROLOGIC MODEL HEC-1[1]

T. J. Cline, A. Molinas, and P. Y. Julien[2]

ABSTRACT: A micro computer based Watershed Information System (W.I.S.) is developed to assist in the preparation of input files for the hydrologic simulation model HEC-1. This system consists of three phases. Phase I utilizes the capabilities of AutoCAD version 9 and three programs, BASINS, PLANES, and CHANNELS, to extract, organize, and display watershed data. Phase II uses the program CN to calculate some HEC-1 parameter values. Phase II utilizes the program HECUPDATE to create HEC-1 input files. The system input includes topographic, soils, land use, watershed geometry data, and a skeletal HEC-1 input file. Output from the system includes a summary User Reference File, a Soils File, a Land Use File, a Watershed Geometry File, a Curve Number File, and a HEC-1 input file, which is ready to run. The W.I.S. has been applied to Macks Creek Watershed in southwest Idaho.
(KEY TERMS: hydrologic modeling; watershed information system; AutoCAD; surface runoff; Model HEC-1; input data files; watershed digitization.)

INTRODUCTION

Hydrologic models are very complex nonlinear systems and can simulate rainfall induced runoff on watersheds with characteristics varying both in space and in time. A major problem confronting watershed modelers is the difficulty in obtaining and handling the quantity of spatially and temporally varying data required to successfully use hydrologic models. Computer and Geographic Information System (G.I.S.) technology have been rapidly evolving in recent years and systems have been developed to facilitate data storage, organization, manipulation, access, and display.

The purpose of this work is to examine the potential of using a commercially available computer-aided drafting package AutoCAD as a micro-computer tool for a three phase Watershed Information System (W.I.S.). The system is developed to obtain, organize, and display watershed data; calculate some model parameter values; and create model input files. The watershed model HEC-1 has been selected for the rainfall-runoff simulation and an example application to Macks Creek Watershed in Idaho is also presented.

The proposed W.I.S. uses a PC's Limited 286 machine, a True Grid 8017 digitizing tablet, AutoCAD version 9 as well as FORTRAN and PASCAL compilers. The model HEC-1 (Hydrologic Engineering Center, 1985; Hydrologic Engineering Center, 1979; Feldman and Goldman, 1982) was selected because it is a widely used model providing a number of options useful to the watershed modeler. The options for which the W.I.S. was developed include the S.C.S. curve number technique for determining excess rainfall and the kinematic wave approximation technique for routing both overland and open channel flow. It is assumed that the reader is familiar with the model HEC-1, as this paper is intended for HEC-1 users who seek computerized ways to prepare input data files.

REVIEW OF AUTOCAD CAPABILITIES AND DATA REQUIREMENTS FOR HEC-1

AutoCAD has several attractive features for the development of a W.I.S. dedicated to hydrologic modeling using HEC-1. These features will be reviewed and the basic data requirements of HEC-1 presented.

Review of AutoCAD Capabilities

AutoCAD is a comprehensive micro computer graphics software package (Raker and Rice, 1987). Although first intended for design and drafting purposes, it seems appealing to examine its capability as

[1]Paper No. 88117 of the *Water Resources Bulletin*. **Discussions are open until February 1, 1990.**
[2]Respectively, Graduate Student and Assistant Professors of Civil Engineering, Engineering Research Center, Colorado State University, Fort Collins, Colorado 80523.

Journal of Hydrology, 124 (1991) 317–344
Elsevier Science Publishers B.V., Amsterdam

[1]

CHANNEL EVOLUTION AND HYDROLOGIC VARIATIONS IN THE COLORADO RIVER BASIN: FACTORS INFLUENCING SEDIMENT AND SALT LOADS

ALLEN GELLIS[1], RICHARD HEREFORD[2], S.A. SCHUMM[3] and B.R. HAYES[3]

[1]*U.S. Geological Survey, GPO Box 4424, San Juan, PR 00936 (U.S.A.)*
[2]*U.S. Geological Survey, 2255 North Gemini Drive, Flagstaff, AZ 86001 (U.S.A.)*
[3]*Department of Earth Resources, Colorado State University, Ft. Collins, CO 80523 (U.S.A.)*

(Received 7 May 1990; revised and accepted 24 August 1990)

ABSTRACT

Gellis, A., Hereford, R., Schumm, S.A. and Hayes, B.R., 1991. Channel evolution and hydrologic variations in the Colorado River basin: factors influencing sediment and salt loads. J. Hydrol., 124: 317–344.

Suspended-sediment and dissolved-solid (salt) loads decreased after the early 1940s in the Colorado Plateau portion of the Colorado River basin, although discharge of major rivers — the Colorado, Green and San Juan — did not change significantly. This decline followed a period of high sediment yield caused by arroyo cutting. Reduced sediment loads have previously been explained by a change in sediment sampling procedures or changes in climate, land-use and conservation practices. More recent work has revealed that both decreased sediment production and sediment storage in channels of tributary basins produced the decline of sediment and salt loads. Sediment production and sediment storage are important components of incised-channel evolution, which involves sequential channel deepening, widening and finally floodplain formation. Accordingly, the widespread arroyo incision of the late nineteenth century resulted initially in high sediment loads. Since then, loads have decreased as incised channels (arroyos) have stabilized and begun to aggrade. However, during the 1940s, a period of low peak discharges permitted vegetational colonization of the valley floors, which further reduced sediment loads and promoted channel stabilization. This explanation is supported by experimental studies and field observations. Both geomorphic and hydrologic factors contributed to sediment storage and decreased sediment and salt loads in the upper Colorado River basin.

INTRODUCTION

The evolution of landforms with time and their response to climatic change are important topics of geomorphologic research. Interest in these topics has been largely academic, but the current need to predict river and hillslope changes has created an incentive to document and understand recent, short-term (e.g. 50 year) landform adjustments. This has led to different explanations of channel incision, floodplain formation and sediment-yield variation. At one extreme, these changes are thought to be inherent in landform evolution (Patton and Schumm, 1975, 1981; Womack and Schumm, 1977), whereas, at the

0022-1694/91/$03.50

Reprinted from MONTHLY WEATHER REVIEW, Vol. 118, No. 10, October 1990
American Meteorological Society

Cloud and Convection Frequencies over the Southeast United States as Related to Small-Scale Geographic Features

HAROLD M. GIBSON AND THOMAS H. VONDER HAAR

Department of Atmospheric Science, Colorado State University, Fort Collins, Colorado

(Manuscript received 4 December 1989, in final form 30 April 1990)

ABSTRACT

Visible and infrared data from the GOES West satellite were collected at 0700 CST and at each hour from 1000 CST to 1700 CST during summer 1986. Use of relatively high spatial and temporal resolution satellite data allowed study of local area cloud variations over broad regions in many new ways. Cloud frequency charts were computed for the area from Mississippi east to Georgia and the Gulf of Mexico north to Tennessee for each of the nine hours as well as convection frequency charts of four convection intensities as defined by the temperature of the cloud top. Strong diurnal cloud variations were observed.

These new data analyses show an average maximum cloud frequency near 45 percent over the land areas at about 1400 local time. The maximum of deep convection, about 8 percent, was one hour later. Cloudiness and deep convection were at a maximum during the nocturnal hours over the Gulf of Mexico. Cloud frequency shows a strong relationship to small terrain features. Small fresh water bodies have cloud minima relative to the surroundings in the afternoon hours. The higher, steep terrain shows cloud maxima and the adjacent lower terrain exhibits afternoon cloud minima due to divergence caused by the valley to mountain breeze.

The sea breeze-induced convergence causes relative cloud maxima over Gulf of Mexico near-shore land areas with the stronger maxima and greater areal coverage over peninsulas. Peninsulas that are of a similar scale or larger as compared to that of the convective cells show a late afternoon maxima of deep convection. Small scale geographical features such as small coastal islands and reservoirs show no relationship to deep convection in the frequency analysis.

1. Introduction

Before satellite images were available, accurate information concerning small-scale cloud distribution was severely lacking. Routine aviation weather observations estimate cloudiness as scattered ($^1/_{10}$ to $^5/_{10}$ coverage), broken ($^6/_{10}$ to $^9/_{10}$ coverage), or overcast. Accuracy at an observation site was therefore no better than two- to three-tenths. The spacing of observation sites results in a still lower accuracy. Consider the lack of maritime observation sites and one may wonder if our ignorance of cloud formation and persistence was greater than our knowledge.

By contrast, a 400 km square visible satellite image with resolution of 0.8 km relates to 250 000 individual locations. These observations are routinely available from geostationary satellites every half to three hours over most of the earth. It is the purpose of this research to use these millions of observations to intensely study the cloud coverage over an area of the southeastern United States centered on Alabama.

Past research shows that the sea breeze significantly contributes to the development of cloud systems and thunderstorms (Byers and Rodebush 1948). Florida has been a favorite location for this research due to the sea breeze-induced convergence field, enhanced by the peninsular shape of the state, resulting in a high frequency of convective cloudiness. Plank (1965) concluded that daily variations in the advection of low level moisture was the strongest contributing factor related to the development of clouds in that area. Frank et al. (1967), using the frequency of radar echoes, noted that the showers tended to form during the morning hours over the windward side of the Florida peninsula and then moved toward the leeward side, reaching a maximum near the leeward sea-breeze front during the afternoon hours. This afternoon maximum coincided with the time of maximum convergence. The Lake Okeechobee area had a minimum of radar echoes, particularly during the afternoon hours, which the authors attributed to the divergence caused by a lake to land breeze.

McQueen and Pielke (1985) investigated the daily trend of convection over south Florida with the use of satellite data. They reported that well-developed convection had a frequency of less than 1.9 percent at 1200 EST on synoptically undisturbed days and increased to 9.5 percent by 1400 EST. A maximum greater than 15 percent occurred by 1600 EST. The frequency dropped sharply during the evening hours.

Corresponding author address: Dr. Harold M. Gibson, Colorado State University, Cooperative Institute for Research in the Atmosphere, Fort Collins, CO 80523.

Radar Receiver Transfer Function Estimate from Correlated Meteorological Echoes

E. GORGUCCI

Istituto di Fisica dell'Atmosfera, Rome, Italy

V. CHANDRASEKAR

University of Alabama in Huntsville, Huntsville, Alabama

G. SCARCHILLI

Istituto di Fisica dell'Atmosfera, Rome, Italy

27 October 1989 and 29 June 1990

ABSTRACT

The precise and continuous calibration of a radar is an important task for maintaining the accuracy of radar measurements. The calibration of radar receiver transfer function slope can be performed using bias measurements of meteorological echoes. The bias measurement is obtained as the difference in the estimate of the mean power given by a logarithmic receiver and a power law receiver. The estimate of the receiver transfer function slope (obtained from bias measurement) and its accuracy are studied in this paper, taking into consideration the correlation structure of the radar time samples. Using the asymptotic theory and computer simulation, the estimate of receiver transfer function slope and its variance are evaluated for many sample sizes and Doppler spectra. Verification of the theoretical results is presented using data collected by the Polar 55-C band radar in Italy.

1. Introduction

Continuous calibration of a radar is important for monitoring radar measurements and maintaining the radar performance. Good knowledge of the receiver transfer function is required for precise measurements from a radar. Radar receivers are normally calibrated by injecting a known test signal at the input of the receiver chain and monitoring the digital signal at the output. Gorgucci et al. (1989) described a method by which the slope of the radar receiver can be estimated using meteorological echoes, observed with a stationary antenna. This technique is based on the principle that meteorological echo amplitudes are Rayleigh distributed, and the estimate of the mean power from nonlinear receivers is biased according to a known function (Scarchilli et al. 1986). The slope of the receiver transfer function can be computed from the measurement of the bias, which is the difference between the mean power estimates obtained by a logarithmic and a nonlinear receiver, which is of a power law form.

The accuracy of this calibration technique is dependent on the properties of the bias measurement. The fluctuations in the bias estimate are controlled by various parameters depending on the radar system as well as meteorological echo characteristics such as sampling time, wavelength of the signal, number of samples used in integration and the spectrum width. This paper deals with the evaluation of the accuracy of the bias measurement for meteorological echoes, and subsequently the radar calibration.

The paper is organized as follows: section 2 deals with the derivations of variance for bias measurement and receiver slope. In this section the standard deviation in the estimate of receiver slope for finite number of correlated time samples is obtained. The expression for the variance of bias measurement involves evaluating the correlation between P_1 and $\ln(P_2)$ where P_1 and P_2 are correlated power measurements obtained from a Rayleigh distributed signal. The evaluation of this more basic result is presented in the Appendix. Also the bias in the estimate of the receiver transfer function slope is obtained, for a finite number of samples, which is asymptotically unbiased. In section 3 data from Polar 55-C radar in Italy are presented to study the estimate of receiver transfer function slope. The results of this section are compared with the properties of the slope estimate suggested by the theoretical results of section 2. Section 4 summarizes the key results of this paper.

Corresponding author address: Dr. V. Chandrasekar, Department of Electrical Engineer, Colorado State University, Fort Collins, CO 80523.

LARGE-EDDY SIMULATIONS OF THERMALLY FORCED CIRCULATIONS IN THE CONVECTIVE BOUNDARY LAYER. PART I: A SMALL-SCALE CIRCULATION WITH ZERO WIND

M. G. HADFIELD*

Industrial and Environmental Meteorology Group, New Zealand Meteorological Service, P.O. Box 722, Wellington, New Zealand

W. R. COTTON and R. A. PIELKE

Department of Atmospheric Science, Colorado State University, Fort Collins, CO 80523, U.S.A.

(Received in final form 14 March, 1991)

Abstract. We have conducted large-eddy simulations (LES) of the atmospheric boundary layer with surface heat flux variations on a spatial scale comparable to the boundary layer depth.

We first ran a simulation with a horizontally homogeneous heat flux. In general the results are similar to those of previous large-eddy simulations. The model simulates a field of convective eddies having approximately the correct velocity and spatial scales, and with the crucial property that kinetic energy is transported vigorously upwards through the middle levels. However, the resolved temperature variance is only about half what is observed in the laboratory or the atmosphere. This deficiency – which is shared by many other large-eddy simulations – has dynamic implications, particularly in the pressure/temperature interaction terms of the heat flux budget. Recent simulations by other workers at much higher resolution than ours appear to be more realistic in this respect.

The surface heat flux perturbations were one-dimensional and sinusoidal with a wavelength equal to 1.3 times the boundary-layer depth. The mean wind was zero. Results were averaged over several simulations and over time. There is a mean circulation, with ascent over the heat flux maxima (vertical velocity $\sim 0.1 w_*$) and descent over the heat flux minima. Turbulence is consistently stronger over the heat flux maxima. The horizontal velocity variance components (calculated with respect to the horizontal average) become unequal, implying that convective eddies are elongated parallel to the surface heat flux perturbations.

A consideration of the budgets for temperature and velocity suggests several simplifying concepts.

Symbols

a	a variable resolved on the model grid
$\langle a \rangle$,	a general average of a
(a),	deviation from $\langle a \rangle$,
a'	deviation of a from horizontal average, $a' \equiv (a)_h$
C_ε	constant in the expression for the grid length scale l_ε
e	subgrid kinetic energy
E_i	ith component of the circulation kinetic energy
g	acceleration due to gravity
h	convective boundary-layer depth
l_g	length scale based on grid spacing
l_s	length scale based on stability

* The research reported in this paper was conducted while the first author was on study leave at Colorado State University.

Boundary-Layer Meteorology **57**: 79–114, 1991.

LARGE-EDDY SIMULATIONS OF THERMALLY FORCED CIRCULATIONS IN THE CONVECTIVE BOUNDARY LAYER. PART II: THE EFFECT OF CHANGES IN WAVELENGTH AND WIND SPEED

M. G. HADFIELD*

Industrial and Environmental Meteorology Group, New Zealand Meteorological Service, P.O. Box 722, Wellington, New Zealand

and

W. R. COTTON and R. A. PIELKE

Department of Atmospheric Science, Colorado State University, Fort Collins, CO 80523, U.S.A.

(Received in final form 14 March, 1991)

Abstract. This paper extends previous large-eddy simulations of the convective boundary layer over a surface with a spatially varying sensible heat flux. The heat flux variations are sinusoidal and one-dimensional. The wavelength is 1500 or 4500 m (corresponding to 1.3 and 3.8 times the boundary-layer depth, respectively) and the wind speed is 0, 1 or 2 m s^{-1}.

In every case the heat flux variation drives a mean circulation. As expected, with zero wind there is ascent over the heat flux maxima. The strength of the circulation increases substantially with an increase in the wavelength of the perturbation. A light wind weakens the circulation drastically and moves it downwind. The circulation has a significant effect on the average concentration field from a simulated, elevated source.

The heat flux variation modulates turbulence in the boundary layer. Turbulence is stronger (in several senses) above or downwind of the heat flux maxima than it is above or downwind of the heat flux minima. The effect remains significant even when the mean circulation is very weak. There are effects too on profiles of horizontal-average turbulence statistics. In most cases the effects would be *undetectable in the atmosphere*.

We consider how the surface heat flux variations penetrate into the lower and middle boundary layer and propose that to a first approximation the process resembles passive scalar diffusion.

1. Introduction

In a previous paper (Hadfield *et al.*, 1991, hereafter HCP1) we presented results from a set of large-eddy simulations (LES) of a convective boundary layer (CBL) in the presence of a one-dimensional, sinusoidal perturbation in the surface sensible heat flux. In that set of simulations, the wavelength λ_p of the heat flux perturbation was 1500 m, or 1.3 times the boundary-layer depth h, and the imposed wind speed u_0 was zero. We found that the perturbation drives a mean circulation, with ascent over the heat flux maxima and descent over the heat flux minima, although the existence of the circulation was established with reasonable confi-

* The research reported in this paper was conducted while the first author was on study leave at Colorado State University.

Boundary-Layer Meteorology **58**: 307–327, 1992.

Passive Microwave Remote Sensing of Cloud Liquid Water Over Land Regions

ANDREW S. JONES AND THOMAS H. VONDER HAAR

U.S. Army Center for Geosciences, Colorado State University, Fort Collins

Techniques for cloud liquid water retrieval over land are developed using data from the Special Sensor Microwave/Imager 85.5 GHz (3.5 mm) channels. To minimize the effect of surface emittance variability on the calculations, the surface emittance was estimated with the aid of surface skin temperature retrievals from the Visible Infrared Spin Scan Radiometer in geosynchronous orbit. The high sensitivity of the 85.5 GHz channels to cloud liquid water allows for the estimation of integrated cloud liquid water based on the microwave brightness temperature depression caused by attenuation and emission of microwave radiation at the colder ambient temperature of the cloud. The method assumes nonscattering radiative processes are dominant, therefore only nonprecipitating cloud liquid water is considered. Integrated cloud liquid water retrievals show good qualitative agreement with other available data sources. Numerical error sensitivity analysis show integrated cloud liquid water error estimates of 0.05–0.50 kg m^{-2} depending on the contrast of cloud over background.

1. INTRODUCTION

Present satellite liquid water retrieval methods are largely limited to areas over ocean surfaces, but with the new Special Sensor Microwave/Imager (SSM/I) instrument, retrieval of liquid water in nonprecipitating clouds over land surfaces has become more feasible as a result of the 85.5 GHz SSM/I channels which are more sensitive to cloud liquid water than channels on previous instruments [*Njoku*, 1982]. The ability to measure cloud liquid water remotely over the oceans has created much climatological interest with several studies probing the questions related to the global atmospheric liquid water distribution and variability such as precipitation patterns and El Niño events [e.g., *Prabhakara et al.*, 1983, 1985, 1986]. In these studies, only the atmosphere over the ocean was considered because of the radiometric properties of an ocean versus a land surface. Earlier, low-frequency microwave radiometers (<40 GHz) were limited in their ability to measure cloud liquid water over land because of the relatively small attenuation cloud liquid water has at those frequencies [*Liebe*, 1985*b*]. In this study a cloud liquid water retrieval algorithm for use over land is developed on the basis of the cloud liquid water radiometric properties at higher frequencies and in particular for the SSM/I 85.5-GHz channels. The surface emittance of the land is estimated using colocated infrared data for clear-sky conditions before clouds appear, thus reducing the effect the land surface emittance variability has on the retrieval process.

A brief review of the microwave radiative transfer equation used in this study is contained in the next section, with an overview of the instruments and data presented in section 3. The two sections which follow explain the retrieval procedure for the surface emittance and cloud liquid water respectively.

Paper number 90JD01376
0148-0227/90/90JD-01376$05.00

2. RADIATIVE TRANSFER IN THE MICROWAVE REGION

Retrieval Over Land Versus Ocean

Satellite-based methods can be divided into retrievals over land and ocean surfaces as a result of the distinct radiometric differences of the surface layers. Ocean surfaces are radiatively cold in the microwave regions because of water's low surface emittance of about 0.5 which increases with wind speed and colder water temperature [*Lane and Saxton*, 1952]. When cloud liquid water is detected in the atmosphere over an ocean surface, the microwave instrument senses higher brightness temperatures for thin clouds as a result of the absorption and emission of microwave radiation by the cloud liquid water, thus clouds appear warm over the ocean, but as the amount of cloud liquid water increases, the microwaves originate primarily from the higher levels of the cloud and the brightness temperature decreases [*Tsang et al.*, 1977]. Over land the surface emittance varies because of soil moisture content and can range from near unity for dry soils to less than 0.6 for wet soils [*Wang and Schmugge*, 1980; *Schmugge*, 1985]. Other factors such as surface roughness and vegetation also contribute to the surface emittance variability [*Choudhury et al.*, 1979; *Schmugge et al.*, 1980; *Owe et al.*, 1988].

Retrieval over an ocean surface. Assuming a relatively transparent atmosphere at microwave wavelengths such that the atmosphere can be assumed to be isothermal (< 40 GHz) allows for the estimation of the apparent microwave brightness temperature as given by *Grody* [1976],

$$T_B = T_s[1 - (1 - \epsilon_p)\tau_p^2] \tag{1}$$

where T_s is the surface skin temperature, ϵ_p is the surface emittance, and τ_p is the atmospheric transmittance for frequency p. A similar form of (1) was derived by *Chang and Wilheit* [1979]. The sensitivity of T_B with respect to τ_p from (1) is

$$\frac{\partial T_B}{\partial \tau_p} = -2T_s(1 - \epsilon_p)\tau_p \tag{2}$$

which is proportional to $(1 - \epsilon_p)$. This means that for high emittance values close to unity (such as land surface values)

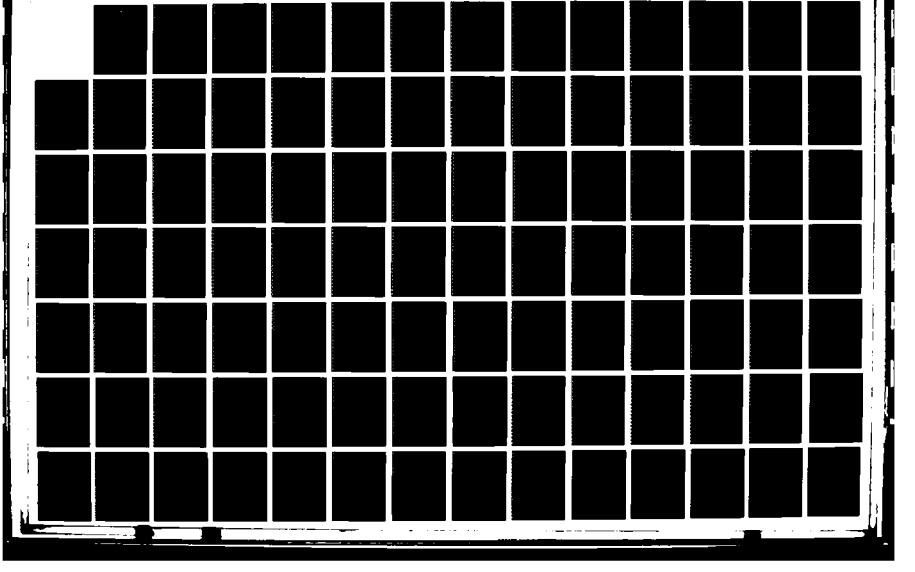

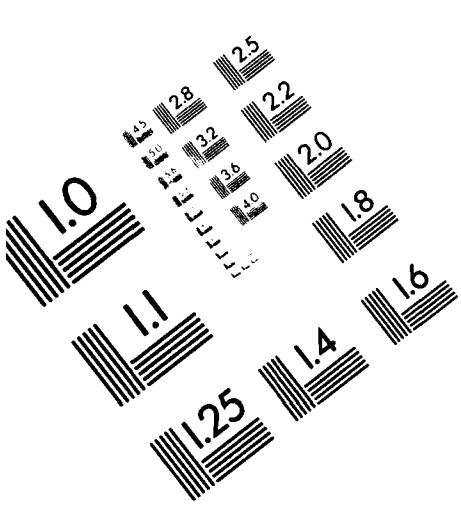

AIIM

Association for Information and Image Management

1100 Wayne Avenue, Suite 1100
Silver Spring, Maryland 20910

301/587-8202

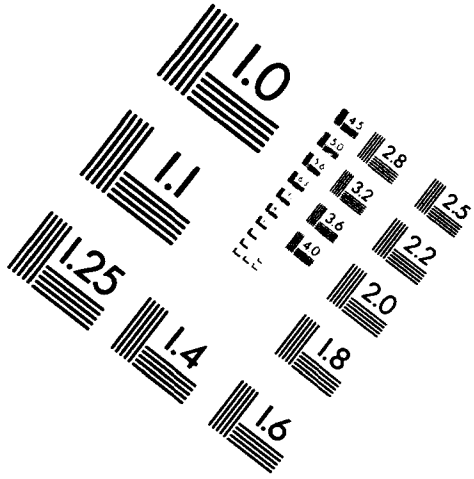

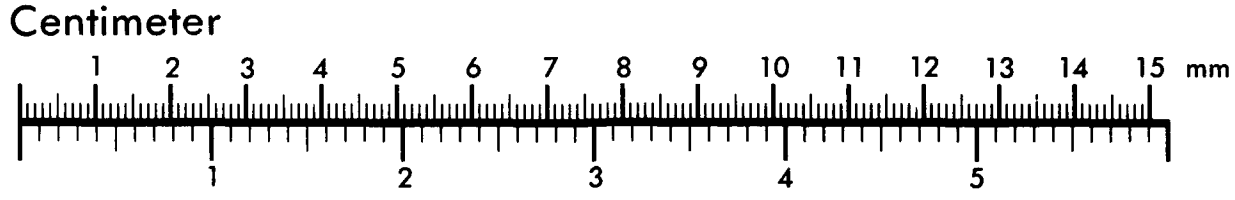

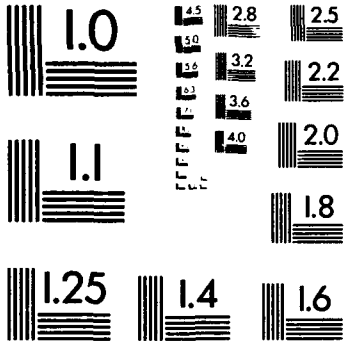

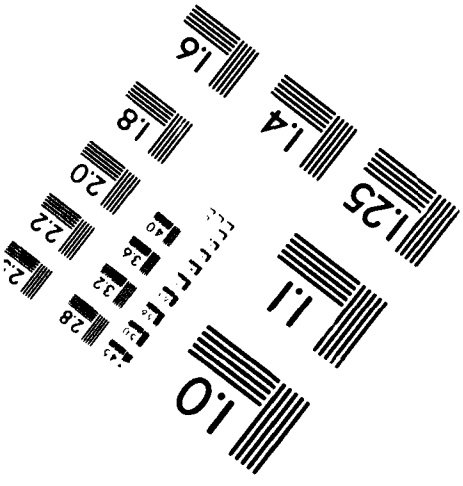

MANUFACTURED TO AIIM STANDARDS
BY APPLIED IMAGE, INC.

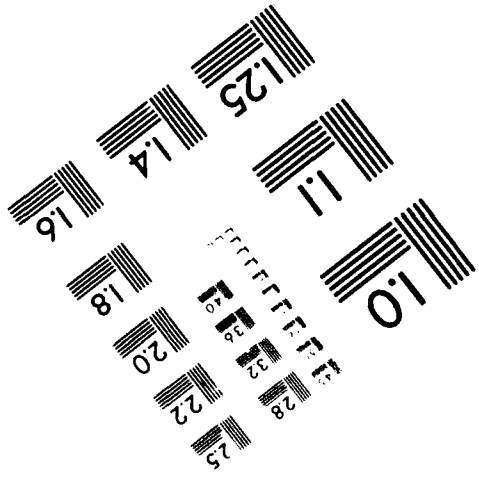

Reprinted from JOURNAL OF ATMOSPHERIC AND OCEANIC TECHNOLOGY, Vol. 6, No. 4, August 1989
American Meteorological Society

Imagery Randomized Block Analysis (IRBA) Applied to the Verification of Cloud Edge Detectors

FRANK P. KELLY AND THOMAS H. VONDER HAAR

Department of Atmospheric Science, Colorado State University, Fort Collins, Colorado

PAUL W. MIELKE, JR.

Department of Statistics, Colorado State University, Fort Collins, Colorado

(Manuscript received 19 February 1988, in final form 20 January 1989)

ABSTRACT

A recently developed statistical method is described for evaluating the effectiveness of numerical models. This method is applied to the verification of the effectiveness of satellite imagery cloud edge detectors. Digital satellite data are objectively modeled as cloud/no-cloud imagery using three different edge detection techniques. The imagery resulting from each technique is then quantitatively compared to a verification image through a recently developed imagery analysis method termed Imagery Randomized Block Analysis. The method also provides an agreement measure for objectively choosing a situationally effective technique among several competitors.

1. Introduction

The systematic detection and classification of clouds are basic to the study of all scales of weather processes. For many years geostationary meteorological satellites have provided us with high spatial and temporal resolution imagery for depicting world wide cloud cover (Suomi and Vonder Haar 1969). Cloud development, movement, and dissipation provide both visual clues and quantitative information about the state of the atmosphere at any one time. The satellite images upon which atmospheric scientists rely are merely "snapshots" of a continuously changing pattern. An operational meteorologist must analyze and subsequently forecast the dynamic character and behavior of the atmosphere from a sequence of static samples. An atmospheric scientist is interested in the different effects local forcing mechanisms (e.g., orographic features and climatic location) have on weather patterns. To maximize the utility of the satellite cloud images, while concurrently minimizing the data analysis requirements of the meteorologist, objective analysis methods are desired. A persistent difficulty is quantitatively choosing the optimum analysis method.

Meteorological satellites provide a favorable perspective for observing the Earth–Atmosphere–Hydrosphere (EAH) system as depicted from observed cloud patterns. Different cloud types and orientations provide information about the underlying physics of the atmosphere. The ability to correctly and objectively detect and classify cloud formations enhances our understanding of the continuum of atmospheric motion. Since the cloud forcing mechanisms and cloud morphology differ in different areas and situations, one cannot expect a single cloud detection/classification scheme to work equally well for all cases. Hence, there exists a need to quantitatively assess method and algorithm effectiveness in determining various cloud fields as seen from satellites.

The intent of any numerical model is to describe each phenomena in question as close to reality as possible for a given set of initial conditions. Objectively classified cloud images are models of the satellite viewed cloud patterns. To evaluate such models, the observed measurements of a given cloud field must be compared directly with the corresponding measurements of this cloud field as depicted by the objectively classified image. Consequently, the observed and model predicted cloud fields must be compared. If an objective cloud detection/classification model is effective, then the observed and model predicted cloud images should be more similar than random pairings of observed and model predicted images. This intuitive concept of similarity utilizes a recently developed permutation method termed multi-response randomized block permutation procedures (MRBP) for evaluation (Mielke and Iyer 1982; Mielke 1984).

The general MRBP method is applied to the specific case of verifying satellite imagery cloud detectors through a process termed Imagery Randomized Block Analysis (IRBA). Because IRBA is based strictly on

Corresponding author address: Dr. Paul W. Mielke, Jr., Department of Statistics, Colorado State University, Fort Collins, CO 80523.

Reprinted from JOURNAL OF ATMOSPHERIC AND OCEANIC TECHNOLOGY, Vol. 7, No. 3, June 1990
American Meteorological Society

On the Use of Satellites in Molniya Orbits for Meteorological Observation of Middle and High Latitudes

STANLEY Q. KIDDER AND THOMAS H. VONDER HAAR

Cooperative Institute for Research in the Atmosphere, Colorado State University, Fort Collins, Colorado

18 August 1989 and 27 October 1989

ABSTRACT

Time and space sampling is an increasingly critical aspect of Earth observation satellites. The highly eccentric orbit used by Soviet Molniya satellites functions much like a high-latitude geostationary orbit. Meteorological instruments placed on a satellite in a Molniya orbit would improve the temporal frequency of observation of high-latitude phenomena such as polar lows. Consideration of this new sampling strategy is suggested for future systems such as the "Earth Probe" satellites in the Mission to Planet Earth program as well as for operational meteorological satellite programs.

1. Introduction

As satellite payload capabilities and the sophistication of remote sensing systems continue to increase, we find time and space sampling to be an increasingly critical aspect of Earth observation satellites. Today's meteorological satellites are primarily in nearly circular orbits of two types: geostationary orbit (GEO) and low-earth orbit (LEO).

GEOs orbit over the equator in synchrony with the Earth so that they appear stationary over a selected meridian. Their main advantage is that points in their field of view can be observed as frequently as instruments allow. The areas they observe (Fig. 1) are restricted, however, to about 60° great circle arc from the subsatellite point. Four or five geostationary satellites usually operate around the globe, so the equatorial regions are well observed. Points poleward of about ±50° are observed poorly or not at all due to increasing atmospheric path length and perspective problems arising from the oblique view.

If they are in orbits with inclination angles close enough to 90° (such as the sunsynchronous NOAA satellites), LEOs can observe the entire globe, but only the polar regions are observed frequently (once each orbit, or approximately once each 100 min). Other locations are observed as infrequently as twice per day (Fig. 2).

The latitude zones between roughly 50° and 80° are not well served by these two orbits. It is the purpose of this paper to point out that an orbit pioneered by Soviet communications satellites could be used to bring the advantages of geostationary satellites to this latitude zone, which contains substantial numbers of people and scientifically interesting, rapidly changing meteorological conditions.

2. The Molniya orbit

The Soviet Union began launching Molniya (Russian: *lightning*) communication satellites in 1965, and they continue to be launched (seven in 1988; Thompson 1989).

The Molniya orbit is highly eccentric and inclined 63.4° from the equator. The perigee is chosen to keep the satellite above most of the atmosphere to avoid drag. The Soviets have chosen the perigee to be about 600 km above the Earth's surface. The apogee is then chosen such that the satellite completes exactly two orbits while the Earth makes one complete rotation (see Appendix). The period for this orbit is 717.74 min. The apogee is 39 750 km above the Earth's surface, compared to the height of a geostationary orbit of 35 787 km. The resulting semi-major axis is 26 553 km, and the eccentricity is 0.737.

The oblateness of the Earth causes changes in Keplerian orbital elements. The semi-major axis, inclination angle, and eccentricity are nearly unaffected by Earth's oblateness. However, the orbital period changes slightly, and both the right ascension of ascending node and the argument of perigee (Fig. 3) change linearly in time due to this perturbation (see Appendix). At an inclination angle of 63.4° [$\sin^{-1}(0.8^{1/2})$], the argument of perigee becomes stationary; thus the apogee is fixed at a given latitude.

Corresponding author address: Dr. Stanley Q. Kidder, Cooperative Institute for Research in the Atmosphere, Colorado State University, Foothills Campus, Fort Collins, CO 80523.

Self-consistent Method for Determining Vertical Profiles of Aerosol and Atmospheric Properties Using a High-Spectral-Resolution Rayleigh-Mie Lidar

D. A. Krueger, L. M. Caldwell, R. J. Alvarez II, and C. Y. She
Department of Physics
Colorado State University
Fort Collins, Colorado 80523

ABSTRACT

A self-consistent method of inverting high-spectral-resolution, Rayleigh-Mie lidar signals to obtain profiles of atmospheric state variables, as well as aerosol properties is presented. Assumed are a known air pressure at a reference height, hydrostatic equilibrium, the ideal gas law, and the theoretical temperature and pressure dependence of Rayleigh/Brillouin line shapes. For measurements over several kilometers, variations in the atmospheric pressure must be included in the data analysis. The inversion of the signal is greatly facilitated by making a quadratic expansion of the lineshape as a function of atmospheric temperature and pressure which is accurate for temperature ranges of $\pm$ 30 K and pressure ranges of $\pm$ 25 kPa around a standard temperature and pressure of 275 K and 76 kPa, respectively. Required measurements are the total lidar signal and signals corresponding to different portions of molecular scattering spectrum. By using interference filters and atomic vapor filters which remove the aerosol contribution, along with their measured transmission functions, these measurements can be made. Since the bandwidth of the interference filters used is fairly broad, the inclusion of rotational Raman scattering is important for accurate lidar inversion. Formulae for determining the vertical profiles of atmospheric temperature, pressure, and density, as well as backscatter ratio, backscatter phase function, extinction ratio, and aerosol extinction coefficient are given and their measurement sensitivities are discussed.

J. Atmos. Ocean. Tech.
December, 1991

Appl. Phys. B 50, 129–132 (1990)

Applied Physics B Photophysics and Laser Chemistry

Collisional Broadening of Ba I Line (553.5 nm) by He or Ar

E. Kuchta, R. J. Alvarez II, Y. H. Li, D. A. Krueger, and C. Y. She

Department of Physics, Colorado State University, Fort Collins, CO 80523, USA

Received 26 May 1989/Accepted 15 September 1989

Abstract. The Doppler-free line shape of the $6s^2\,{}^1S_0-6s^16p^1\,{}^1P_1$ transition at 553.5 nm in natural Ba in the presence of an argon or helium buffer gas has been measured at 744 K for gas pressures from 0.2 to 100 Torr. Using the measured data for pressures above 5 Torr, the broadening rate coefficients for the half width at half maximum (HWHM) are determined to be $(4.9\pm0.5)\otimes10^{-9}$ and $(5.0\pm0.5)\otimes10^{-9}$ s^{-1} cm^{-3} for helium and argon respectively.

PACS: 32.70.Jz, 34.40.+n

The effect of neutral nonresonant collisions on atomic spectral lines has long been of theoretical and experimental interest. The rate coefficients of rare-gas induced broadening of alkali principle series lines have been measured extensively. Alkali-earth atoms have been studied much less. A rather complete tabulation of collision induced halfwidth and shift has been given in a recent review by Allard and Kielkopf [1]. No data on barium spectral lines were given in their table. In the recent work of Ueda et al., the rate coefficients of He-, Ar-, and Kr-induced broadening in $(6s)^2\,{}^1S_0-(6s)(np)^1P_1$ series for $n=7$–10 have been measured by the conventional hook-total-absorption method [3]. Although the far-wing collisional redistribution line shape and alignment decay rates have been measured with a broadband laser (1 cm^{-1} linewidth) for Ba–Ar and Ba–Xe [2], a direct determination of the rate coefficient for the strongest $6s-6p$ transition at 553.5 nm from a line-broadening experiment is not reported. The rate coefficient for a transition of large oscillator strength, $f_0=1.59$, is of obvious interest. In addition, its value is necessary for performance optimization in a novel laser radar application where a barium vapor absorption cell is proposed [4] and is being used [5] as a narrow-band blocking filter. For these reasons, we have performed an experiment which measured He- and Ar-induced broadening rate coefficients of the natural barium $(6s)^2\,{}^1S_0-(6s)(6p)^1P_1$ transition.

Although laser-induced fluorescence [6] and Doppler-free two-photon spectroscopy [7] have been commonly applied to the collisional broadening problem for different reasons, we use saturation absorption spectroscopy [8] to measure the Doppler-free, thus pressure-dependent, lineshape of a vapor containing natural barium in the presence of a buffer gas of helium or argon. From the HWHM as a function of buffer gas pressure, the rate coefficients of He- and Ar-induced broadening are determined.

1. Experimental

The experimental setup is shown in Fig. 1. The vapor cell (30.5 cm long by 2.54 cm diameter) is shown enlarged. It contains solid Ba and a buffer gas which is heated to 744 K at the center and is cooled to about 325 K at the ends to prevent barium from coating the end windows. Although the vapor cell uses a heat-pipe construction, the cell is not a heat-pipe oven because of its much lower temperature of operation. The barium vapor partial pressure at the center is approximately $6\otimes10^{-5}$ Torr. The total pressure ranges from 0.2 to 100 Torr and is essentially due to the buffer gas. The three cw laser beams originate in a ring dye laser which has a linewidth of about 1 MHz. The pump beam which is chopped at 1 kHz has a power of approximately 0.6 mW. If the frequency is on a barium resonance, it will populate the upper atomic level. This

Mesoscale Analysis by Numerical Modeling Coupled with Sounding Retrieval from Satellites

ALAN E. LIPTON* AND THOMAS H. VONDER HAAR

Department of Atmospheric Science, Colorado State University, Fort Collins, Colorado

(Manuscript received 31 March 1989, in final form 18 December 1989)

ABSTRACT

The development and evaluation of a system for time-continuous mesoscale analysis is presented, with a focus on retrieving water vapor concentrations and ground surface temperatures from VISSR Atmospheric Sounder (VAS) data. The analysis system is distinguished by an intimate coupling of retrieval and numerical modeling processes that avoids some of the problems researchers have encountered when satellite-retrieved parameters have been input to models. The system incorporates virtually all of the temporal, vertical and horizontal structure that can be resolved in VAS soundings while maintaining model-generated gradients. The two primary components of the system are a version of the CSU Regional Atmospheric Modeling System (RAMS) and an algorithm for retrieving meteorological parameters from VAS data.

The analysis system was evaluated by means of simulations, with a domain that consisted of a vertical cross section through a broad mountain slope. The purposes were to determine the accuracy of coupled analysis results under controlled conditions and to compare results of the coupled scheme with those of other analysis schemes. For water vapor analysis, vertical gradients were more accurately resolved with the coupled method than with conventional retrieval from satellite data. The coupled method's incorporation of VAS data from multiple observation times was valuable for making mesoscale horizontal gradients stand out more clearly amid the noise in the water vapor analyses. In addition, the method was relatively robust when confronted with a common problem in analysis of the preconvective atmosphere—contamination of the satellite data by increasing amounts of small convective clouds. Analyses in which surface temperatures were derived from satellite-based retrievals were compared with the alternative of relying on energy balance computations without mesoscale data about soil characteristics. The surface temperatures from the two methods differed by as much as 5 K, giving rise to prominent differences in the induced mesoscale circulations. The energy balance computations were so sensitive to soil characteristics that the satellite retrieval method gave more accurate results even with cloud contamination.

1. Introduction

Our ability to understand and forecast mesoscale weather phenomena has been impeded by a lack of comprehensive mesoscale datasets and the difficulty of assembling large quantities of data into a useable form. These problems have been particularly troublesome to operational forecasters (Smith et al. 1986). A valuable but limited way to supply the necessary mesoscale data is to sound the atmosphere from satellites. Hillger and Vonder Haar (1981) and Mostek et al. (1986) showed that infrared sounder data can be used to detect variations in low-level water vapor concentrations; consequently, they are useful for assessing the potential for deep convection over the Great Plains. The VISSR Atmospheric Sounder (VAS) can be operated at high horizontal and temporal resolution (Menzel et al. 1983) and, therefore, it has particular potential as a mesoscale analysis tool. However, the VAS (and other present-day satellite sounders) is limited in that the retrieved profiles are of mediocre absolute accuracy and poor vertical resolution. In addition, clouds are a major obstacle to retrievals from infrared data.

Mesoscale data are generally most useful when they are available in gridded form, as in a numerical model. Mesoscale models are useful for analyzing and forecasting regions of destabilization and are particularly well suited to situations in which terrain variations strongly force atmospheric circulations (Pielke 1984). When used for analysis, the model complements the observational data by filling in gaps between observations (in space and time) and providing estimates of parameters that were not measured. Synoptically forced (Anthes et al. 1983) and ground-surface forced (Segal and Pielke 1981) weather events have been studied by these means.

Data for initialization and updating of models can be retrieved from satellite sources provided that a sufficient number of retrievals can be performed within

* Present affiliation: Atmospheric Sciences Division, Geophysics Laboratory, Air Force Systems Command, Hanscom Air Force Base, Massachusetts.

Corresponding author address: Dr. Alan E. Lipton, GL(AFSC)/LYS, Hanscom AFB, MA 01731.

Preconvective Mesoscale Analysis over Irregular Terrain with a Satellite–Model Coupled System

ALAN E. LIPTON* AND THOMAS H. VONDER HAAR

Department of Atmospheric Science, Colorado State University, Fort Collins, Colorado

(Manuscript received 31 March 1989, in final form 18 December 1990)

ABSTRACT

Influences on the mesoscale distribution of summertime convective cloud development in the northeastern Colorado region are described using a new system for time-continuous mesoscale analysis. The analysis system is distinctive in that there is an intimate coupling between integration of a numerical model and retrieval of temperatures and water vapor concentrations from VISSR Atmospheric Sounder (VAS) data. We present a case study to compare results of the coupled analysis method with those of related methods, focusing on the roles of variations in ground surface temperatures and water vapor concentrations.

The horizontal and time variations represented in satellite-based (coupled) surface temperature analyses closely corresponded to information from conventional shelter temperature observations, but had much greater detail. In contrast, temperatures based on energy balance computations tended to increase too quickly during the morning and were lacking in mesoscale feature. In the water vapor analyses, when the first set of satellite data is less reliable than the later sets, some of the contamination lingers throughout the time-continuous coupled analysis results. However, the coupled method generally appears to be the most valuable method considered in this study because it exploits the major strengths of the numerical model and the satellite data while making it relatively easy to recognize and compensate for any impacts of their weaknesses. In addition, the coupled analysis results illustrated that there can be very large mesoscale gradients in temperatures at the ground surface even on relatively flat terrain. These gradients, in combination with terrain height variations, can play an important role in preconvective water vapor kinematics through their influences on vertical and horizontal winds. The analysis system proved to be valuable for forecasting through the close correspondence between derived stability indices and later convective development in the case we studied.

1. Introduction

In a previous paper (Lipton and Vonder Haar 1990) we described a system for time-continuous mesoscale analysis in which there is an intimate coupling of numerical modeling with the retrieval of atmospheric parameters from satellite data. The coupled method was compared to other methods by means of two-dimensional simulated analyses. For water vapor analysis we showed that vertical gradients were more accurately resolved with the coupled method than with conventional retrieval from satellite data. The coupled method's incorporation of VAS data from multiple observation times was valuable for making mesoscale horizontal gradients stand out more clearly amid the noise in the water vapor analyses. In addition, the method was relatively robust when confronted with a common problem in analysis of the preconvective atmosphere—contamination of the satellite data by increasing amounts of small convective clouds. We also compared results from two methods for dealing with surface temperatures in mesoscale analysis. In the coupled method surface temperatures were derived from satellite-based retrievals. The alternative was to rely on energy balance computations in the absence of mesoscale data on soil characteristics. The surface temperatures from the two methods differed by as much as 5 K, giving rise to prominent differences in the induced mesoscale circulations. The energy balance computations were so sensitive to soil characteristics that the satellite retrieval method gave more accurate results even with cloud contamination.

In this paper we present results from a case study for the northeast Colorado region (Fig. 1) on 21 August 1983. The primary goals of the study were to evaluate the coupled system's performance under real-world conditions and to explore the kinematics of the mesoscale preconvective environment over irregular, high terrain. A summertime case was preferred for study because convective storms are common even in the absence of strong synoptic-scale forcing. The particular date was chosen because high-quality satellite sounder data were available and the meteorological conditions

* Present affiliation: Atmospheric Sciences Division, Geophysics Laboratory, Air Force Systems Command, Hanscom Air Force Base, Massachusetts.

Corresponding author address: Dr. Alan E. Lipton, GL(AFSC)/LYS, Hanscom AFB, MA 01731.

New primary ice nucleation parameterizations in an explicit cloud model

Michael P. Meyers, Paul J. DeMott and William R. Cotton
Colorado State University
Department of Atmospheric Science
Fort Collins, Colorado 80523

November 18, 1991

J. Appl. Met., 31 (7), 708-721

Abstract

Two new primary ice nucleation parameterizations are examined in the RAMS cloud model via sensitivity tests on a wintertime precipitation event in the Sierra Nevada region. A model combining the effects of deposition and condensation-freezing nucleation is formulated based on data obtained from continuous flow diffusion chambers. The data indicate an exponential variation of ice nuclei concentrations with ice supersaturation, reasonably independent of temperature between −7 and −20°C. Predicted ice concentrations from these measurements exceed values predicted by the widely used temperature-dependent Fletcher approximation by as much as one order of magnitude at temperatures warmer than −20°C. A contact-freezing nucleation model is also formulated based on laboratory data gathered by various authors using techniques which isolated this nucleation mode. Predicted contact nuclei concentrations based on the newer measurements are as much as three orders of magnitude less than values estimated by Young (1974a) which have been widely used for predicted schemes.

Simulations of the orographic precipitation event over the Sierra Nevada indicate that the pristine ice fields are very sensitive to the changes in the ice nucleation formulation, with the pristine ice field resulting from the new formulation comparing much better to the observed magnitudes and structure from the case study. Deposition/condensation-freezing nucleation dominates contact-freezing nucleation in the new scheme, except in the downward branch of the mountain wave, where contact-freezing dominates in the evaporating cloud. Secondary ice production is a more dominant at warm temperatures in the new scheme producing more pristine ice crystals over the barrier. The old contact-freezing nucleation scheme overpredicts pristine ice crystal concentrations, which depletes cloud water available for secondary ice production. The effect of the new parameterizations on the precipitating hydrometeors is substantial with nearly a 10% increase in precipitation across the domain. Graupel precipitation increased dramatically due to more cloud water available with the new scheme.

Evaluation of the Potential for Wintertime Quantitative Precipitation Forecasting over Mountainous Terrain with an Explicit Cloud Model. Part I: Two-Dimensional Sensitivity Experiments

MICHAEL P. MEYERS AND WILLIAM R. COTTON

Colorado State University, Department of Atmospheric Science, Fort Collins, Colorado

(Manuscript received 21 August 1990, in final form 2 February 1991)

ABSTRACT

A prolonged orographic precipitation event occurred over the Sierra Nevada in central California on 12–13 February 1986. This well-documented case was investigated via the nonhydrostatic version of the Colorado State University (CSU) Regional Atmospheric Modeling System (RAMS). The two-dimensional, cross-barrier simulations produced flow fields and microphysical structure, which compared well with observations. The feasibility of producing quantitative precipitation forecasts (QPF) with an explicit cloud model was also demonstrated.

The experiments exhibited a profound sensitivity to the input sounding. Initializing with a sounding, which is representative of the upstream environment, was the most critical factor to the success of the simulation. The QPF was also quite sensitive to input graupel density. Decreasing the density of graupel led to increases in the overall precipitation. Sensitivities to other microphysical parameters as well as orography and dynamics were also examined.

1. Introduction

The Sierra Cooperative Pilot Project (SCPP) was initiated in the 1970s to study the natural cloud processes occurring in Sierra Nevada storms. The objectives of the experiment were to identify the conditions when cloud seeding results in an increase or decrease in precipitation, and to monitor the magnitude of those changes (Reynolds and Dennis 1986). The subsequent benefits of SCPP have been a multitude of new insights into the microphysics and dynamics of orographic precipitation. Based on the extensive documentation accumulated during SCPP, a challenge has also been put forth to the modeling community to test their ability to simulate orographic cloud systems and examine the dominant physical controls in these storms.

The structure and organization of cyclonic storms affecting the Sierra Nevada region often resemble the characteristic split-front type (Browning and Monk 1982) evident in the Pacific Northwest (Hobbs 1978) and the United Kingdom (Browning 1985). One contributing factor to the split front is orographic blocking. Blocking results when the cross-barrier flow cools adiabatically as it is forced up the barrier, producing a positive pressure perturbation (Godske et al. 1957; Smith 1979), and a corresponding pressure-gradient force directed upstream from the mountain. This pressure-gradient force decelerates the low-level flow and, in some cases, can even reverse the direction. When a cold front approaches, the cold air advances faster at the higher levels than at lower levels below the mountain crest due to the low-level blocking. This blocking results in cold air being advected over warmer air, commonly leading to a convectively unstable condition (Hobbs et al. 1975; Reynolds and Dennis 1986).

Another symptom of orographic blocking is the mountain parallel wind component, often in the form of a low-level jet (LLJ). This mountain parallel jet was recognized in the polar regions by Schwerdtfeger (1974, 1975). Modeling studies (Parish 1982; Pierrehumbert and Wyman 1985; Smolarkiewicz et al. 1988; Smolarkiewicz and Rotunno 1990) have examined blocked flow in a stratified fluid upstream of ridgelike obstacles. The Sierra Nevada "barrier jet" (Parish 1982) develops when the cross-barrier flow becomes subgeostrophic due to orographic blocking, accelerating the flow toward low pressure in response to the unbalanced pressure gradient in the y direction, and producing a positive v component of the wind. If the flow lasts for several hours the wind field will adjust to the new mass field. This adjustment results in a terrain-locked flow in which the winds in the lowest levels blow nearly parallel to the terrain contours in the form of a barrier jet.

A typical measure of the upstream blocking is expressed by the Froude number

$$\mathrm{Fr} = U/Nh_m,$$

Corresponding author address: Mr. Michael P. Meyers, Colorado State University, Department of Atmospheric Sciences, Fort Collins, CO 80523.

Meteorol. Atmos. Phys. 40, 189–193 (1989)

Meteorology and Atmospheric Physics

551.5:51

Department of Atmospheric Science, Colorado State University, Fort Collins, U.S.A.

A Terrain-Following Coordinate System – Derivation of Diagnostic Relationships

R. A. Pielke and J. Cram

With 1 Figure

Received October 9, 1987
Revised September 23, 1988

Summary

Generalized hydrostatic and geostrophic equations can be derived from the equations in the terrain-following framework. The generalized hydrostatic equation permits some non-hydrostatic motions (as obtained from a Cartesian framework) to remain when a non-zero slope exists. Correspondingly, the generalized geostrophic wind permits a horizontal divergent component (in addition to divergence caused by the change of Coriolis parameter with latitude) to occur when the slope angle is not zero.

1. Introduction

Since Phillips (1957) introduced the concept of a terrain-following coordinate system, this framework to represent the conservation equations has been applied extensively in meteorology. The advantage of this approach is that the ground surface coincides with a coordinate surface. Phillips applied the chain rule of calculus to transform from the Cartesian coordinate system to a terrain following coordinate framework expressed in terms of pressure divided by surface pressure.

Dutton (1976) discussed the use of tensor transformation procedures to convert from one coordinate system to another. The value of applying tensor analysis is that physical invariance is guaranteed to be preserved. Pielke and Martin (1981, 1983), Clark (1977), Pielke et al. (1985), and Pielke and Cram (1987) made use of tensor transformation techniques in deriving appropriate equations for use in meteorological models and analyses. Gal-Chen and Sommerville (1975) provided the original work in employing a z-based terrain following coordinate system to a non-hydrostatic model.

The purpose of this paper is to apply the results of tensor transformation in order to obtain new useful diagnostic relations valid on a terrain following coordinate surface.

2. Summary of Tensor Transformation Requirements

From Dutton (1976) and Pielke (1984), there are several transformation relations which will be useful when the value of this technique is discussed in Section 3. In this paper, the coordinate transformation

$$\begin{aligned}
\tilde{x}^1 &= x \\
\tilde{x}^2 &= y \\
\tilde{x}^3 &= \sigma = s[z - z_G(x,y)]/[s - z_G(x,y)] \\
x &= \tilde{x}^1 \\
y &= \tilde{x}^2 \\
z &= (\sigma/s)[s - z_G(\tilde{x}^1,\tilde{x}^2)] + z_G(\tilde{x}^1,\tilde{x}^2) \qquad (1)
\end{aligned}$$

will be used to illustrate the mathematical rigor of this approach, although any single-valued functional relation between x, y and z, and a new

NOTE

The Relationship Between Numerical and Physical Models of Atmospheric Flow

Roger A. Pielke
Colorado State University
Fort Collins, CO 80523

April 6, 1988

Environ. Software, 3, 39-41

Introduction[1]

There are two fundamental methods of simulating atmospheric flows ysical models and *mathematical models*. With the first technique, e model replicas of observed ground surface characteristics (e.g., to- raphic relief, buildings) are constructed and inserted into a chamber as a wind tunnel or a water tank. The flow of air or other gases iquids in this chamber is adjusted so as to best represent the larger e, observed atmospheric conditions. Mathematical modeling, by con- t, utilizes such basic analysis techniques as algebra and calculus to e directly the conservation laws of motion, heat, moisture, and other spheric constituents.

Physical models

ng order of magnitude estimates for the dependent variables and as- uing that L and S are the representative length and velocity scale of circulation of interest (i.e., $\frac{S^2}{L}$ = maximum of $\left[\frac{W^2}{L_z}, \frac{WU}{L_x}, \frac{WV}{L_y}, \frac{U^2}{L_x}\right]$), n a scaled version of the conservation of motion equation can be writ- as

$$\begin{aligned}\left[\frac{S^2}{L}\right]\frac{\partial \hat{u}_i}{\partial \hat{t}} = &-\left[\frac{S^2}{L}\right]\hat{u}_j\frac{\partial \hat{u}_i}{\partial \hat{x}_j} - \left[\frac{c_u^2}{L}\right]\frac{\partial}{\partial \hat{x}_j}\overline{\hat{u}_j''\hat{u}_i''} \\ &- \left[\frac{Rg\ell}{L}\right]\hat{\theta}_0\frac{\partial \hat{\pi}'}{\partial \hat{x}_i} - \left[\frac{Rg\ell}{L}\right]\hat{\theta}_0\left\{\frac{\partial \hat{z}_0}{\partial \hat{x}}\delta_{i1} + \frac{\partial \hat{z}_0}{\partial \hat{y}}\delta_{i2}\right\} \qquad (1) \\ &+ \left[\frac{g\ell}{c_u^2}g\right]\hat{\theta}'\delta_{i3} - [\Omega S]2\varepsilon_{ijk}\hat{\Omega}_j\hat{u}_k - \left[\frac{\nu S}{L^2}\right]\frac{\partial^2 \hat{u}_i}{\partial \hat{x}_j\partial \hat{x}_j}\end{aligned}$$

re a circumflex (ˆ) over a dependent or independent variable indi- es that it is nondimensional. The scaling parameter e_{u_i} is a measure he subgrid scale velocity correlations that can be estimated from the n subgrid scale kinetic energy i.e.,

$$e_{u_i} = [\overline{u_i''^2}/2)]^{1/2}.$$

Including an estimate for the molecular viscous dissipation and mul- lying (1) by L/S^2 (to obtain a nondimensional equation for the local eleration) results in

$$\begin{aligned}\frac{\partial \hat{u}_i}{\partial \hat{t}} = &-\hat{u}_j\frac{\partial \hat{u}_i}{\partial \hat{x}_j} - \left[\frac{c_u^2}{S^2}\right]\frac{\partial}{\partial \hat{x}_j}\overline{\hat{u}_j''\hat{u}_i''} - \left[\frac{Rg\ell}{S^2}\right]\hat{\theta}_0\frac{\partial \hat{\pi}'}{\partial \hat{x}_i} \\ &- \left[\frac{Rg\ell}{S^2}\right]\hat{\theta}_0\left\{\frac{\partial \hat{z}_0}{\partial \hat{x}}\delta_{i1} + \frac{\partial \hat{z}_0}{\partial \hat{y}}\delta_{i2}\right\} + \left[\frac{gL\ell\theta}{\theta_0 S^2}\right]\hat{\theta}'\delta_{i3} \qquad (2) \\ &- \left[\frac{\Omega L}{S}\right]2\varepsilon_{ijk}\hat{\Omega}_j\hat{u}_k - \left[\frac{\nu}{LS}\right]\frac{\partial^2 \hat{u}_i}{\partial \hat{x}_j\partial \hat{x}_j}.\end{aligned}$$

use a scaled physical model to represent accurately the conservation- notion relation in the atmosphere, it is essential that

1. the individual bracketed terms be equal in the model and in the atmosphere, or
2. the bracketed terms that are not equal must be much less in magnitude than the other bracketed terms in Eq. (2).

When these conditions are met the actual and modeled atmospheres are said to have *dynamical similarity*.

Two of these bracketed terms are defined as

$$\Omega L/S = 1/R_o$$

and

$$\nu/LS = 1/Re,$$

where R_o is the Rossby number and Re the Reynolds number; and

$$gL(\delta\theta/\theta_o)/S^2 = \mathrm{Ri}_b$$

is the *bulk Richardson number*. ($\delta\theta$ represents the potential temperature perturbation and is the same order as the temperature perturbation δT).

From Eq. (2), to maintain dynamic similarity, it is implied that to represent all of the terms in the equation properly:

1. the ratio of the subgrid scale kinetic energy to the grid-volume average kinetic energy must be kept constant;
2. reducing the length scale L in the physical model requires:
   (a) an increase in the magnitude of the horizontal temperature perturbation $\delta\theta$ or a reduction in the simulated wind flow speed S or both,
   (b) an increase in the rotation rate Ω or a reduction in S or both,
   (c) a decrease in the viscosity ν or an increase in S or both;
3. an increase in $\delta\theta$ in the pressure gradient term necessitates that S also increase.

Unfortunately, it is impossible to satisfy all of these requirement si- multaneously in existing physical models of mesoscale atmospheric circu- lations. Such physical models are constructed inside of buildings, which limits the dimensions of the simulated circulations to the size of meters, whereas actual mesoscale circulations extend over kilometers.

To illustrate the difficulty of obtaining dynamic similarity in a phys- ical model for all terms in Eq. (2), let the horizontal scale of a mountain ridge be 10 km, whereas the physical model of this geographic feature uti- lizes a 1 m representation. The scale reduction is, therefore, 10^4. Thus, if $S = 10$ m s^{-1} in the real situation and air is used in the scaled model atmosphere, then the simulated wind speed would have to be 10^5 m s^{-1} to maintain identical Reynolds number similarity! In addition, to have the same Rossby number for this example, the physical model must ro- tate 10,000 times more rapidly than the earth or the wind speed must be reduced by 10,000. Reducing the speed, of course, is contradictory to what is required to obtain Reynolds number similarity! Only if the results are relatively insensitive to changes in these nondimensional quan- tities, as suggested, for example, by Cermak (1975) for large values of the Reynolds number in simulations of the atmospheric boundary layer, can one ignore large differences in the nondimensional parameters.

[1] This note was extracted and modified somewhat from that presented in Pielke (1984, Chapter 8).

Reprinted from JOURNAL OF APPLIED METEOROLOGY, Vol. 27, No. 2, February 1988
American Meteorological Society

The Extrapolation of Vertical Profiles of Wind Speed within the Marine Atmospheric Surface Layer Using the p Formula

M. SEGAL AND R. A. PIELKE

Department of Atmospheric Sciences, Colorado State University, Fort Collins, Colorado

(Manuscript received 18 October 1986, in final form 21 July 1987)

ABSTRACT

Values of p for the exponent-type wind profile formulation, used in vertical extrapolations of wind speed, were derived for the marine atmospheric surface layer. Nomograms were constructed, providing p values as dependent on a single elevation measurement of the air temperature, wind speed, and the surface water temperature. The range of p values in the unstable surface layer is between 0.02 to 0.2, while for stable situations the range is 0.1 to possibly ~1.0. The values of p converge to about 0.2 for high wind speeds.

1. Introduction

Extrapolation of wind speed profiles, within the first tens of meters above the land, based on single height wind data, are common in both research and applied studies. The necessity for such extrapolations emerges because of the substantial expenses associated with measured vertical profiles of the wind. Probably the most common extrapolation is based on an exponent type wind profile which is referred to as the wind power formula (e.g., Panofsky and Parsad, 1965; Panofsky and Dutton, 1983)

$$p=\frac{d(\ln u)}{d(\ln z)}=\left(z\frac{du}{dz}\right)\Big/u=\left(\frac{\mathrm{Ri}_B}{\mathrm{Ri}}\right)^{1/2} \tag{1}$$

or on its common approximation through

$$\frac{u}{u_1}=\left(\frac{z}{z_1}\right)^p. \tag{2}$$

In (2), u refers to the wind speed, z to elevation, the subindex, 1, indicates the reference measurement level, Ri is the Richardson number, Ri_B is the bulk Richardson number as defined by (8), and p is a constant which is a function of the thermal stability in the surface layer. Many studies have been involved with the evaluation of the magnitude of p over a land surface. In recent years, Touma (1977), for example, carried out a comprehensive analysis based on wind data from many sites, to determine by observational means the values of p as a function of the near-surface thermal stability.

The necessity for such extrapolation is even more frequent over large water bodies where vertical profiles of the wind speed are obviously very expensive to acquire. Over the open sea, where even single elevation wind data are rare, utilizing the wind power formula may provide important additional information as to the wind profile within the surface layer. Alternatively, it can provide a formulation for conversion of wind speed measured at different locations and elevations to a standard level. Such evaluations can be obtained, of course, by a detailed computation of the surface layer characteristics (e.g., Smith, 1980; Liu, 1984). However, in analogy to the land case, using the wind power formula approximation over water can be beneficial in many situations (e.g., when a single elevation wind speed is given and the thermal stratification has to be determined subjectively, or when a bulk evaluation is needed).

Unlike the numerous studies relating to p over land surfaces, however, no special attention has been given to a refined investigation of its characteristics over open water surfaces. Davenport (1965) suggested $p \approx 0.1$ as being representative over the open sea. It is the purpose of this paper to provide further refinements in the scaling of p over water surfaces.

The sea–atmosphere interfacial characteristics are commonly categorized in three classes: (i) smooth surface conditions; (ii) transition surface conditions; and (iii) rough surface conditions. Following Kondo (1975), for example, the first class is involved with wind speeds of less than 2–3 m s^{-1} (at 10 m height), the second class is involved with a typical wind speed range of 3–8 m s^{-1}, and the third one with stronger wind speeds. In the bulk approximation for p values, derived in section 2, these characteristics of the sea surface state, as well as refinements involved with computation of the potential temperature of the air at the top of the sublayer at the surface, are not considered. In section 3, however, these two aspects are introduced and the involved modifications of the bulk approximation for p are evaluated.

Corresponding author address: Dr. Moti Segal, Dept. of Atmospheric Sciences, Colorado State University, Fort Collins, CO 80523.

Reprinted from MONTHLY WEATHER REVIEW, Vol. 117, No. 4, April 1989
American Meteorological Society

The Impact of Crop Areas in Northeast Colorado on Midsummer Mesoscale Thermal Circulations

M. SEGAL,* W. E. SCHREIBER,† G. KALLOS,‡ J. R. GARRATT,*,§ A. RODI,† J. WEAVER*,¶ AND R. A. PIELKE*

* *Department of Atmospheric Science, Colorado State University, Fort Collins, Colorado*
† *Department of Atmospheric Science, University of Wyoming, Laramie, Wyoming*
‡ *Department of Applied Physics, University of Athens, Greece*
¶ *NOAA/NESDIS/RAMM Branch*

(Manuscript received 13 May 1988, in final form 18 October 1988)

ABSTRACT

The present study provides a preliminary evaluation of mesoscale circulations forced by surface gradients of heating arising from irrigated areas adjacent to dry land, utilizing a combination of satellite, observational, and modeling approaches. The irrigated crop areas of northeast Colorado were chosen for the study. For the cases studied satellite surface infrared temperature data indicated a typical temperature contrast of approximately 10 K at noon, between the irrigated area and the adjacent dry land. Surface observations and aircraft measurements within the lower region of the atmospheric boundary layer indicated, in general, a significant temperature contrast and moisture difference, thereby implying a potential thermally driven circulation. The anticipated thermally induced flows, however, were reflected in the measurements only by modest changes in the wind speed and wind direction across the contrast location. It is suggested that the daytime, elevated, terrain-forced flow in the area, and the synoptic flow, combined to mask to varying degrees the thermally induced circulation due to the irrigated land-dry land area effect. Numerical model simulations which were carried out over the studied area support this hypothesis. In addition, the impact of the irrigated areas on the moisture within the boundary layer, as well as on potential convective cloud development, is discussed.

1. Introduction

Summer irrigated crop areas generally have a significantly lower Bowen ratio (the ratio of surface sensible heat flux, H_s, to that of evapotranspiration flux, H_L) when compared to dry land areas. Since the available net radiation at the surface, less the soil heat fluxes, is partitioned between H_s and H_L at the surface, it follows that the presence of a large irrigated area adjacent to a dry area, within a mesoscale domain, should result in substantial horizontal gradients in H_s. Consequently, a horizontal temperature gradient within the lower atmosphere, analogous to that found along a seacoast, should result, and a sea-breeze-like circulation [termed in this paper a *nonclassical mesoscale circulation* (NCMC) to distinguish it from the sea breeze which is also forced by horizontal gradients in H_s] is expected to be induced. Theoretical and conceptual evaluations of the kinematic and thermodynamic processes associated with NCMC in such situations have been provided in recent years, for example, by Smith and Mahrt (1981), Anthes (1984), Segal et al. (1984), and Pielke and Segal (1986). Numerical model studies by Mahfouf et al. (1987) and Segal et al. (1988) suggested that for dense, well-watered and *extended* crop areas, mesoscale circulations of an intensity close to that of a sea breeze may be produced. In Segal et al. (1988), a short review of previous studies relevant to NCMCs was included. Also worth noting are observational studies in the early fifties in the semiarid Trans Volga steppe in the Soviet Union (although they involved relatively coarse resolution measurements), which suggested the existence of NCMCs involved with irrigated areas (Dzerdzeevskii 1963). It has been suggested that NCMCs along irrigated wet land–dry land contrasts may be of some significance in convective cloud initiation under supportive synoptic conditions (Sun and Ogura 1979; Anthes 1984; Yan and Anthes 1988). Likewise, cloud-scale model simulations by Smolarkiewicz and Clark (1985) suggested that inhomogeneities in soil and vegetation characteristics are likely to be important in the early stages of cumulus cloud formation.

Since in the aforementioned model simulation studies, prescribed vegetation characteristics were used, observational studies should next be carried out in order to evaluate thoroughly whether real-world, large

§ Permanent affiliation: CSIRO, Division of Atmospheric Research, Mordialloc, Victoria, Australia.

Corresponding author address: Motie Segal, Colorado State University, Dept. of Atmospheric Science, Fort Collins, CO 80523.

Atmospheric Environment Vol. 22, No. 3, pp. 471–486, 1988.
Printed in Great Britain.

0004–6981/88 $3.00 + 0.00
Pergamon Press plc

ON THE IMPACT OF VALLEY/RIDGE THERMALLY INDUCED CIRCULATIONS ON REGIONAL POLLUTANT TRANSPORT

M. SEGAL, C.-H. YU,* R. W. ARRITT and R. A. PIELKE
Department of Atmospheric Science, Colorado State University, Fort Collins, CO 80523, U.S.A.

(*First received* 12 *January* 1987 *and in final form* 13 *August* 1987)

Abstract—The impact of thermally induced valley/ridge circulations on the regional-scale transport of pollutants is examined using a modeling approach. The approach consists of applying a numerical meteorological model which provides the wind and turbulence fields used as input to a Lagrangian dispersion model. A variety of generic simulations were performed. Results indicate a significant effect of the induced local flows and the thermal stratification on the regional-scale transport. Both the time of the day in which the cross valley/ridge transport occurs and the season of the year are found to be crucial in determining the magnitude and form of the alterations. Conceptual generalizations of the model results are presented.

Key word index: Thermally-induced circulations, local circulations and their effect on regional transport, numerical model transport evaluations, dispersion modeling, mesoscale thermally forced circulations and their effect on regional transport.

1. INTRODUCTION

During the past two decades, interest in regional-scale (i.e. from ~200 to ~2000 km) transport of polluted air masses has continuously increased (e.g. Eliassen, 1980; Bhumralkar and Teasley, 1984). This interest has been motivated mostly by concerns such as acid deposition and visibility impairment from distant sources. Evaluations of the regional transport of pollutants are usually done by means of trajectory analysis (e.g. Wolff *et al.*, 1977; Haagenson and Shapiro, 1979; Heffter, 1980; Henmi and Bresch, 1985; Samson, 1980; Artz *et al.*, 1985 among others). Wind data for the trajectory analyses are usually provided directly by the synoptic meteorological radiosonde network or more recently by numerical models (e.g. Warner *et al.*, 1983). However, because of the horizontal resolution of this network (~300 to ~500 km), it is incapable of resolving the impact of mesoscale systems such as valley/ridge thermally induced flows which are generally of a horizontal scale less than 200 km. Additionally, the temporal resolution of observational synoptic networks (typically 12 h) is comparable to the lifetime of these mesoscale systems; thus, even the temporal variations in the mesoscale induced flows cannot be adequately sampled. The regional numerical models generally have a grid spacing in the range of 25–100 km, so only atmospheric features larger than around 100–400 km can be resolved (assuming that at least four grid intervals are needed to resolve the feature).

The mesoscale systems involved with valley/ridge thermal forcing are anticipated to produce major alterations of the regional pollution transport. They are widespread in nature with typical examples including geographical locations such as the rugged terrain of the Colorado River basin, the Appalachians ridge–valley region, and the Rhine valley in Germany, among others.

The present study is oriented toward an illustration and evaluation of the impact of thermally induced valley/ridge circulations on regional transport. For this purpose several generic numerical mesoscale model simulations were carried out while considering regional transport across an elongated valley/ridge region. Refined horizontal and vertical grid resolutions were adopted in order to adequately resolve the meteorological fields induced by these terrain features. The numerical model provides the meteorological wind and turbulence fields used as input to a Lagrangian dispersion scheme (as outlined in section 2). Adopting these modeling tools, pollutant volumes represented by fields of particles were followed as they crossed the terrain. For these experiments, each assumed volume consisted of a dense array of particles initially located on the boundary of the simulated domain with a horizontal extent of 15 km and a depth of several hundred meters. Such volumes were released at different hours of the day, for summer and winter conditions. Using the discrete volume releases it is possible to infer the behavior of continuous transport which can be viewed as an ensemble of such discrete masses. Results of the model simulations are given in section 3, while in section 4 a conceptual evaluation for the generalized phenomenon is outlined.

2. MODELING ASPECTS

2.1. *Numerical mesoscale meteorological model*

The formulation of the numerical mesoscale model used in the present study is given in detail in Pielke

Contemporary Physics, 1990, volume 31, number 4, pages 247–260

Remote measurement of atmospheric parameters: new applications of physics with lasers

C. Y. She

Basic optical processes, e.g. absorption, fluorescence, Raman and Rayleigh scattering, that are relevant to lidar applications are briefly described and the principle and relative merits of existing lidar (light detection and ranging) techniques reviewed. The potential and physics of high-spectral-resolution lidar techniques, which currently are in the developmental stage, are discussed in this paper.

1. Introduction

There are at least two motivations for investigating the Earth's atmosphere: that of scientific curiosity and that of practical necessity. It is of fundamental interest to understand the structure of Nature and processes within it, and we must evaluate the effect of man's activity on the fragile balance of Earth's environment. The recent discovery of the ozone hole in the Antarctic (Farman *et al.*, 1985) which could reduce Nature's protection against harmful u.v. radiation, and the recent measurement of the steady increase in CO_2 concentration in the atmosphere, which could lead to (what is still controversial) global warming (Slingo 1989), are examples which kindle public concerns and command urgent scientific activities. In order to understand the dynamics of the atmosphere and the interaction of her natural components and her reaction to air pollutants, direct measurements of atmospheric parameters and species concentrations in a temporally- and spatially-resolved manner are essential.

With the advent of lasers, such measurements can be done remotely from earth-based (stationary or mobile) and/or airborne stations. Many interactive processes between optical radiation and atoms and molecules have been exploited and used to measure parameters of interest to atmospheric as well as enviromental scientists. These include atmospheric temperature and pressure, winds, and aerosol and minor species concentrations. Most of these processes are well known and have been studied earlier in the laboratory. In fact, all operation lidar (light detection and ranging) techniques for remote measurements can be best understood when described in terms of, and compared with, experiments in a physics laboratory. Therefore, this paper will first discuss relevant optical processes, such as optical absorption, fluorescence, Raman and Rayleigh scattering, in the context of a laboratory experiment before reviewing the principles of different types of existing lidar techniques and their up to date achievements.

However, aspects of the interactions involving spectrally-resolved characteristics in a resonance and/or scattering process which require the use of narrowband ($\sim$100 MHz) tunable lasers for their investigation, are quite new. The advantages of using high-spectral-resolution techniques for atmospheric measurements are just being realized. The potential and physics of high-spectral-resolution lidar (HSRL) techniques, including a proposed application for measuring atmospheric temperature from ground to mesopause some 100 km up, will then be discussed.

It is well known that as a result of photo-ionization in the upper atmosphere, photo-dissociation of ozone molecules, and solar heating of the earth's surface, the atmosphere is divided into layers of altitudes according to its temperature structure as the Σ-shape curve shown in figure 1. The layer boundaries, marked by short horizontal lines, are denoted as 'pause' with an identifying prefix referred to the layer below it. The altitude and thickness of the tropopause has a seasonal as well as geographical dependence; its mean height in the mid-latitudes is about 11 km. Dynamically speaking, the transport of atmospheric constituents depends upon both processes of molecular diffusion and turbulent mixing. At the turbopause, these two processes are equally effective; below it, turbulent mixing or eddy diffusion dominates the dynamics of air motion

Author's address: Department of Physics, Colorado State University, F. Collins, Colorado 80523, U.S.A.

Optics Letters, 17(7), 541-543 (1992)

High-spectral-resolution Rayleigh-Mie lidar measurement of aerosol and atmospheric profiles

C. Y. She, R. J. Alvarez, II, L. M. Caldwell, and D. A. Krueger

Department of Physics, Colorado State University, Fort Collins, Colorado 80523

Received January 17, 1992

ABSTRACT

We report what is, to our knowledge, the first demonstration simultaneous measurement of tropospheric temperature and aerosol extinction coefficient profiles using a high-spectral-resolution Rayleigh-Mie lidar. With the pressure at a single reference height independently provided, our lidar inversion is capable of deducing the vertical atmospheric profiles, including temperature, pressure, and density, as well a aerosol profiles, including backscatter ratio, extinction coefficient, and backscatter phase function.

Appl. Phys., B55, 154-158 (1992)

High-Spectral-Resolution Rayleigh-Mie Lidar Measurement of Vertical Aerosol and Atmospheric Profiles

C. Y. She, R. J. Alvarez II, L. M. Caldwell, and D. A. Krueger

Physics Department, Colorado State University

Fort Collins, CO 80523, U. S. A.

FAX (303)-491-7947

Abstract. A new two-channel ground-based high-spectral-resolution Rayleigh-Mie lidar and its operation is described. Upon the inversion of data collected during the night of August 14-15, 1990 with this unique lidar system, vertical profiles of atmospheric parameters including temperature, potential temperature, pressure and density, as well as aerosol parameters including backscatter-ratio, extinction coefficient and backscatter phase function are determined.

PACS: 42.68.R, 94.10.D, 92.60.M

1. Introduction

Vertical profiles of aerosol and atmospheric properties are of considerable importance to atmospheric studies. The necessary information can be determined from Rayleigh-Mie scattering of the atmosphere, if aerosol and molecular scattering components can be effectively separated[1]. In 1983, we suggested [2] that the use of a narrowband lidar system along with atomic resonance blocking filters has the sensitivity needed for a simultaneous measurement of backscatter ratio and atmospheric temperature. After years of technical development as well as theoretical improvements to include rotational Raman scattering and the pressure dependence of Rayleigh scattering into the data analysis, we have recently reported the first determination[3] of vertical profiles of atmospheric temperature, and aerosol extinction coefficient up to a height of 5 km with a 8 inch receiving telescope. The details on the principle and practice of the self-consistent lidar inversion technique[4] for the high-spectral-resolution Rayleigh-Mie lidar and the result of the atmospheric

GEOPHYSICAL RESEARCH LETTERS, VOL. 17, NO. 7, PAGES 929-932, JUNE 1990

TWO-FREQUENCY LIDAR TECHNIQUE FOR MESOSPHERIC Na TEMPERATURE MEASUREMENTS

C. Y. She, H. Latifi, J. R. Yu, R. J. Alvarez II and
*Department of Physics, Colorado State University

R. E. Bills, C. S. Gardner
+Department of Electrical and Computer Engineering, University of Illinois at Urbana-Champaign

Abstract. We describe a new two-frequency lidar for measuring Na temperature profiles that uses a stabilized cw single-mode dye laser oscillator (rms frequency jitter < 1 MHz) followed by a pulsed-dye power amplifier (140 MHz FWHM linewidth) which is pumped by an injection-locked Nd:YAG laser. The laser oscillator is tuned to the two operating frequencies by observing the Doppler-free structure of the Na D_2 fluorescence spectrum in a vapor cell. The lidar technique and our initial observations of the temperature profile between 82 and 102 km at Ft. Collins, CO (40.6°N,105°W) are described. Absolute temperature accuracies at the Na layer peak of better than ±3 K with a vertical resolution of 1 km and an integration period of approximately 5 min were achieved.

Introduction

Studies of the middle atmosphere are incomplete without accurate knowledge of the temperature structure. High temporal and spatial resolution are needed for probing short-wavelength gravity and tidal waves. Unfortunately, the mesopause region is one of the most difficult to study experimentally even with remote sensing techniques. Rocket launched falling spheres [Philbrick et al., 1985] and grenades [Theon et al., 1972], airglow observations [e.g. Sivjee and Hamwey, 1987] and nadir viewing satellites such as Nimbus 6 and 7 [e.g. Andrews et al., 1987] have all provided useful information on the temperature near the mesopause. However, none of these techniques are capable of providing the accuracy, resolution and long-term coverage needed for detailed studies of small scale temperature fluctuations.

Lidar techniques offer the greatest promise for high resolution observations of the temperature structure of the stratosphere and mesosphere. Rayleigh lidars are now used routinely to infer temperature profiles from about 30 to 80 km altitude [Chanin et al., 1985] and theoretically, can be designed to measure temperatures at altitudes exceeding even 100 km. However at mesopause heights, laser powers of ~ 100 W and telescope diameters of ~ 8 m are required to obtain reasonable vertical resolution (~ 1 km) and integration periods (~ 5 min) [Gardner, 1989].

High resolution temperature profiles of the mesopause region can also be obtained by active probing of the thermally broadened Na resonance line using comparatively low-power narrowband lidars. This idea was first applied by Gibson et al. [1979] who were able to deduce the temperature near the peak of the Na layer. More recently, Fricke and von Zahn [1985] have routinely obtained Na temperature profiles above Andoya, Norway using an excimer-pumped dye laser system. Because the frequency of their pulsed laser system was neither reproducible nor predictable, the relative frequency of each individual laser pulse was measured with a wavelength meter and the laser output was scanned over a relatively wide frequency range to adequately cover the Na fluorescence spectrum. In addition, the laser lineshape function could not be accurately measured. The absolute frequencies of the laser pulses were calibrated against all Na returns obtained during each night. By using this technique the authors report an uncertainty of ±5 K at the layer peak with an integration period of 10 min and a vertical resolution of 1 km [Neuber et al., 1988].

We present our initial measurements of the mesopause region temperatures above Ft. Collins, CO (40.6°N, 105°W) obtained using the new two-frequency Na lidar system. The laser configuration, expected temperature measurement accuracies, and the initial observations are discussed.

Paper number 90GL00868
0094-8276/90/90GL-00866$03.00

Technique and Lidar System

The ratio of the Na fluorescence signal near the minimum between the D_{2a} and D_{2b} peaks to the value near the stronger D_{2a} peak is a very sensitive indicator of temperature. To measure temperature accurately using the two-frequency technique, the absolute frequency and lineshape of the tunable laser must be known precisely and remain constant from pulse to pulse at a given frequency setting. In this experiment the cw laser was tuned precisely to the fluorescence features of a Na vapor cell. Because the cell was heated to about 48°C, the Doppler-broadened width of the Na fluorescence line (1.36 GHz FWHM) was too broad to be useful as a frequency reference. However, the rear window of the vapor cell was designed to retro-reflect a fraction (~ 10%) of the laser beam. Under simultaneous illumination of 2 counter-propagating beams at a saturated intensity (~ 0.4 mW/mm^2), the Na fluorescence spectrum exhibits Doppler-free features at the D_{2a} and D_{2b} peaks (f_a and f_b) and at the cross-over resonance (f_c). These features are similar to those observed with Doppler-free saturated absorption spectroscopy [Hansch et al., 1971].

A Na cell fluorescence spectrum measured during our lidar observations is plotted in Figure 1 along with the theoretical unsaturated spectrum for Na at a temperature of 187 K. The 3 Doppler-free features are distinctly visible in the saturated spectrum. Due to theoretical and experimental uncertainties we can only determine the location of these features to within ±10 MHz at f_a = -648.8 MHz, f_b = 1066.9 MHz and f_c = 200.3 MHz.

We chose f_a and f_c as the 2 operational frequencies for mesospheric temperature measurements. Since f_a is at the D_{2a} peak and f_c is close to the minimum between the D_{2a} and D_{2b} peaks (f_{min} = 300 MHz @ 200K), the fluorescence signal level from the Na layer at these 2 frequencies is relatively insensitive to small frequency errors in the laser. Unlike f_{min} which depends on temperature, both f_a and f_c are temperature independent, a characteristic that simplifies the calculation of temperature from the measured ratio of the fluorescence signals.

Figure 2 is a block diagram of our laser transmitter. The major lidar system parameters are summarized in Table 1. The transmitter includes a cw frequency-stabilized single-mode dye laser oscillator followed by a pulsed dye amplifier. The oscillator is optically pumped by an Ar^+ laser and the amplifier is pumped by an injection-locked frequency-doubled Nd:YAG laser. Since the Nd:YAG laser is injection-seeded, the pulse shapes of the Nd:YAG laser and the dye amplifier are smooth

Na TEMPERATURE LIDAR MEASUREMENTS OF GRAVITY WAVE PERTURBATIONS OF WIND, DENSITY AND TEMPERATURE IN THE MESOPAUSE REGION

C. Y. She, J. R. Yu, J. W. Huang and C. Nagasawa

Department of Physics, Colorado State University

C. S. Gardner

Department of Electrical and Computer Engineering, University of Illinois at Urbana-Champaign

Abstract. High resolution temperature profiles of the mesopause region above Fort Collins, CO (40.6°N,105°W) were measured with a Na lidar on the nights of March 2-3 and April 15-16, 1990, during the ALOHA-90 campaign. This paper reports the initial scientific analysis of these data which were used to compute (1) the altitude profiles of relative atmospheric temperature perturbations, (2) the mean Brunt-Vaisala frequency in the mesopause region, and (3) the vertical shear variance of horizontal winds. On March 2-3 and April 15-16, the rms temperature perturbations were 5.7 % and 7.1 %, the average Brunt-Vaisala periods were 4.9 min and 4.6 min, and the wind shear variances were 878 $(ms^{-1}/km)^2$ and 967 $(ms^{-1}/km)^2$, respectively.

Introduction

Gravity waves play a major role in establishing the temperature and wind structure of the mesopause region and have a significant influence on the spatial and temperature structure of the Na layer. Horizontal wind perturbations, u', caused by gravity waves are readily measured by radar [e.g. Vincent and Fritts, 1987], while the relative atmospheric density perturbations, $(\rho'_a/\bar{\rho}_a)$, can be measured by Rayleigh and Na lidars [e.g. Gardner et al., 1989]. Note we use the standard notation of denoting perturbation quantities with a prime and mean quantities with an overbar. Gravity wave perturbations in air density, temperature and winds are related by the polarization and dispersion relations first derived by Hines [1960]. The gravity wave polarization relations can be used to express the variances of horizontal winds in terms of the relative density perturbations as

$$< (u')^2 > = (g/N)^2 < (\rho_a'/\bar{\rho}_a)^2 > \qquad (1)$$

where g is the gravitational acceleration and N is the Brunt-Vaisala (angular) frequency which may be calculated from atmospheric temperature lapse rate, $\alpha = dT/dz$, as

$$N^2 = [\ (\gamma - 1) + \gamma\,(dH/dT)\ ]\ g^2/c^2 = g\,(\alpha - \alpha^*)/T \qquad (2)$$

where H, T, c and α^*(= 9.5 K/km in the mesopause region) are, respectively, scale height, temperature, adiabatic sound speed, and adiabatic lapse rate. In order to substantiate the commonly held view that the perturbations in density, temperature and winds observed at mesopause heights are caused by the propagating gravity waves, simultaneous lidar-radar experiments are required to compare the variances of horizontal winds and the relative density perturbations and to verify Eq. (1). This comparison also requires an accurate measurement of the Brunt-Vaisala frequency, N.

In the mesopause region, molecular scattering is too weak to permit the use of existing Rayleigh lidars for the measurement of atmospheric temperature profiles with high accuracies and resolution [Gardner et al., 1989]. Until recently, the only relevant information that could be derived from a (broadband) Na lidar was the relative atmospheric density perturbation, $\rho_a'/\bar{\rho}_a$, which may be determined from the measured relative Na density perturbation, $\rho_s'/\bar{\rho}_s$, through [Senft and Gardner, 1991]

$$\rho_s'(z,t)/\bar{\rho}_s = \{[1 - \gamma H(z - z_0)/\sigma_0^2]/(1 - \gamma)\}\,\rho_a'(z,t)/\bar{\rho}_a \qquad (3)$$

where z_0 and σ_0 are the centroid height and rms thickness of the unperturbed Na layer. Since the altitude dependent scaling factor in Eq. (3) vanishes near the Na layer peak, it is not possible to determine atmospheric density perturbations near z_0. Furthermore, since the Brunt-Vaisala frequency can not be measured with a broadband Na lidar, the relationship between wind and density perturbation, Eq.(1), can not be established accurately.

With the new two-frequency narrowband Na lidar, high-resolution atmospheric temperature profiles can now be measured continuously throughout the mesopause region [She et al., 1990; Bills et al., 1991]. Since pressure fluctuations in the atmosphere are negligible in comparison with the associated density and temperature fluctuations, relative atmospheric density perturbations are equal to the negative of the measured relative temperature perturbations, $(\rho_a'/\bar{\rho}_a) = -(T'/\bar{T})$. Therefore, the measured temperature profile can also be used to determine the variance of the relative density perturbation, $< (\rho_a'/\bar{\rho}_a)^2 >$, as well as the temperature lapse rate, α, and, thereby the Brunt-Vaisala frequency, N. These results together can be used to calculate variance of the horizontal wind perturbation, $< (u')^2 >$. The relative temperature perturbation can also be used to calculate the vertical gradient (or shear) of relative density perturbations and horizontal winds, and their variances, $<[d(\rho_a'/\bar{\rho}_a)/dz]^2>$ and $< (du'/dz)^2 >$. These results can then be used to quantify the dynamic stability of the region by computing the Richardson number [Hines, 1991; Senft and Gardner, 1991]

$$R_i = N^2 / < (du'/dz)^2 > = N^4 / [g^2 < [d(\rho_a'/\bar{\rho}_a)/dz]^2 >] \qquad (4)$$

By using the temperature profiles measured by the Colorado State narrowband Na lidar during ALOHA - 90 campaign, we report the first determination of the vertical profiles of relative density perturbation and the mean Brunt-Vaisala frequency of gravity waves in the mesopause region. In addition, the inferred rms horizontal winds and the vertical shear variance of horizontal winds as well as the Richardson number are determined.

Paper number 91GL01517
0094-8534/91/91GL-01517$3.00

High-spectral-resolution fluorescence light detection and ranging for mesospheric sodium temperature measurements

C. Y. She, J. R. Yu, H. Latifi, and R. E. Bills

The principle and practice of narrow-band light detection and ranging (lidar) for temperature measurements are discussed with the emphasis on a new two-frequency technique for measuring mesospheric Na temperature and density profiles. The uniqueness of this narrow-band lidar lies in the transmitter whose line-shape function can be measured directly. The frequency of the laser output can be monitored simultaneously during data acquisition with Doppler-free fluorescence spectroscopy by using a laboratory Na cell. These measurement techniques, along with the procedures for data analysis are described in detail. At present the absolute temperature accuracy at the ~a layer peak is ± 3 K (± 4 K), with a vertical resolution of 1 km and an integration period of 5 min (2.5 min). Potential applications and further improvements in this lidar technique are also discussed.

Key words: Na temperature lidar, mesopause.

Reprinted from JOURNAL OF THE ATMOSPHERIC SCIENCES, Vol. 47, No. 24, 15 December 1990
American Meteorological Society

Analytical Solutions to the Collection Growth Equation: Comparison with Approximate Methods and Application to Cloud Microphysics Parameterization Schemes

JOHANNES VERLINDE,* PIOTR J. FLATAU AND WILLIAM R. COTTON

Colorado State University, Department of Atmospheric Science, Fort Collins, Colorado

(Manuscript received 24 January 1990, in final form 11 May 1990)

ABSTRACT

A closed form solution for the collection growth equation as used in bulk microphysical parameterizations is derived. Although the general form is mathematically complex, it can serve as a benchmark for testing a variety of approximations. Two special cases that can immediately be implemented in existing cloud models are also presented. This solution is used to evaluate two commonly used approximations. The effect of the selection of different basis functions is also investigated.

1. Introduction

The numerical treatment of the collection growth of precipitation particles has long been a problem in two- and three-dimensional cloud modeling. This paper examines exact and approximate solutions to the collection equation as applied to the prediction of mixing ratios of hydrometeor species in cloud models (Wisner et al. 1972; Cotton et al. 1982). The form of the collection equation that is used is the integrated form of the stochastic collection equation as applied to two different species interacting. This equation plays an important role in the bulk parameterization schemes of cloud microphysics in two- and three-dimensional cloud models, and is employed in several models currently in use (Orville and Kopp 1977; Passarelli and Srivastava 1979; Hsie et al. 1980; Cotton et al. 1982; Lin et al. 1983; Rutledge and Hobbs 1983). The solution is derived for the general form where water content may be distributed according to any of the family of gamma-type distributions. Fast solutions for self-collection as well as hail/rain interaction are obtained. Approximation schemes that are currently in use are compared to the exact solution of this integral.

The paper is organized as follows: Bulk parameterization schemes and their use in cloud and mesoscale models are discussed first. Subsequently, the collection equation defining the change in mixing ratio due to conversion between two water categories is discussed. The accretional (continuous) growth approximation and the approximation suggested by Wisner et al. (1972) are discussed there. The general solution is then derived. This is the main theoretical result of this paper. The special cases of hail collecting rain and selfcollection are also discussed. Comparisons between the approximate and the new analytical solution are given for several typical types of interactions. Finally, some discussion on the application of these results are given.

2. Bulk parameterization schemes

The primary aim of bulk parameterization schemes is to capture in a few simple formulas the essential physics embodied in more general theoretical models. It is assumed that the water content in a cloud can be categorized in different species, which, for this problem, interact through collision and coalescence. A typical division of species would be to discriminate between cloud water, rain water, pristine ice, snow/aggregates and graupel/hail. It is further assumed that for each of these categories the water content is distributed according to a specified continuous size distribution, typically one of the gamma-type family, lognormal, or even monodispersed.

The bulk microphysics approach is to assume that only the moments of size distributions such as total water content (the third moment) or the total concentration (the zeroth moment) are important for cloud evolution. Exact knowledge of the spectrum evolution is considered to be of lesser importance. Typically, only one moment of the distribution is carried as a prognostic variable in the model, although some of the more sophisticated models use two moments as prognostic variables. For a three-parameter distribution this then implies that either one or two distribution parameters have to be fixed. Equations describing the physics of the process are integrated over the assumed distribu-

* On special leave from the South African Weather Bureau.

Corresponding author address: Johannes Verlinde, Department of Atmospheric Science, Colorado State University, Fort Collins, CO 80523.

Reprinted from JOURNAL OF THE ATMOSPHERIC SCIENCES, Vol. 47, No. 5, 1 March 1990
American Meteorological Society

Multiparameter Radar Modeling and Observations of Melting Ice

J. VIVEKANANDAN, V. N. BRINGI AND R. RAGHAVAN

Department of Electrical Engineering, Colorado State University, Fort Collins, Colorado 80523

(Manuscript received 25 January 1989, in final form 29 August 1989)

ABSTRACT

This paper uses a microphysically detailed graupel and hail melting model, described by Rasmussen and Heymsfield, which is coupled to a radar model that computes multiparameter variables such as differential reflectivity, linear depolarization ratio, the specific propagation differential phase shift and X-band specific attenuation. The microphysical model is initialized with two different summer-time sounding profiles (Colorado and Alabama). Sensitivity studies are performed with respect to particle shape and orientation distributions. The hail melting model is also initialized with a summertime sounding from the Munich, FRG area, and C-band differential reflectivity is computed for application to radar data from the DFVLR radar. A simple spherical hail melting model is also used to study the effects of absorption and scattering on the X-band attenuation. NCAR CP-2 radar measurements from the MIST (Microburst and Severe Thunderstorm) project and from CINDE (Convective Initiation and Downburst Experiment) are used to illustrate the usefulness of multiparameter data in studying the melting of ice in convective storms.

1. Introduction

Downdrafts that cause strongly divergent and damaging winds near the surface pose a serious problem for aviation safety leading to many studies of the downburst phenomena, Fujita (1985). Wet downbursts are accompanied by an intense precipitation shaft. Srivastava (1987) has used a numerical model to study intense downdrafts forced by the melting and evaporation of precipitation. He found that the melting and evaporation of precipitation and precipitation loading below cloud base were sufficient to produce wet downbursts. Cooling due to ice melting was found to be concentrated in a narrow layer of the atmosphere. He also found that, "As the stability of the lapse rate is increased, higher precipitation contents, precipitation in the form of ice, and relatively higher concentrations of small precipitation particles are required to force an intense downdraft".

Multiparameter radar measurements based on dual-polarization and dual-frequency techniques (in addition to conventional Doppler parameters) can play an important role in the remote sensing of the microphysics of the precipitation downdraft. Wakimoto and Bringi (1988) and Tuttle et al. (1989) have used the NCAR CP-2 multiparameter radar as the central tool in studying the microphysical evolution of an intense microburst-producing storm during the summer of 1986 near Huntsville, Alabama. They found that the differential reflectivity (Z_{DR}) and the specific attenuation at X-band (A_X) were important measureables related to the microphysical evolution of the cloud. In particular, the vertical profiles of Z_{DR} and A_X within the storm core could be related to the precipitation content, type and phase, well before the strongly divergent winds appeared at the surface.

Both dual-polarized and dual-frequency techniques are now fairly well established and can yield significantly more microphysical information than the conventional reflectivity factor. Hall et al. (1980, 1984) were the first to show that Z_{DR} could be used to differentiate between rain and ice, while Bringi et al. (1986a) used a coupled graupel melting and radar model together with aircraft 2D-PMS data to show that the vertical profile of Z_{DR} was an excellent indicator of the onset and progression of melting ice into raindrops. Hail detection using the Z_{DR} technique is well documented by Bringi et al. (1984, 1986b) and Illingworth et al. (1987). The measurement of attenuation using dual-frequency methods is documented in Eccles and Mueller (1973), Eccles (1979), and Tuttle and Rinehart (1983). In rainfall and at long wavelengths Z_{DR} is an excellent estimator of the reflectivity-weighted mean axis ratio of the raindrops filling the radar resolution volume, while the X-band specific attenuation is related to approximately the fourth moment of the raindrop size distribution, Jameson (1983a,b). Recently, the specific propagation differential phase shift (K_{DP}) in rainfall has been measured using an algorithm derived by Mueller (1984) at the National Severe Storms Laboratory (NSSL), Sachidananda and Zrnić (1986, 1987) and by Golestani et al. (1989) using the CP-2 radar. This parameter is related to nearly the 4th mo-

Corresponding author address: Dr. V. N. Bringi, Dept. of Electrical Engineering, Colorado State University, Fort Collins, CO 80523.

Reprinted from JOURNAL OF APPLIED METEOROLOGY, Vol. 30, No. 10, October 1991
American Meteorological Society

Ice Water Path Estimation and Characterization Using Passive Microwave Radiometry

J. VIVEKANANDAN, J. TURK AND V. N. BRINGI

Department of Electrical Engineering, Colorado State University, Fort Collins, Colorado

(Manuscript received 6 September 1990, in final form 14 March 1991)

ABSTRACT

Microwave emission emerging from a precipitating cloud top and lying in a radiometer's field of view represents the culmination of a complex interaction between emitted microwave radiation and its ongoing extinction through overlapping regions of liquid, melting phase, and ice. The encounter with the ice region represents the final interaction between the upwelling microwave radiation and the cloud constituents. Hence, an ice phase characterization perhaps represents a more inherently retrievable property from a combination of scattering-based channels above 37 GHz than the underlying rainfall. Model computations of top-of-atmospheric microwave brightness temperatures T_B from layers of precipitation-sized ice of variable bulk density and ice water content (IWC) are presented. The 85-GHz T_B is shown to depend essentially on the ice optical thickness, while the possibility of using the 37- and 85-GHz brightness temperature difference ΔT_B to estimate the integrated ice water path (IWP) is investigated. The results demonstrate the potential usefulness of using scattering-based channels to characterize the ice phase and suggest a top-down methodology for retrieval of cloud vertical structure and precipitation estimation from multifrequency passive microwave measurements.

Radiative transfer model results using the multiparameter radar data initialization from the Cooperative Huntsville Meteorological Experiment (COHMEX) in northern Alabama are also presented. The vertical behavior of the simulated multifrequency T_B, albedo, and extinction is presented along with the associated multiparameter radar measurements during the cloud lifecycle. Ice water path values estimated from the radar measurements are compared with the above theoretical computations for the corresponding T_B values and show agreement for values of IWP less than 1 kg m^{-2}. Above this, assumptions in the form of the ice-size distribution fail to adequately characterize the ice scattering process. Brightness temperature T_B warming effects due to the inclusion of a cloud liquid water profile are shown to be especially significant at 85 GHz during later stages of cloud evolution.

1. Introduction

The fundamental behavior of top-of-atmosphere (TOA) brightness temperatures at millimeter wavelengths is well known (Wu and Weinman 1984; Wilheit 1986; Spencer et al. 1989). Emission-based schemes function over oceans near operating frequencies of 19 GHz, where light to moderate precipitation rates cause a brightness temperature T_B increase over the radiometrically cold ocean surface. Scattering effects saturate the emission signal beyond a rain rate R of 20 mm h^{-1}. As the operating frequency increases, rapid increases of the volume scattering coefficient ultimately give rise to significant scattering of the cumulative upwelling radiation away from the radiometer field of view. Near 90 GHz, the single scattering coefficient for ice exceeds that of rain past a rain rate of about 10 mm h^{-1}, resulting in a cold TOA T_B. Unlike the emission-based method, the dynamic range of the scattering-based method is high (i.e., the slope of any theoretical T_B versus R curve is highly negative over a wide range of rain rates) when precipitation-sized ice particles are present and the underlying surface is essentially opaque past a few millimeters per hour.

Combinations of both emission- and scattering-based methods perhaps represent the best hope for passive spaceborne sensing of precipitation, independent of the underlying surface (Simpson et al. 1988). Essentially, the emission signal originates in the liquid and melting phase hydrometeors (lower altitudes, lower frequencies), while the scattering "signal" modulates the emission signal, mainly in regions of ice (higher altitudes, higher frequencies). Since TOA brightness temperatures represent a vertically integrated effect at the frequency of interest, the vertical structure of the hydrometeor phase and type and the associated size and shape distributions determine the intensity of the microwave emission and extinction. Recently, significant contributions to the understanding of the evolution of T_B behavior have resulted from coupling of either cloud model output or radar observations to microwave radiative transfer models. Smith and Mugnai (1988) and Mugnai and Smith (1988) examined the time evolution of the cloud-drop distribution in a time-dependent cloud model, noting the tendency for cloud

Corresponding author address: Dr. Vivekanandan, Dept. of Electrical Engineering, Colorado State University, Fort Collins, CO 80523.

Reprinted from JOURNAL OF APPLIED METEOROLOGY, Vol. 29, No. 7, July 1990
American Meteorological Society

Microwave Radiative Transfer Studies Using Combined Multiparameter Radar and Radiometer Measurements during COHMEX

J. VIVEKANANDAN AND J. TURK

Department of Electrical Engineering, Colorado State University, Fort Collins, Colorado

G. L. STEPHENS

Department of Atmospheric Sciences, Colorado State University, Fort Collins, Colorado

V. N. BRINGI

Department of Electrical Engineering, Colorado State University, Fort Collins, Colorado

(Manuscript received 26 June 1989, in final form 7 December 1989)

ABSTRACT

Theoretical calculations of the upwelling microwave radiances from clouds containing layers of rain, ice, and a melting region were performed at frequencies of 18, 37, and 92 GHz. These frequencies coincide with high-resolution microwave radiometer measurements taken aboard the NASA ER-2 high-altitude aircraft during the summer 1986 COHMEX (Cooperative Huntsville Meteorological Experiment) in Alabama. For purposes of brightness temperature computations, the storms were modeled with rain, melting phase, and ice layers. The melting phase region was composed of water-coated ice spheres defined by a "melt index" in terms of the volume fraction of water. Single scatter albedo, scattering, and extinction coefficients were computed at the above frequencies as a function of the rain rate and melt index. In addition, multiparameter radar observations of the storm were mapped into a cartesian space and averaged over regions comparable to the radiometer footprint. Vertical profiles of these data under the ER-2 flight path were constructed to reveal quantitative estimates of regions of rain, melting, and ice phases, and also to retrieve a two-parameter exponential size distribution. This information was used to compute extinction coefficients and Mie phase matrices for each layer of specified microphysical characteristics. Upwelling multifrequency brightness temperatures were computed using plane-parallel radiative transfer modeling, and compared with those observed by the ER-2 airborne radiometers.

1. Introduction

With the increasing importance of the satellite remote sensing of global rainfall patterns, interpretation of microwave radiometer measurements over both land and ocean offers a fundamental advantage over traditional visible imager techniques. Whereas satellite-borne visible imagers see only the tops of both precipitating and nonprecipitating clouds, passive microwave radiometers are able to see through regions of overlying ice or high cirrus clouds, depending on the frequency of operation. The behavior of the brightness temperatures T_B upwelling from regions of both liquid and ice phase hydrometeors at or near the typical operating frequencies of 18, 22, 37, and 90 GHz is well documented. Early work of Wilheit et al. (1977) considered the emission from rain as measured at 19 GHz by the Electronically Scanning Microwave Radiometer (ESMR-5) over the Gulf of Mexico, and compared the results of a radiative transfer model to the rain rates as derived from radar. At this frequency, extinction by most precipitation-sized hydrometeors is dominated by absorption. As the rainfall rate increases, the resulting emission will result in an increase in the upwelling brightness temperature over a cold ocean surface. Emission methods have limited dynamic range; however, as the 18 GHz emission signal saturates beyond a certain rain rate, typically near 15 mm h^{-1} (Spencer 1986), so the brightness temperature will level off due to emission from increasingly higher altitude (colder) rain. This threshold occurs at successively lower rain rates as the passive emission frequency increases. In addition, the emission at this microwave frequency can be caused by either rain or nonprecipitating cloud water. Also, the variable gain across the large earth footprint of radiometers at these frequencies in relation to the horizontal dimensions of the rain region will typically lead to an underestimate of the higher rain rates (Lovejoy and Austin 1980), due to effects from finite clouds and the underlying surface,

Corresponding author address: Dr. J. Vivekanandan, Dept. of Electrical Engineering, Colorado State University, Fort Collins, CO 80523.

Journal of Applied Meteorology - August 1991

Ice Water Path Estimation and Characterization Using Passive Microwave Radiometry

J. VIVEKANANDAN, J. TURK AND V. N. BRINGI

Department of Electrical Engineering, Colorado State University, Fort Collins, Colorado

(Manuscript received 6 September 1990, in final form 14 March 1991)

ABSTRACT

Microwave emission emerging from a precipitating cloud top and lying in a radiometer's field of view represents the culmination of a complex interaction between emitted microwave radiation and its ongoing extinction through overlapping regions of liquid, melting phase, and ice. The encounter with the ice region represents the final interaction between the upwelling microwave radiation and the cloud constituents. Hence, an ice phase characterization perhaps represents a more inherently retrievable property from a combination of scattering-based channels above 37 GHz than the underlying rainfall. Model computations of top-of-atmospheric microwave brightness temperatures T_B from layers of precipitation-sized ice of variable bulk density and ice water content (IWC) are presented. The 85-GHz T_B is shown to depend essentially on the ice optical thickness, while the possibility of using the 37- and 85-GHz brightness temperature difference ΔT_B to estimate the integrated ice water path (IWP) is investigated. The results demonstrate the potential usefulness of using scattering-based channels to characterize the ice phase, and suggest a top-down methodology for retrieval of cloud vertical structure and precipitation estimation from multifrequency passive microwave measurements.

Radiative transfer model results using the multiparameter radar data initialization from the Cooperative Huntsville Meteorological Experiment (COHMEX) in northern Alabama are also presented. The vertical behavior of the simulated multifrequency T_B, albedo, and extinction is presented along with the associated multiparameter radar measurements during the cloud lifecycle. Ice water path values estimated from the radar measurements are compared with the above theoretical computations for the corresponding T_B values, and show agreement for values of IWP less than 1 kg m^{-2}. Above this, assumptions in the form of the ice size distribution fail to adequately characterize the ice scattering process. Brightness temperature T_B warming effects due to the inclusion of a cloud liquid water profile are shown to be especially significant at 85 GHz during later stages of cloud evolution.

1. Introduction

The fundamental behavior of top-of-atmosphere (TOA) brightness temperatures at millimeter wavelengths is well known (Wu and Weinman 1984; Wilheit 1986; Spencer et al. 1989). Emission-based schemes function over oceans near operating frequencies of 19 GHz, where light to moderate precipitation rates cause a brightness temperature T_B increase over the radiometrically cold ocean surface. Scattering effects saturate the emission signal beyond a rain rate R of 20 mm h^{-1}. As the operating frequency increases, rapid increases of the volume scattering coefficient ultimately give rise to significant scattering of the cumulative upwelling radiation away from the radiometer field of view. Near 90 GHz, the single scattering coefficient for ice exceeds that of rain past a rain rate of about 10 mm h^{-1}, resulting in a cold TOA T_B. Unlike the emission-based method, the dynamic range of the scattering-based method is high (i.e., the slope of any theoretical T_B vs R curve is highly negative over a wide range of rain rates) when precipitation-sized ice particles are present and the underlying surface is essentially opaque past a few millimeters per hour.

Combinations of both emission- and scattering-based methods perhaps represent the best hope for passive spaceborne sensing of precipitation, independent of the underlying surface (Simpson et al. 1988). Essentially, the emission signal originates in the liquid and melting phase hydrometeors (lower altitudes, lower frequencies), while the scattering "signal" modulates the emission signal, mainly in regions of ice (higher altitudes, higher frequencies). Since TOA brightness temperatures represent a vertically integrated effect at the frequency of interest, the vertical structure of the hydrometeor phase and type and the associated size and shape distributions determine the intensity of the microwave emission and extinction. Recently, significant contributions to the understanding of the evolution of T_B behavior have resulted from coupling of either cloud model output or radar observations to microwave radiative transfer models. Smith and Mugnai (1988) and Mugnai and Smith (1988) examined the time evolution of the cloud-drop distribution in a time-dependent cloud model, noting the tendency for cloud liquid water to bias those theoretical T_B-R relations

Corresponding author address: Dr. Vivekanandan, Dept. of Electrical Engineering, Colorado State University, Fort Collins, CO 80523.

136 JOURNAL OF ATMOSPHERIC AND OCEANIC TECHNOLOGY VOLUME 5

Four-Dimensional Imaging for Meteorological Applications

T. H. VONDER HAAR, A. C. MEADE, R. J. CRAIG AND D. L. REINKE

Cooperative Institute for Research in the Atmosphere (CIRA) and Department of Atmospheric Science, Colorado State University, Fort Collins, Colorado

2 January 1987 and 3 June 1987

ABSTRACT

Advanced software routines have been developed for digital imaging systems to obtain three- and four-dimensional computer-generated images from meteorological satellite, radar, and conventional data. Time sequences of these digital images provide a truly four-dimensional view of evolving atmospheric conditions. Applications of this technique for convective storms research and teaching, for forecaster information, and for pilot briefing are presented.

1. Introduction

The advent of rapidly improving digital image processing systems has opened new horizons for extraction of information from three- and four-dimensional datasets describing atmospheric features. Digital imaging is a subarea of the field of digital signal processing and is more technologically advanced than, but with roots in, the older field of digital image processing (Hord, 1982).

The science of meteorology is no exception to the use of 3-D displays and in fact is able to take advantage of this unique capability to gain a new window into the complex structures that exist in the atmosphere. Meteorology is a "four-dimensional" science in its attempt to quantify the structure of the earth's dynamic atmosphere and predict its future state accurately.

The potential applications for 3-D analysis and displays in atmospheric science, however, are quite different from the majority of the graphic display work done by structural engineers. An engineer is most often interested in the display and manipulation of a solid surface with unique curves, angles and edges. A meteorologist is more concerned with not only the physical boundaries of an entity, such as a cloud or moisture field, but also with the properties inside of the boundaries such as the temperature and moisture gradient or the wind field inside the core of a cyclone or thunderstorm complex. Indeed, recent studies of forecaster preferences for computer-generated products (Walker and Schultz, 1985) indicate a strong preference for image products.

We see the capability, via 3-D analysis and display techniques, to "fly through" an image of a block of the atmosphere and examine the structure and content of the meteorological parameters of interest at any point within that block. The potential applications of this capability are enormous, including aviation navigation and system performance, both weather prediction and postanalysis, severe weather analysis and prediction, quantifying the effects of the atmosphere on remote sensing throughout the spectrum, and invaluable educational and research tools.

The capability to model the atmosphere in 3-D with large computers is not new. These models have been the mainstay of our automated weather forecasting products for several decades. What has become a challenging new frontier, however, is the 3-D digital display and interrogation of observed weather parameters which have until now been limited to two-dimensional cross sections or single point measurements.

Recent work in the area of combining conventional observational data to produce 3-D displays suggests that there is indeed a tremendous potential for the current generation of meteorological analysis and display systems such as the IRIS, McIDAS, and SDHS (Satellite Data Handling System). By combining remotely sensed digital data from radar and satellite and merging in available surface, rawinsonde and airep data, a unique 3-D view of the current state of the atmosphere may be generated.

During the last several years, a team of atmospheric scientists and electrical engineers at Colorado State University has developed new algorithms (and adapted those designed for other applications) for 3-D and 4-D perspective display. This paper presents an overview of the results of our research. We have tested the new methods on both research and operational applications. Four-dimensional model output and actual 4-D weather datasets have been studied. Algorithms have been developed to scale down the computer requirements for the 3-D perspective software.

Corresponding author address: Dr. Thomas H. Vonder Haar, CIRA/NOAA, Colorado State University, Foothills Campus, Fort Collins, CO 80523.

LARGE-EDDY SIMULATIONS OF THE EFFECTS OF HILLY TERRAIN ON THE CONVECTIVE BOUNDARY LAYER

ROBERT L. WALKO, WILLIAM R. COTTON, and ROGER A. PIELKE

Department of Atmospheric Science, Colorado State University, Fort Collins, CO 80523, U.S.A.

(Received in final form 18 June, 1991)

Abstract. Large-eddy simulations of the convective boundary layer are compared over hilly versus flat surfaces. Moderate values for the height and horizontal spacing of the hills were selected. Thermally-direct hill-valley circulations are induced by the uneven terrain, accounting for a significant fraction of the resolved energy in the boundary-layer eddies. The probability of upward eddy motion reaches up to 70% over the hilltops and down to 15% over the valleys. Above-average values of both subgrid scale turbulent kinetic energy and upward eddy heat transport are found above the higher terrain. Horizontal spectra of vertical motion are strongly biased toward the horizontal scales of the terrain. Vertical profiles of atmospheric variables obtained by horizontal averaging, however, exhibit no significant differences between hilly and flat terrain simulations.

1. Introduction

Hilly or mountainous topography often has a strong impact on atmospheric dynamics. Its direct effects include forcing low-level vertical motion when the horizontal wind vector intersects the topography contours and providing a sensible and latent heat source or sink to the atmosphere at altitudes which vary with the horizontal coordinates. These surface effects are transmitted to greater heights following the laws which govern atmospheric motions, and produce many well-known phenomena such as mountain and valley circulations and mountain waves.

The effect of hilly topography on the properties of the convective boundary layer (CBL) has received relatively little study, even though boundary layers over much of the earth's land surface are located above or near sloping terrain. Investigators have tended to concentrate on the simpler problem of CBL formation over a flat surface in order to isolate and interpret the basic statistical properties of the boundary-layer eddies. This has been particularly true of Large-eddy Simulations (LES) of the CBL, which have nearly always been conducted on a domain bounded by a flat, uniform lower surface, and have employed cyclic rather than open lateral boundary conditions to remove any influence of mesoscale gradients on the solutions (e.g., Deardorff, 1974; Moeng and Wyngaard, 1984, 1988; Schmidt and Schumann, 1989). Field studies are likewise often conducted at sites specifically selected for their uniformity of terrain (e.g., Businger *et al.*, 1971; Carras and Williams, 1981; King *et al.*, 1989). Such studies have established most of the important statistical properties of the CBL over a uniform surface and provide a yardstick against which investigations of more complicated CBL situations can be compared.

Boundary-Layer Meteorology **58**: 133–150, 1992.

Atmospheric Research, 25 (1990) 235-276
Elsevier Science Publishers B.V., Amsterdam — Printed in The Netherlands

Observations of Blocking-Induced Convergence Zones and Effects on Precipitation in Complex Terrain

DOUGLAS A. WESLEY and ROGER A. PIELKE

Colorado State University, Department of Atmospheric Science, Fort Collins, CO 80523 (U.S.A.)

(Received January 23, 1989; accepted May 12, 1989)

ABSTRACT

Wesley, D.A. and Pielke, R.A., 1990. Observations of blocking-induced convergence zones and effects on precipitation in complex terrain. Atmos. Res., 25: 235-276.

Through an extensive set of observations, including standard surface measurements, Doppler radar, routine National Weather Service radiosondes and special Cross-chain Loran Atmospheric Sounding System (CLASS) data, two case studies of wintertime storms on the east slopes of the Rocky Mountains of Colorado are presented (9-10 February 1988 and 30-31 March 1988). The emphases are the effects of blocking-induced convergence zones on snowfall distributions, snow crystal production mechanisms and banded reflectivity structure. As shown by the analysis of a typical Front Range storm, cold air damming can frequently lead to convergence zones and enhanced precipitation east of the mountains. The meso-fronts often form in place just east of the foothills, and are sensitive to the nature of the low-level synoptic easterly flow. For other upslope situations, the convergence zone does not appear as a meso-front, but as a less distinct area of convergence. Measured vertical profiles associated with the blocked surface patterns reveal a distinctly layered temperature and wind structure. These soundings, along with surface measurements of wind, moisture and snow crystal types, enable some microphysical interpretation to be made concerning snowfall production in zones of ascent aloft, which are related to frontal surfaces as well as lifting at the top of the blocking-induced cold pool. Predominance of heavily rimed, dendritic aggregates implies lifting associated with the layered vertical structure in both storms. Bands of enhanced Doppler reflectivity exhibit significant correlation with snowfall intensity. The two case studies demonstrate that distinctly different patterns of blocking and convergence can appear in Colorado Front Range storms, each resulting in a unique snowfall distribution.

RESUME

A l'aide d'un ensemble fourni d'observations, incluant des mesures classiques au sol, des données de radar Doppler, des radiosondages du réseau du National Weather Service, et des sondages spéciaux du "Cross-chain Loran Atmospheric Sounding System" (CLASS), on présente deux études de cas de perturbations hivernales sur la pente orientale des Montagnes Rocheuses du Colorado (9-10 février 1988, et 30-31 mars 1988). On montre spécialement les effets des zones de convergence induites par blocage sur la distribution des chutes de neige, les mécanismes de production des cristaux de neige, et la structure en bande de la réflectivité. Comme le montre l'analyse d'une

0169-8095/90/$03.50

Radiative and Nonlinear Influences on Orographic Gravity Wave Drag

MICHAEL J. WEISSBLUTH AND WILLIAM R. COTTON

Department of Atmospheric Science, Colorado State University, Fort Collins, Colorado

(Manuscript received 19 September 1988, in final form 22 May 1989)

ABSTRACT

Vertical divergence of the mountain wave's momentum flux has recently been hypothesized to be an important contribution to the global momentum budget. Wavebreaking theories and envelope orography have been employed to explain the divergence of the momentum flux. Here, cloud-top radiational cooling is shown to locally destabilize the environment and disrupt the propagation of the mountain wave in idealized two-dimensional simulations, thus drastically altering the expected momentum flux profile. Also, simulations of two-dimensional mountain waves indicate that nonlinearities can increase the wave response if the lower layer is decoupled from the flow aloft or decrease the wave response by providing multiple reflection levels for the incident mountain wave. The onset of wavebreaking and the level at which the wave breaks can be influenced by the ambient thermodynamic profile.

1. Introduction

Gravity waves have long been known to play important roles in atmospheric processes occurring over a broad range of space and time scales. In large eddy simulations (LESs) and mesoscale models, gravity waves have been for the most part explicitly modeled since the grid spacing has been small enough to capture the forcing and response of the atmosphere. In particular, mesoscale models have been successfully used to simulate the mountain waves produced when there is flow over topography (e.g., Durran and Klemp 1983). Durran and Klemp (1983) also examined the behavior of mountain waves in the presence of moisture and found that there is a small change in the vertical wavelength and amplitude of the mountain wave due to the slight decrease in the Brunt–Väisälä frequency.

General circulation models (GCMs), however, are inherently unable to explicitly simulate orographic gravity waves due to their present grid spacing. The inability of GCMs to resolve this important class of waves can be conceptualized by considering the atmosphere's response to stratified flow over idealized topography as in Emanuel (1986). Two regimes of oscillatory flow are possible; the first is when the wavelength of the topography lies between $2\pi U/N$ and $2\pi U/f$ (inertia–gravity waves) and the second is when the wavelength of the topography is greater than $2\pi\sqrt{U/\beta}$ (planetary-scale Rossby waves). Here U is the constant zonal wind speed flowing over the topography, f is the Coriolis parameter N is the Brunt-Väisälä frequency and β is the meridional change of f. This implies that the grid spacing needed to minimally resolve the longest gravity wave wavelength is 150 km using $U = 10$ m s^{-1} and $f = 10^{-4}$ s^{-1}. GCMs may be approaching this now, but obviously there will always be a significant amount of gravity wave energy that may never be captured by these models.

Recently, the inability of the GCM to capture the mountain wave has been hypothesized to cause systematic biases in the model fields (Slingo and Pearson 1986). Correct estimates of the Southern Hemisphere's wind fields in the summer and winter and Northern Hemisphere's wind fields in the summer lend credibility to the model physics, but the Northern Hemisphere's wind fields are systematically overestimated in the winter. The problem, then, may be linked to the strong winter flow over mountain ranges (which are relatively sparse in the Southern Hemisphere). Therefore, two mechanisms have been proposed to induce drag in the Northern Hemisphere's winter westerlies. Envelope orography (Wallace et al. 1983) reduced systematic errors in the European Centre for Medium-Range Weather Forecasting's GCM by enhancing the land surface elevations preferentially over major mountain ranges. This reduced the westerly momentum through pressure torques exerted on the mountain by the prevailing westerly current. Unfortunately, systematic errors then appeared in the Northern Hemisphere's summer due to unrealistic elevated heating.

Another approach used more successfully was the introduction of a gravity wave drag parameterization proposed by Palmer et al. (1986). The basis for this scheme is as follows. Flow over topography produces mountain waves which, in the absence of transience or dissipation, create a stress profile independent of

Corresponding author address: Dr. W. R. Cotton, Department of Atmospheric Science, Colorado State University, Fort Collins, CO 80523.

3.2 PH.D. DISSERTATIONS

ABSTRACT

MEASUREMENT OF TROPOSPHERIC TEMPERATURE AND AEROSOL EXTINCTION HIGH SPECTRAL RESOLUTION LIDAR

Raul John Alvarez, II
Physics Department

A high spectral resolution Rayleigh-Mie lidar system capable of measuring relative temperature and aerosol profiles in the troposphere has been developed. The use of a narrowband laser transmitter along with an atomic vapor cell as a variable width bandstop filter allows for the separation of molecular and aerosol scattering signals. Using two of these filters with different widths and a newly developed lidar inversion method it is possible to determine relative temperature, pressure, and density profiles of the troposphere. This separation also makes a quantitative measurement of aerosol extinction coefficient profiles possible.

In principle, the information required in addition to the lidar signals for determining atmospheric and aerosol properties with this Rayleigh-Mie lidar is: the theoretical Rayleigh-Brillouin spectrum for scattering of narrow bandwidth laser light, independent measurements of the filter transmission functions, the assumption that the atmosphere acts as an ideal gas in hydrostatic equilibrium, and an approximate atmospheric pressure at one reference altitude. Profiles of the tropospheric state variables of temperature, pressure, and density are determined from signals averaged over 20 minutes. Once profiles of the atmospheric variables are determined, the aerosol extinction coefficient profiles are calculated.

A systematic offset in the lidar temperature profiles is seen however in practice when compared to balloon sonde measurements. Further laboratory experiments have established that the systematic offset is real and is consistent between laboratory and field measurements. This repeatable offset can be eliminated by normalizing the temperature at a reference altitude to an independently measured or estimated value.

The development and implementation of this high spectral resolution lidar and the first simultaneous measurements of tropospheric temperature and aerosol profiles from 0.2 km to 8 km are presented. The precision at 1 km altitude is ±10 K for temperature measurement, ±3% for backscatter ratio, and ±5% for aerosol extinction coefficient. At 5 km, these values are ±12 K for temperature, ±4% for backscatter ratio, and ±100% for extinction coefficient. Suggestions to determine the cause of the offset and to reduce the relative uncertainties are also discussed.

ABSTRACT

REGIONAL-SCALE FLOWS IN COMPLEX TERRAIN: AN OBSERVATIONAL AND NUMERICAL INVESTIGATION

James E. Bossert
Atmospheric Science Department

An observational program has been conducted to obtain information concerning thermally-driven flows in complex terrain on meso-β to meso-α scales (100 - 500 km). Data were collected from remote surface observing systems at exposed mountaintop locations throughout the state of Colorado, over the summers of 1984-1988. These field experiments have been called the Rocky Mountain Peaks Experiments (ROMPEX). The observations from ROMPEX have been supplemented with data from other remote surface networks, special soundings, upper-air observations, and radar and lightning strike information to provide an adequate description of the flows and weather of interest.

The observations have shown the development of a recurrent "regional-scale" circulation system across the Colorado mountain barrier, operating on a diurnal time scale. The basic structure of the flow system consists of a daytime inflow phase toward the mountains along the Continental Divide, and a nocturnal outflow away from this high terrain. Long-term averages show this circulation system to be the dominant wind pattern at several high altitude stations, revealing its climatological significance. Attention has been focused upon the nocturnal phase of the circulation system along the western slope of the mountain barrier. Here, the winds are particularly strong and from a southeasterly direction, which is generally counter to the upper-level winds, and onset abruptly in early evening with steady flow thereafter. Soundings have shown this nocturnal current to be shallow and within a distinct stable air mass. Convective storms are found to enhance this southeasterly flow regime.

Numerical simulations have been performed with the Colorado State University Regional Atmospheric Modelling System (CSU-RAMS) to provide further insight into the physical mechanisms forcing the observed regional-scale circulation system. The model simulations include both idealized two- and three-dimensional experiments, as well as a three-dimensional case study experiment using actual data for the initialization. The three-dimensional simulations use two-way interactive grid nesting and a realistic representation of topography over the region of interest.

The idealized three-dimensional experiment showed that thermal forcing over realistic topography in conditions of negligible, or weak ambient flow, is capable of producing many of the flow features observed throughout the diurnal cycle. This experiment further showed how the deep mountain-plains solenoid along and above the Front Range crest evolves in late afternoon into a shallower density current, which then propagates westward over the mountains of the western slope. This unexpected flow phenomenon is the primary process responsible for the strong nocturnal southeasterly winds found in observations. Sensitivity experiments show that the particular terrain configuration through an east-west cross-section of the Colorado mountains is important to the generation of this unusual circulation. The strong thermal gradient produced by differential heating of the topography is the primary driving force in the density current evolution. Coriolis influence maintains the steady nocturnal south-southeast winds over the western slope. Additional experiments show that the diurnally evolving regional-scale circulation system over the

Colorado Rocky Mountains is a robust feature which can occur over a range of ambient flow and stratification conditions. Soil moisture experiments reveal that wet soil along the eastern slope and dry along the western slope aids the development of the westward propagating density current.

The diurnal evolution of the circulation system on the case study day was in fair agreement with many of the observed circulation features. This experiment also revealed that synoptic-scale forcing can influence the development of the regional-scale circulations in preferential regions along the eastern slope of the mountain barrier. As a result of the numerical experiments four phases of the thermally forced regional-scale diurnal circulation system have been identified. These consist of a daytime mountain boundary layer development phase, a late afternoon transitional phase, an evening propagating density current phase, and a late night adjustment phase.

ABSTRACT OF DISSERTATION

HYDRODYNAMIC NETWORK SIMULATION THROUGH CHANNEL JUNCTIONS

A numerical model based on the conservation of mass, momentum and energy is developed for more accurate unsteady flow simulation in channel networks. The model utilizes a new matrix solution algorithm for channel networks to convert the matrix of coefficients resulting from the governing equations into a form exhibiting banded matrix features. In this algorithm, separate recurrent equations for converging channels, diverging channels, converging channel junctions, and diverging channel junctions are used. Through the use of an algorithm taking advantage of the banded matrix structure, the new channel network model developed in this dissertation has a vastly reduced computer storage requirement. Also, because of the use of recurrent equations during simulation the computational times are faster.

The relative magnitude of the terms of the full dynamic equation are also investigated in the dissertation based upon a dimensionless parameter, Froude number and the channel bed slope. Based on the relative magnitude of the five terms used in the full dynamic equation, the applicability of full dynamic, diffusion, and kinematic wave models is investigated. The verification of the proposed model is accomplished through two phases. In the first phase, the conservation of mass is verified in single channels and in a channel network. In the second phase, using the model developed in this dissertation the simulated results are compared with the experimental data. The model is applied for the runoff simulation in the Macks Creek Watershed in conjunction with a two dimensional finite element overland

model developed by Marcus (1991). In the simulation runs, spatially and temporally varied input data are used for demonstrating the applicability of the model to complicated test conditions. The comparison between observed and simulated runoff hydrographs at basin outlet shows good agreement. As shown in the simulation runs, the model developed in this dissertation is an effective tool in simulating flow in complicated channel networks.

Gye Woon Choi
Department of Civil Engineering
Colorado State University
Fort Collins Co. 80523
Spring, 1991

ABSTRACT OF DISSERTATION

SIMULATION OF THE SPATIAL AND TEMPORAL EFFECTS OF ARMY MANEUVERS ON WATERSHED RESPONSE

The environmental impacts of large scale mechanized military maneuvers on U.S. Army training lands are a critical natural resources management issue for the 1990s. Many Army training lands are located in semiarid regions of the United States where infrequent rainfall events play a major role in sustaining and shaping the landscape and its water resources. The extent to which maneuvers alter the rainfall-runoff response of natural watersheds within these training lands is not widely understood and is the focus of this dissertation research.

Detailed field investigations and computer simulations have been performed for a 50-square mile watershed, the Taylor Arroyo, located within the U.S. Army Pinon Canyon Maneuver Site (PCMS) in southeastern Colorado. Innovative land management practices have been implemented within the watershed to minimize the effects of maneuvers and preserve its natural characteristics. The possible effects of hypothetical maneuver scenarios on the watershed under a range of rainfall conditions have been simulated using a two-dimensional, physically based hydrologic model, CASC2D. CASC2D is an event-based model which divides the watershed into grid elements and can represent the spatial variability present in the watershed. The principal hydrologic processes of infiltration, overland flow, and channel flow are

simulated and can be spatially analyzed. The model also incorporates dynamic visualization graphics portraying the areas disturbed by maneuvers and their time varying hydrologic response to rainfall excitation.

The Geographic Resources Analysis Support System (GRASS), a raster-based GIS, has been used to spatially characterize the Taylor Arroyo watershed for model input. The spatial outputs from CASC2D have been imported into GRASS for detailed analysis and map display. The integrated use of GRASS and CASC2D facilitates raster data manipulation and transfer and enhances the spatial and temporal analysis of maneuver impacts on the watershed. This integrated approach provides a valuable research tool for the scientific study of watershed impacts. It also provides the land manager with a decision-support system which can analyze the spatial effects of maneuvers and enhance the understanding of this complex management issue.

William W. Doe III
Department of Civil Engineering
Colorado State University
Fort Collins, CO 80523
Summer 1992

ABSTRACT OF DISSERTATION

MULTIPARAMETER DOPPLER RADAR THEORY, SIMULATION, TIME SERIES AND APPLICATIONS

Conventional radars for meteorological measurements radiate and receive waves of single polarization. Power measurements combined with the Doppler capabilities of present-day conventional systems provide information about the presence, range and the first three moments of the Doppler spectrum. Distributions of microphysical properties such as size, shape, orientation and composition can yield ambiguous results in the single power measurement. Nonsphericity and preferred orientation of the hydrometeors, especially raindrops, cause polarization dependent scattering properties, thus permitting the measurement of additional echo characteristics. The term multiparameter generally refers to dual-polarization or dual-wavelength measurements made in addition to radar reflectivity, but excluding Doppler spectrum parameters. With all the progress achieved using multiparameter radars there is now little doubt that it can significantly enhance our capability of remotely sensing cloud microphysical evolution.

However, detailed modelling and experimental data for different polarization states is currently not available. This thesis represents a study and refinement of multiparameter radar modelling and observations in rainfall and mixed phase precipitation media. In meteorology, multiparameter modelling can help in understanding and providing early warning of convective storms, which can produce hail and flooding resulting in loss of life and property. Multiparameter radar studies are essential

in terrestrial and earth-satellite communications where the ever-increasing demand for communications is causing frequency-spectrum congestion. Also, modelling can help in accurate rainfall rate estimation needed for watershed management, rainfall runoff and flood control studies.

The exact and/or direct analysis of real physical problems is usually quite complicated. In such circumstances simulation has proven to be a powerful method to handle analytically intractable problems. The innovation algorithm has been used here for the first time to study the error in differential propagation phase shift, Φ_{DP}, and its dependency on Doppler spectrum parameters. It is noticed that because of the high zero-lag correlation coefficient between the backscattered H and V signals, $\rho_{HV}(0)$, at S-band a lower $\sigma_{\Phi_{DP}}$ can be obtained. K_{DP} and A_x which are, respectively, the rate of change of Φ_{DP} and the specific attenuation at X-band are shown to be noisy quantities; thus, a new processing technique is developed to derive K_{DP} and A_x which succeded in reducing the fluctuations to small levels, so that the mean properties can be observed. Using model simulation and experimental observations a linear relationship between K_{DP} and A_x, as predicted from theory, was obtained, suggesting that K_{DP} measurements at S-band could be used to predict specific attenuation at higher microwave frequencies.

A new parameter, ZDP, was introduced here for the first time which is useful in the study of rain/ice mixtures. The high correlation between ZDP and Z_H in rain and the deviation from "rain line" in mixed phase are used to determine rain/ice mixtures.

Rainfall rates, R, based on three different methods, viz, $R(Z_H)$, $R(Z_H, Z_{DR})$ and $R(K_{DP})$ are obtained, where Z_{DR} is differential reflectivity between backscattered H and V polarized signals. Based on our findings which are consistent with theory we conclude that, for R<20 mm/hr use $R(Z_H)$, for R >20 mm/hr use $R(Z_H, Z_{DR})$ and for R >80 mm/hr use $R(K_{DP})$ relationships. Also, for the first time the staggered

pulsing scheme was used on the NCAR CP-2 radar in 1988 to gather time series data. Using the collected data all the radar parameters were measured within the expected accuracy range, suggesting that, from both reseach and operational viewpoints, the staggered pulsing scheme is likely to be an important advance in the kinematic and microphysical sensing of severe storms.

Yahya Golestani
Department of Electrical Engineering
Colorado State University
Fort Collins, Colorado 80523
Summer 1990

Abstract of Dissertation

THE RESPONSE OF THE ATMOSPHERIC CONVECTIVE BOUNDARY LAYER TO SURFACE INHOMOGENEITIES

Large-eddy simulations (LES) of the atmospheric convective boundary layer have been conducted with a surface sensible heat flux that either is constant or varies on a spatial scale comparable to the boundary layer depth.

The horizontally homogeneous simulations have been compared with previous LES, laboratory and atmospheric studies. The dynamics of the simulated turbulence and the model's sensitivity to the subgrid diffusivity have been investigated. In general the present model gives results similar to previous large-eddy simulations. All the LES models simulate a field of convective eddies having approximately the correct velocity and spatial scales, and with the crucial property that kinetic energy is transported vigorously upwards through the middle levels. Several failings of the models have been identified, including a tendency to underpredict temperature variance and to overpredict vertical velocity skewness in the upper boundary layer.

The surface heat-flux variations are one-dimensional and sinusoidal with a wavelength between one and four times the boundary layer depth. Simulations have been carried out with zero wind or with a light mean wind perpendicular to the perturbations. Several effects have been identified, though some are evident only after a great deal of averaging. They include mean circulations in phase with the surface perturbations, modulation of the turbulence throughout the boundary layer and modifications (usually slight) to the profiles of horizontally averaged statistics. The mean boundary layer depth remains horizontally uniform. Most of the effects increase as the wavelength of the surface perturbation is increased and decrease with an imposed mean wind.

The processes maintaining the mean temperature field and the mean circulation have been analysed. A time scale for kinetic energy transfer from the circulation to the turbulence has been defined and found to be surprisingly short in some cases. The turbulent stress budgets have also been examined: the effects of turbulent buoyancy fluctuations and of interactions between the circulation and the turbulence have been distinguished.

Elevated-plume dispersion has been studied using a Lagrangian particle model. Circulations driven by the surface heat-flux perturbations affect the ground level concentration.

Mark Gregory Hadfield
Atmospheric Science Department
Colorado State University
Fort Collins, CO 80523
Fall 1988

ABSTRACT

SPATIAL AND TEMPORAL SHORT RANGE TOTAL CLOUD COVER ESTIMATION BY METRIC ANALYSIS OF COMPOSITE IMAGERY

The compositing of regional scale satellite cloud imagery for the purpose of estimating climatological cloud occurrence frequencies is well formulated. Several studies by the author and colleagues within the last five years have combined image processing methods with digital satellite data to produce cloud climatologies. These efforts have investigated averaged cloud fields over areas of Montana, Colorado, Nebraska, Florida, and the Southeast U.S. The main emphasis for these climatologies has been qualitative and descriptive.

This study presents results from an initial attempt to estimate future cloud cover based on cloud composites. Visible and infrared satellite data from the GOES satellite system are assembled into frequency and newly developed conditional probability of occurrence composites. The study region is located over the Island of Cuba and the data was collected and processed for the period from 12 July to 30 September, 1986. This research also introduces the new concepts of index image generation (i.e., combining frequency and conditional probability composites into a single image). It also extends the current research on cloud cover estimation in new ways by generating an Estimated Cloud Image (ECI). The ECI model generates cloud cover estimates for a one-hour time interval based on the combination of real-time imagery with the frequency and conditional probability of occurrence composites as depicted by index images.

Recently developed non-classical statistical methods are also applied as they relate to (a) the analysis of cloud imagery (Multi-Response Permutation Procedures, MRPP) and the (b) verification of the estimated cloud cover (Multi-Response Randomized Block Permutation Procedures, MRBP) by our method as contrasted to commonly used persistence approaches. Binary images generated by an objective cloud detection algorithm are quantitatively grouped based on the image structure derived from a method which applies MRPP to digital satellite imagery. Composites are then generated based on MRPP derived groupings and total cloud cover estimates are constructed for two case studies. The results of the estimation (i.e., ECI) are then tested with a verification ("ground-truth") image by a metric imagery comparison technique. This method provides a measure of agreement between any two images and also p-value which quantifies the degree of significance of the test versus a null hypothesis of a completely random match. The coefficient of agreement (CA) of the test attains unity for an ideal exact match between an ECI and the verification image. The total cloud cover estimation model developed and described in the present study results in CA values of 0.40 to 0.80. The utility of the model is quantified and its potential for spatial and temporal short range cloud cover estimation is described. The newly developed applications of MRPP and MRBP are also discussed.

Francis Peter Kelly
Department of Atmospheric Science
Colorado State University
Fort Collins, Colorado 80523
Fall, 1988

ABSTRACT OF DISSERTATION

DYNAMIC MODELING OF MEANDERING ALLUVIAL CHANNELS

The migration of meandering alluvial channels is investigated theoretically, numerically, and experimentally. An equation for the rate of bank erosion is derived from a two-dimensional continuity equation for sediment transport linked with the depth-averaged dynamic flow equations.

A simple one-dimensional theoretical analysis of lateral meander migration leads to a relationship between the migration rate and the relative channel curvature, defined as the ratio of flow depth and the radius of channel curvature. The simple model appropriately simulates the pattern and rate of meander expansion and migrations of the White River, Indiana and the East Nishnabotna River, Iowa. The genesis of meandering development from a sine-generated alluvial channel is also analyzed. The migration of meanders is found to reach its maximum when the relative radius of curvature, defined as the ratio of valley meander length and the radius of curvature, reaches about 4.8, or the sinuosity of meander approaches 1.3.

A two-dimensional numerical model, DYNAMIC, which predicts both lateral and longitudinal migration of alluvial channels is then developed, based on a system of quasi-steady depth-averaged flow dynamic equations, a sediment continuity equation, and a bank erosion equation. A linear analysis of the two-dimensional model leads to a convolutional relation between the rate of meander migration and flow and sediment properties. In the two-dimensional numerical analysis, a

numerical algorithm called FLOWSOL, based on the numerical scheme SIMPLER by Patankar and Spalding, is developed to solve the flow dynamic equations. The flow algorithm is then linked to the sediment continuity equation and bank erosion equation to simulate bed deformation and bank erosion. The developed two-dimensional model is applied to calculate the velocity profiles in Rozovskii's experiments and the bed deformation and shear stress in Hooke's experiments. Good agreement is obtained between the calculated and measured velocities, shear stresses and bed profiles in all experiments. Some techniques in handling the flow problem in sharp bends are also developed.

A flume study of the migration of meandering alluvial rivers is also conducted in the Hydraulic Laboratory at the Engineering Research Center. Small scaled meandering rivers, starting from either straight or sinuous channel, are developed successfully on a floodplain with or without cohesive materials (about 3%) in a wide recirculating flume. The lateral migration of miniature rivers under relatively constant flow discharge is documented and analyzed.

The laboratory experiments on laboratory migration of meanders were properly simulated by the two-dimensional numerical model finally.

Yongqiang Lan
Department of Civil Engineering
Colorado State University
Fort Collins, CO 80523
Fall, 1990

ABSTRACT OF DISSERTATION

MESOSCALE ANALYSIS BY NUMERICAL MODELING COUPLED WITH SATELLITE-BASED SOUNDING

This dissertation deals with the development of a system for time-continuous mesoscale analysis and its use in studying the mesoscale distribution of summertime convective cloud development in the Northeastern Colorado region. There were two basic components of the system — a version of the CSU Regional Atmospheric Modeling System (RAMS) and an algorithm for retrieving temperatures and water vapor concentrations from VISSR Atmospheric Sounder (VAS) data. The system was designed to avoid some of the problems that researchers have encountered when satellite-retrieved parameters have been input to models. The primary distinguishing feature of the new method is that there is an intimate coupling of the retrieval and modeling processes. Water vapor concentrations and ground surface temperatures were the foci of the analyses.

In preparation for analysis experiments we tested the sensitivity of a two-dimensional version of the model to various controls on the behavior of water vapor concentrations and surface temperatures. For water vapor mixing ratios, variations that might be caused by analysis errors had very little impact on the dynamics of circulations in the pre-convective stage. In contrast, ground surface temperature variations were shown to have a large impact on circulations, so analysis errors are very relevant to pre-convective dynamics.

The first comparisons of the coupled analysis method with other, related, methods was by means of two-dimensional simulations. Analyses in which surface temperatures were derived from satellite-retrievals were compared with the alternative of relying on energy balance computations. The energy balance computations were so sensitive to soil characteristics, which were simulated as unknown, that the satellite retrieval method gave better results even with cloud contamination. In water vapor analysis comparisons no single

method was superior in every respect, but the coupled method performed relatively well. Vertical gradients and horizontal gradients were well represented, and the method was relatively insensitive to a common problem in pre-convective analysis — contamination of satellite data by increasing amounts of small convective clouds.

Analysis methods were further compared in a three-dimensional case study for 21 August 1983. The horizontal and time variations of satellite-retrieved surface temperatures closely corresponded to the conventional shelter temperature observations, but had much greater detail. In contrast, the energy balance-based temperatures tended to increase too quickly during the morning and lacked some of the observed gradients. According to the retrievals, there can be very large mesoscale gradients in temperatures at the ground surface even on the relatively flat plains. In the case study water vapor analyses there were substantial differences among the results of the several methods that were intercompared. The study demonstrated that, when the first set of satellite data is less reliable than the later sets, some of the contamination lingers throughout the time-continuous coupled analysis results. However, the coupled method generally appeared to be the most valuable of the methods considered in this study because it exploited the major strengths of the numerical model and the satellite data while making it relatively easy to recognize any impacts of their weaknesses.

The results of this dissertation support the hypothesis that both ground surface temperatures and terrain variations can play important roles in pre-convective water vapor kinematics through their influences on vertical and horizontal winds. The development of convective clouds corresponded largely, but not exclusively, with convergence and deepening of low-level water vapor. The analysis system proved to be valuable for forecasting through the close correspondence between derived stability indices and later convective development. The new method is a step in the expanding capability of meteorologists to combine tools and sources of data for understanding and forecasting mesoscale phenomena.

Alan E. Lipton
Department of Atmospheric Science
Colorado State University
Fort Collins, Colorado 80523
Fall, 1988

ABSTRACT OF DISSERTATION

TWO-DIMENSIONAL FINITE ELEMENT MODELING OF SURFACE RUNOFF FROM MOVING STORMS ON SMALL WATERSHEDS

A distributed finite element model is developed to simulate moving storm events on natural watershed areas. The model consists of a two-dimensional surface flow model for the simulation of surface runoff on a watershed. The two-dimensional kinematic wave approximation is combined with the Manning resistance formula for the surface runoff calculation. The Green and Ampt infiltration equation is used to determine the excess rainfall. In the two-dimensional surface flow model, the Galerkin weighted residual method is used to formulate the space domain while an implicit finite difference scheme is used to approximate the time domain. The model uses quadrilateral elements with different shape functions. The finite element isoparametric formulation is used to describe the spatial variability of the input parameters in terms of slope, roughness, and excess rainfall. The model uses nodal input data rather than element averaged data thereby continuity of the calculated variables are insured. Different flow regimes ranging from laminar to turbulent flows can be handled by the model.

Three phases of testing were conducted to validate the model. First, the model results are compared to analytical solutions with excellent results for simple cases of constant input data. Second, the model is compared to experimental case studies. It is found that the two-dimensional approximation retains the geometric representation of the flow domain thereby giving better results than the one-dimensional approximation. Third, the influence of the non-linear behavior of the input data represented by the excess rainfall, slope, and roughness on the output result is analyzed. Slope and roughness have pronounced effects on discharge calculations, particularly near the time to equilibrium while rainfall shows little effect. Since the slope and roughness reside in the convective terms of the constitutive governing flow equation, the non-linearity of these terms must be carefully dealt with. In the above analyses, the mass balance has been verified.

The model is finally applied to the Macks Creek drainage basin in Idaho for simulating runoff generated from a moving storm recorded by eight rain gages. The spatial and temporal variation of the moving storm determine the variability of the flow on the drainage basin. The visualization of the flow dynamics caused by the storm mobility is successfully accomplished on the Macks Creek drainage basin. The model displays excess rainfall intensity, infiltration rate, cumulative infiltration, flow depth, and flow discharge. Flow routing of the channel part is performed using the model developed by Choi(1991). The concept of spatially and temporally responsive modeling shows areas mostly contributing to the magnitude and timing of the flow discharge. The spatio-temporal variation of rainfall represented by several rain gages is required for accurate simulation of a moving storm and therefore accurate

for simulation of the spatial and temporal variability of flow characteristics. The depression storage and the antecedent moisture content corresponding to the different soil types on the Macks Creek drainage basin are found to be important in determining the timing and magnitude of peak flow and runoff volume. The simulated hydrograph at the outlet of the Macks Creek drainage basin shows good comparison with the measured hydrograph.

Khalid Behnam Marcus
Civil Engineering Department
Colorado State University
Fort Collins, Colorado 80523
Summer 1991.

ABSTRACT

TWO-DIMENSIONAL RUNOFF MODELING WITH WEATHER RADAR DATA

Fred L. Ogden
Civil Engineering Department

The objective of this study is to examine the effect of precipitation data spatial and temporal resolution on the surface runoff calculated by one-dimensional and two-dimensional, physically based, distributed parameter runoff models.

The model sensitivity to rainfall data temporal resolution is examined on both one-dimensional and two-dimensional impervious surfaces. Studies are performed using a Monte Carlo approach, where fifty simulations are performed for each value of temporal sampling resolution and rainfall duration. Results indicate that the sensitivity of both one-dimensional and two-dimensional runoff geometries increases with increasing temporal sampling resolution and with increasing rainfall duration. The sensitivity reaches an asymptote as the rainfall duration exceeds the time to equilibrium, defined by the average rainfall intensity. The asymptotic value of relative sensitivity increases with the square root of the temporal sampling interval.

The sensitivity of the two-dimensional runoff model to the spatial variability of precipitation intensity is explored. Both stochastically generated and polarimetric weather radar estimated static rainfall fields are input to the runoff model for differing rainfall durations and spatial resolutions. The sensitivity of the runoff model to rainfall intensity spatial variability is observed to decrease with increasing rainfall duration for all spatial resolutions tested. The effect of precipitation data resolution is observed by comparison with results from the finest resolution input data. The statistical deviations in model performance due to resolution coarsening are presented.

The effect of storm motion on the outflow calculated by the two-dimensional runoff model is observed using rectangular, constant intensity precipitation fields. The precipitation fields are moved in 16 directions over the watershed, at ten speeds per direction. A dimensionless storm speed and storm direction is identified which produces the largest effect on the magnitude of the outflow hydrograph peak. This dimensionless storm velocity is on the order of the runoff length divided by the time to equilibrium for an equivalent stationary storm.

Real-time polarimetric weather radar estimated rainfall fields are input to the two-dimensional runoff model in simulations with and without infiltration on one 32 km^2 and one 121 km^2 watershed to determine the effect of input data spatial resolution on model performance. In simulations without infiltration, the smaller watershed is more sensitive to input data resolution because of increased variability in rainfall volume. Statistical deviations from finest resolution results are presented. In simulations with infiltration, the interaction between the scale of the input rainfall data and infiltration processes in considerable. As input rainfall data resolution is coarsened, excess rainfall amounts decrease substantially, indicating that two-dimensional, distributed parameter, physically based runoff models must be calibrated for one input data resolution. If the resolution of the precipitation data is changed, the model must be re-calibrated.

ABSTRACT

THE EFFECT OF MOVING RAINSTORMS ON OVERLAND FLOW USING ONE-DIMENSIONAL FINITE ELEMENTS

Jerry R. Richardson
Civil Engineering Department

Rainfall events are rarely stationary. That is to say that over any watershed, storms are spatially and temporally variable. Unfortunately, most rainfall-runoff models usually consider precipitation to be stationary and uniform. However, evidence in the literature indicates that the movement of storms can have a significant influence on runoff hydrographs. Therefore, a need for numerical models which can accommodate the movement of precipitation is recognized. This dissertation provides a better understanding of the influence of block moving precipitation on surface runoff hydrographs. Two one-dimensional finite element models were developed and used for these investigations.

Analytical expressions for each partial derivative of the momentum equation are developed for stationary storms. For moving rain storms, the behavior of the terms of the momentum equation is shown to be very complex. However, based on the analysis of the momentum equation for stationary and block moving storms, it is found that only the full-dynamic and kinematic forms of the momentum equation are suitable for simulation of overland flow. The kinematic approximation is suitable for overland flow simulation for most cases of stationary and moving storms. The time to peak of moving storms was shown to depend on the traverse time of storms and can be several times greater than the time to equilibrium for stationary storms. For partial-equilibrium hydrographs, the maximum peak discharge of equivalent block moving storms, was shown to occur when the dimensionless storm velocity was equal to 0.3 for laminar flow and 0.5 for turbulent flow using Manning's equation. The maximum peak discharge occurs when the flood wave and the storm front arrive at the downstream end of the plane at the same time. Using the results of these studies, and the finite element model, successful simulation of block moving storms over a laboratory watershed was conducted. These simulations indicate that the one-dimensional finite element model can be used to simulate runoff from moving storms over a system of planes and channels.

ABSTRACT OF DISSERTATION

HYDROLOGIC ANALYSIS OF WATERSHED RESPONSE TO SPATIALLY VARIED INFILTRATION

A two-dimensional finite difference technique is used to simulate distributed rainfall-runoff events on watersheds. The model consists of three major processes: overland flow, channel flow, and infiltration. The Green-Ampt scheme is formulated to compute the infiltration losses. Surface flow is routed by applying diffusive wave approximation along with the Manning resistance equation. The spatial variability of the catchment characteristics are represented by square grid cells. Physical properties such as surface roughness and soil infiltration parameters are assumed uniform within each grid element.

An analytical relationship for computing the catchment kinematic time to equilibrium is derived. The relationship accounts for spatial variability of impervious watershed and rainfall characteristics. Numerical integration techniques are required for determining the equilibrium time.

The effects of spatially varied watershed characteristics on surface runoff are examined in terms of overland surface roughness for impervious basins and soil hydraulic conductivity for pervious areas. Results are presented in dimensionless

form thereby allowing general conclusions regarding spatially varied characteristics. The outcome of a two-dimensional Monte Carlo simulation confirm that the ratio of storm duration over equilibrium time (or a hypothetical equilibrium time in the presence of infiltration) is the key element in analyzing the influence of spatially varied parameters. The spatial sensitivity of surface runoff due to spatial variability of watershed properties generally decreases for longer duration storms and/or shorter equilibrium times, unless the mean value of watershed hydraulic conductivity is close to the rainfall intensity. It is necessary to capture the spatial distribution when the storm is short or when the rainfall rate is near the spatially averaged hydraulic conductivity. As the watershed scale increases, basin response becomes more nonlinear for a given storm since the time to equilibrium and the spatial variability of watershed characteristics increase. Spatially varied watersheds typically produce higher peak discharges than watersheds with uniform infiltration characteristics.

Bahram Saghafian
Civil Engineering Department
Colorado State University
Fort Collins, CO 80523
Fall 1992

ABSTRACT

MECHANICS OF HEADCUT MIGRATION IN RILLS

Otto R. Stein
Civil Engineering Department

The proposed conceptual model relates two-dimensional headcut migration to sediment detachment just upstream and just downstream from a headcut. If upstream erosion dominates, the headcut tends to obliterate itself as it migrates upstream, eventually becoming indistinguishable from the eroding channel's bed slope. If downstream erosion dominates, the headcut face erodes from below and a definable headcut with a near vertical face migrates upstream with time.

A criterion to determine which migration mode occurs is formulated using both dimensional analysis and by equating hydraulic and sediment detachment equations. Dimensional analysis results in a time scale ratio of upstream to downstream erosion related to the upstream and downstream sediment detachment, bed slope, Reynolds number and the drop number, which represents the dimensionless headcut drop height. A physically based analysis of hydraulics and sediment detachment yields a relationship between the dimensionless terms. The resulting equation for headcut stability is favorably compared with a total of eleven laboratory measurements of headcut migration on cohesive soil.

The maximum scour depth and the total volume of eroded material produced by the impinging jet just downstream from a headcut are analyzed. A previously developed method for the prediction of the ultimate, or equilibrium, scour depth in non-cohesive bed material is modified to include scour from cohesive bed material. This method equates the sediment detachment potential of the bed material to the diffusion of a jet.

The same approach is used to determine the time rate of the maximum scour depth. Dimensional analysis relates the ratio, maximum scour depth at any time over the predicted ultimate scour depth, to the jet Reynolds number, Froude number and a dimensionless time scaled to jet properties. The change in scour depth is analytically shown to proceed at two distinct rates. For some period of time from the initiation of scour, scour rate is independent of time because the bed is within the jet potential core and diffusion has not reduced the maximum jet velocity. Beyond this time period jet diffusion decreases the rate of scour and this rate decreases with increasing time and scour depth. In the limit the predicted ultimate scour depth is approached. The dimensional and physically based analyses for scour depth compare favorably with experimental data. This data includes measurements of the ultimate scour depth and the change in scour depth with time for ten runs on cohesive soil, eight runs on sand d_{50} = 1.5mm and six runs on sand d_{50} = 0.15mm.

ABSTRACT OF DISSERTATION

NUMERICAL SIMULATION OF A MESOSCALE CONVECTIVE COMPLEX: MODEL DEVELOPMENT AND NUMERICAL RESULTS

A mesoscale numerical model has been developed and used to study the complex circulations of a baroclinic environment which supported the development of a mesoscale convective complex (MCC). The hydrostatic numerical model was first written as a separate version of the CSU cloud/mesoscale model. The non-hydrostatic cloud model and the hydrostatic meso-/synoptic-scale model were combined in 1983 to form the CSU Regional Atmospheric Modelling System (RAMS). Some of the aspects of RAMS developed during the coarse of this research were a hydrostatic "time-split" time differencing scheme, a prognostic soil temperature and moisture model, a new form of the higher ordered forward upstream advection scheme, an improved version of the Fritsch and Chappell convective parameterization scheme, a simple form of the Kuo-type convective parameterization scheme, and an isentropic data analysis package.

The goal of the numerical simulations was to employ the numerical model to study an MCC with higher space and time resolution than is available through observational means, not to reproduce the observations that were available. The model results were compared with the observations, however, to examine the credibility of the model. While there were many differences, the coarse resolution (about 110 km) control run simulated an MCC whose meso-α-scale structure and environment evolved similarly with the observed convective system to establish the credibility of the numerical model. Two additional coarse resolution simulations were used to examine the predictability of the model formulation and sensitivity to initial conditions These simulations showed more research still needs

to be done on basic modelling problems in order to apply these models to operational forecasting.

Higher resolution simulations (about 45 km) were made to increase the spatial resolution. A comparison between the coarse resolution and higher resolution runs showed only small differences in the gross behavior of the simulated MCC disturbance. The results of the higher resolution control run were examined for the important forcing mechanisms of this MCC. For the development of the MCC, an important forcing mechanism was the development and propagation of the mountain/plains solenoidal circulation which was forced by the baroclinicity created by the physiographic features of the topography slope and horizontal gradients of soil moisture. Other factors present in the simulation that were hypothesized to be important were a low-level "heat low" in the Montana-Wyoming region, the Bermuda high providing a favorable pressure gradient over the central plains for the development of a strong nocturnal low-level jet, a weak front moving southward from Canada, and an upper level jet core in a favorable position to provide upper-level divergence.

Results from a two-dimensional simulation, in which a simplified physiographic forcing was used to create a solenoid, verified many features of the solenoid's behavior. The solenoid may also be responsible for the nocturnal preference for MCCs and the frequently observed mid-level shortwave that often accompanies the convective systems.

Two higher resolution sensitivity simulations were performed. The first, in which the convective parameterization was not used, showed the expected result that no mesoscale circulations developed that exhibited the characteristics of an MCC. This dry run, as with the control run, produced a low-level solenoidal circulation which propagated across the Dakotas. At the end of the simulation, the dry solenoid looked very similar to the solenoid in the control run after the MCC disturbance outran the solenoid. The second sensitivity experiment with the resolved microphysical parameterizations activated showed that the gross behavior of the MCC was similar to the control run although there were differences in

the details of the mesoscale vertical motion fields and locations of convection underneath the anvil.

Craig J. Tremback
Department of Atmospheric Science
Colorado State University
Fort Collins, Colorado 80523
Spring, 1990

ABSTRACT

MICROWAVE REMOTE SENSING OF A PRECIPITATING ATMOSPHERE

Joseph Turk
Electrical Engineering Department

Throughout the 10-100 GHz spectrum, the scattering and absorption properties of atmospheric hydrometeors and gases vary widely. As a result, multifrequency techniques for passive microwave estimation of precipitation have been proposed. The emission-based, lower frequency observations (< 37 GHz) effectively respond at lower altitudes, while the scattering-based higher frequencies (≥ 37 GHz) respond at higher altitudes, thus providing a potential means to link self-consistent precipitation estimates to the multifrequency brightness temperatures T_B. Unlike many schemes which link T_B to the liquid water content, this study emphasizes the use of scattering-based channels to infer information on the ice water content. The high altitude ice region remains fairly unobscured to a spaceborne sensor, suggesting the implementation of the scattering-based channels in a top-down methodology as the first step in a retrieval of the cloud vertical structure.

Extensive model simulations of the upwelling T_B were performed throughout clouds whose bulk microphysical properties were deduced from multiparameter radar data and cloud model output obtained during the 1986 Cooperative Huntsville Meteorological Experiment (COHMEX). A highly accurate plane-parallel microwave radiative transfer model with Mie phase matrices was used to solve the equation of transfer in a scattering atmosphere with a land surface. COHMEX aircraft radiometer measurements at 18, 37, and 92 GHz were compared with the output of the multiparameter radar-initialized radiative transfer model. Deviations at 92 GHz were attributed to uncertainties in the bulk density and size distribution of the ice region. Using both multiparameter radar observations and cloud model output, the 37-85 GHz T_B difference (ΔT_B) was found to be sensitive to the amount of integrated ice water path (IWP) lying above the rain, independent of ice density. Presence of coexisting cloud water and ice had the net effect of compressing the ΔT_B for a given IWP. Over convective regions, 85 GHz T_B depressions < 200 K were noted to be relatively insensitive to the amount of underlying liquid water content, and mainly dependent upon the optical thickness of the ice layer.

ABSTRACT

THE INFLUENCE OF TOPOGRAPHY ON COLORADO FRONT RANGE SNOWSTORMS

Douglas A. Wesley
Atmospheric Science Department

This study utilizes both an extensive set of observations and mesoscale model simulations to isolate and describe the important influences of complex terrain on Colorado Front Range winter storms, with an emphasis on snowfall distributions. Specifically, the interaction of various types of cold, low-level air masses with topography and the larger-scale flow is described. Frequently, the heaviest snowfall does **not** coincide with the steepest terrain gradients, as might be expected, due to this interaction. Field measurements of several snowstorms during the 1987-89 time period include special CLASS (Cross-chain Loran Atmospheric Sounding System) vertical profiles, standard National Weather Service (NWS) and National Meteorological Center (NMC) surface and rawinsonde data, surface observations collected by a trained snow-spotter network, profiler data, Doppler reflectivity and velocity scans, and Geostationary Operational Environmental Satellite (GOES) images. The numerical predictions are produced by the CSU Regional Atmospheric Modeling System (RAMS), using two- and three-dimensional non-hydrostatic simulations. The versions of the model employed in this study utilized both horizontally homogeneous initializations and initial fields made up of NMC upper-air grids and rawinsondes. Most simulations employed full microphysics. A omit comparison between model-predicted dynamic and microphysical fields and observational data is described for the 30-31 March 1988 snowstorm along the Colorado Front Range.

Of particular interest in this study is the role of trapped cold air masses over the foothills and adjacent plains during the evolution of snow-producing synoptic scale disturbances. Specifically, these include two types of precipitating easterly ("upslope") flows along the Colorado Front Range: cold-air damming situations and arctic outbreaks. By no means are the dynamical features of these two types of storms mutually exclusive. The investigation includes detailed case studies of each storm type. The cold air damming process concentrates snowfall, typically in the foothills and adjacent areas to the east. A blocked low-level stable layer causes overrunning in a north-south band over and near the foothills. A quite different scenario, the cold outbreak, requires the establishment of an arctic air mass in the low levels. In this case, overrunning occurs as moist westerly winds aloft flow over the arctic air mass, producing snowfall in the foothills and plains.

The problems with forecasting precipitation amounts during these situations are well-known. This project isolates two of the primary mechanisms which have caused many of these problems. Both of these dynamical processes must be considered by the wintertime forecaster as major contributors to heavy snowfall in this region.

3.3 M.S. THESES

ABSTRACT

STAGE DEPENDENT CHANNEL ADJUSTMENTS IN A MEANDERING RIVER, FALL RIVER, COLORADO

Deborah J. Anthony
Earth Resources Department

Dam failure increased bedload supply to Fall River, a very sinuous, low gradient, snowmelt-fed stream, by a factor of 1000. This sediment is mobile at nearly all discharges, and thus channel topography is able to change with stage. In a two-bend study reach, the relationships between flow and mobile bed material were studied by measuring bedload transport rates, bed and water surface topography, and downstream and cross-stream velocity patterns on 22 cross sections. Measurements were made at different discharge levels through the 1986 runoff season.

At bankfull discharge, bend cross sections showed maximum asymmetry, with point bar platforms built up to the water surface and thalwegs excavated to their greatest depth. Cross-stream flows included zones of high turbulence, containing bed and bank cells in the thalweg region, with helical flow occurring over the point bar slope and outward flow only occurring over the point bar platforms. Bedload transport was greatest over the point bar slope, and almost zero through the thalweg. Sorting was continuous through each bend.

At intermediate flows, cross section symmetry increased due to lateral erosion of the point bar platform. Helical flows occupied a larger portion of individual cross sections, including the thalweg. In planform, however, the zone of helical flow had split into two smaller cells in each bend. Bedload transport had shifted outward from its high flow position, due to point bar progradation towards the cutbank, so that some sediment movement was recorded in the thalweg.

At low flows, characteristic of fall and winter, cross section symmetry was at a maximum. Additional erosion of the high point bars had occurred, but the greatest change was due to thalweg filling. Cross-stream flows were weak and chaotic for the most part, and bedload transport was more uniform across the channel than at higher discharges. Sorting was discontinuous, and it was confined to small pools in the otherwise flat channel.

In this mobile bed channel, bed topography is a function of cross-stream flow and bedload transport patterns, which are controlled by stage.

ABSTRACT

RADAR-DERIVED ESTIMATES OF LATENT HEATING RATES IN A CONVECTIVE STORM

Charlotte A. Atwater
Atmospheric Science Department

The importance of latent energy in storm dynamics and the global energy balance has long been recognized by atmospheric researchers. This study focuses on the latent heating and cooling in an isolated, microburst-producing thunderstorm in Alabama on the 20th of July, 1986. Data used in this work were recorded by NCAR CP-2 radar. 10 cm horizontal and vertical reflectivity signals (Z_H and Z_V, respectively) are used to calculate the difference reflectivity, $Z_{DP} = 10\log(Z_H - Z_V)$, which is then used to calculate the fraction of the horizontal reflectivity signal arising from ice hydrometeors. This information is then used to quantify liquid and ice water contents and the rainfall rate. The time rate of change of these three quantities are then used to derive latent heating rates.

The fraction of the reflectivity signal arising from ice hydrometeors is based on the degree of decorrelation between the Z_{DP} and Z_H signals in mixed-phase regions. Liquid water contents are calculated using a combination of 1) an empirical relation relating liquid water content to radar reflectivity for mixed-phase regions and 2) calculating liquid water contents from radar-derived parameters of the raindrop size distribution for pure liquid water regions. Ice water contents are calculated from an empirical relation relating liquid water content to radar reflectivity with corrections made to account for differences between the indices of refraction and typical densities of liquid and ice hydrometeors. Finally, rainfall rates are calculated using an empirical relation relating rainfall rate to coincident differential reflectivity, Z_{DR}, and Z signals. Estimated error levels, including instrument error, are approximately ±10% for the time rate of change of liquid water content, ±70% for the time rate of change of ice water content, and ±40% for rainfall rate.

Calculated vertical ice fraction profiles indicate that the storm consisted almost entirely of liquid water during its early stages. Glaciation began at the top of the storm and continued to progress downward through the storm with the descent of the core of maximum reflectivity signal. The ice fraction profile increased slightly from nearly 0.0 to about 0.1 at the surface at the time the microburst was observed to impact the ground. This increase is most likely a result of pea-sized hail reaching the surface. These conclusions confirm those drawn in other studies of the 20 July 1986 case.

The latent heating results indicate that heating and cooling caused by condensation and evaporation, respectively, account for roughly 90% of the total heating and cooling in this storm, with the remaining 10% coming from melting and freezing processes. Net latent heating rates (total heating rate minus total cooling rate) increased nearly steadily from the early stages of the storm until about 10 minutes before the microburst occurred, at which point it began to decrease. The net latent heating rate went from positive to negative less than 5 minutes before the microburst impacted the ground. Towards the end of the decaying stage of the storm, net latent heating was approaching zero.

ABSTRACT

DEVELOPMENT OF A WATERSHED INFORMATION SYSTEM FOR HEC-1 WITH APPLICATION TO MACKS CREEK, IDAHO

Thaddeus Cline
Civil Engineering Department

A micro computer based Watershed Information System (W.I.S.) is developed to assist in the preparation of HEC-1 input files. This system consists of three phases. Phase I utilizes the capabilities of AutoCAD version 9 and three AutoLISP programs: BASINS, PLANES and CHANNELS, to extract, organize and display watershed data. Phase II uses a FORTRAN program: CN, to calculate some HEC-1 parameter values. Phase III utilizes a PASCAL program: HECUPDATE, to create HEC-1 input files. Input into the system includes topographic, soils, land use, watershed geometry data, and a skeletal HEC-1 input file. Output from the system consists of a summary User Reference File, a Soils File, a Land Use File, a watershed Geometry File, a Curve Number File and HEC-1 input file which is ready to run. This thesis presents the W.I.S.: describing its use, applying it and providing program listings.

The W.I.S. is applied in a HEC-1 modeling study of Macks Creek Watershed: a small, arid mountainous watershed located in southwest Idaho. First the W.I.S. generates a database and HEC-1 input files. Then these files are used to calibrate the model to a rainfall-runoff event on June 5 and 6, 1967. The input files from the calibrated model are then used to simulate the response of the watershed to a heavy rainfall event on August 23, 1965. The W.I.S. developed and applied in this thesis greatly facilitates watershed data extraction and organization, data display, HEC-1 parameter calculation and the creation of HEC-1 input files. Two FORTRAN programs HECQ.FOR and HEC123.FOR reformat HEC-1 output into files which can be imported by a spreadsheet program for graphical representation of simulation results. HECQ.FOR also compares the simulated and the measured hydrographs by calculating absolute and relative error, the mean and standard deviation of these errors and the volume of the difference between the simulated and the measured hydrographs.

It is shown that using abnormally low values for roughness coefficients in HEC-1 had the same effect on the simulated hydrograph as the introduction of collector channels. It is also shown that using the base flow correction option of HEC-1 modifies output hydrographs in a way that can erroneously indicate that volume of direct runoff is not preserved when varying routing parameters. This is due to a "masking" effect justifying caution in hydrograph analysis using this option. Finally, a sensitivity analysis of some HEC-1 parameters is performed. Results of this analysis are useful for developing and operating the W.I.S. and for model calibration. The sensitivity analysis shows that HEC-1 is very sensitive to values of curve number and initial abstraction, moderately sensitive to values of overland flow roughness coefficient and overland flow length, and slightly sensitive to open channel flow roughness coefficient and computational time interval.

ABSTRACT

CLOUD AND CONVECTION FREQUENCIES RELATIVE TO SMALL-SCALE GEOGRAPHIC FEATURES

Visible and infrared data of GOES West were collected for nine hours each day during the summer of 1986. Cloud frequency charts were computed for the area from Mississippi east to Georgia and the Gulf of Mexico north to Tennessee for each of the nine hours as well as convection frequency charts to four convection intensities as defined by the temperature of the cloud top. Strong diurnal tendencies were noted. As was expected, these charts show that over the land areas cloudiness is at a maximum during the early afternoon hours with convection at a maximum in the late afternoon and evening. Cloudiness and convection are at a maximum during the nocturnal hours over the Gulf of Mexico.

Cloud frequency shows a strong relationship to small terrain features. Small fresh water bodies have cloud minima in the afternoon hours relative to the surrounding terrain while higher terrain, especially if there is a sharp slope, have cloud maxima. The adjacent lower terrain exhibits afternoon cloud minima due to divergence caused by the valley to mountain breeze.

The sea breeze-induced convergence causes relative cloud maxima over near-shore land areas with the stronger maxima over peninsulas. It is shown that the sea breeze results in convergent low level flow regardless of the whether over a peninsula or over land adjacent to a bay or inlet. Cloud frequencies tend to be larger both in magnitude and areal extent over peninsulas. Small scale geographical features show no relationship to convection, but larger peninsulas and extensive higher terrain show late afternoon convection maxima.

Harold M. Gibson
Department of Atmospheric Science
Colorado State University
Fort Collins, Colorado 80523
Fall 1988

MODELING CLOUDY AND CLEAR INTERVAR LENGTH PROBABILITIES USING SPACE SHUTTLE IMAGERY

ABSTRACT

Interval length probabilities provide an alternative to other char. terizations of cloudy and clear regions as viewed from atop the atmosphere. This work attempts to accurately model these probabilities using very high resolution space shuttle orbiter images. Probabilities extracted from these images are compared with three model representations. Metric and congruent statistical methods based on absolute deviations are used to determine model goodness-of-fit. An exponential model is shown to exhibit the least error of the three. Further examination shows that the parameters used to fit the exponential model to observed probabilities can be obtained from the cloud field itself (in the form of mean cloudy and mean clear interval lengths). These mean values are determined for image fractions as small as 1/32 and used to predict probabilities for the entire image.

George Franklin Howard III
Department of Atmospheric Science
Colorado State University
Fort Collins, Colorado 80523
Summer, 1987

ABSTRACT

VISUALIZATION OF THREE-DIMENSIONAL SCIENTIFIC DATA USING OCTREES

Russell J. Huonder
Computer Sciences Department

Meteorological sensors with three-dimensional digital output have created an interest in graphical rendering of atmospheric conditions for scientific visualization. The goal of visualization is improved understanding of atmospheric phenomena. The renderings should be fast, and should accurately represent the data. A traditional approach to three-dimensional object rendering is to display the data using a geometric modeling system, but because these systems model object surfaces, volumetric data sets can not be effectively represented. The smooth surfaces these systems produce are also undesirable since data integrity can be lost.

In this thesis, the *octree* structure is presented as a data structure which efficiently and effectively represents the observational data. An introduction to this structure is presented along with advantages and disadvantages. Observational data sets used are discussed along with a description of how the data is encoded. Various existing algorithms for displaying the structure are reviewed, and then a new algorithm for visualization of the octree using arbitrary rotations is presented. Within this discussion various illumination models are considered, as well as other parameters which permit a focused view of the data such as slicing and thresholding. A technique for fusing data sets is then presented with recommendations for future work in this area.

The algorithms developed for manipulation of the octree allow three-dimensional visualization of scientific data. Arbitrary rotation, data fusion, thresholding, slicing, and the various illumination models are demonstrated using infrared satellite data and radar data. The results are illustrated via multiple photographs of octrees.

ABSTRACT OF THESIS

A COMPARISON OF RESPONSE MODALITIES FOR RATING HAZE INTENSITY

There has been a great deal of research which has focused on the assessment of the visual impact of air pollution with specific emphasis on depicting how visitors' perception, appreciation and enjoyment of scenic areas vary with some physical measures of changes in air quality (Bell, Malm, Loomis, & McGlothin, 1985; Latimer, Hogo, & Daniel, 1981; Loomis, Kiphart, Garnand, Malm, & Molenar, 1984; Malm, Kelley, Molenar, & Daniel, 1981; Middleton, Stewart, & Dennis, 1983; Ross & Malm 1984; Ross, Haas, Loomis, & Malm, 1984). The majority of the past research has utilized categorical rating techniques (typically 10-point scales) for judgments of scenic beauty, visual air quality, and specific attributes of haze layer. Disadvantages associated with the use of these methods include: the inability of categorical scales to produce estimates of the perceptual magnitudes of the stimuli, the inability of category scales to routinely reflect intervals, the limitation of the number of response options which may restrict judgments, and the inability to express relative or absolute values between perceived differences in stimulus intensity (Lodge, 1981; Shinn, 1974). As a result, some researchers (Lodge, 1981; Shinn, 1974; Stevens, 1971) recommend the use of magnitude/ratio estimation methods over category scales. Since there is little empirical evidence comparing the efficacy of these different methods

for judgments of visual air quality, the present study attempted to explore how well different scaling techniques relate to each other and to the stimulus of haze intensity. Seventy-two undergraduate students participated in the experiment which required each student to rate the intensity of a computer-generated haze layer depicted in a slide of a scenic view (3 randomized sets of 8 different intensities) utilizing one of six different response techniques. There were two types of cross-modality matching techniques (a loudness response technique and a frequency response technique), two types of magnitude (numeric) estimation techniques (free-modulus and standard-modulus), and two types of category techniques (a 10-point and a 20-point scale). Utilizing Stevens power law to determine the shape of the function for each type of scaling technique, the two category methods produced larger power function exponents than either of the other two types of response methods. Results also indicated linear relationships between the various response techniques. Linear relationships suggest that subjects, when viewing haze, may be responding to the qualitative differences in the haze such as color wavelength rather than to the quantitative differences such as brightness.

Marc Eugene Fusco
Psychology Department
Colorado State University
Fort Collins, CO 80523
Spring 1987

ABSTRACT

MICROWAVE REMOTE SENSING OF CLOUD LIQUID WATER AND SURFACE EMITTANCE OVER LAND REGIONS

Andrew S. Jones
Atmospheric Science Department

Microwave remote sensing of cloud liquid water has largely been limited to areas over ocean surfaces. This study uses data from a new microwave instrument, the SSM/I on a polar-orbiting DMSP satellite, and infrared and visible data from the VISSR instrument on the GOES satellite in geostationary orbit. The region selected for the study was an area of 500 km x 500 km centered on northeast Colorado during the first week of August 1987. The SSM/I instrument has new high frequency channels (85.5 GHz) which are more strongly attenuated by cloud liquid water than channels on previous instruments. This allows for the estimation of integrated cloud liquid water based on the microwave brightness temperature depression caused by attenuation and emission of microwave radiation at the colder cloud levels. Atmospheric attenuation due to oxygen and water vapor is determined using a millimeter-wave propagation model (MPM). The Rayleigh approximation is used for the calculation of cloud liquid water attenuation.

Surface emittance measurements at the SSM/I frequencies were made with the aid of co-located GOES infrared data during clear sky conditions. Images produced of the retrieved surface emittances suggest a strong influence by wet surfaces caused by precipitation and irrigation. Error analysis results indicate absolute errors of ±0.012 for surface emittance retrievals for the 85.5 GHz channels.

Integrated cloud liquid water retrievals show good qualitative agreement with other available data sources. Numerical error sensitivity analysis and comparison of integrated cloud liquid water retrievals for the vertical and horizontal polarizations show error estimates of 0.15 $kg \cdot m^{-2}$ including instrument noise. A bias between the horizontal and vertical polarizations of the 85.5 GHz channels was noticed in the retrieved integrated cloud liquid water amounts. The bias appears to be due to a relative instrument error between channels of approximately 1.5 K. Absolute error estimates of the integrated cloud liquid water retrievals are unavailable but calibration of the method should be possible if quantitative integrated cloud liquid water amounts are known.

ABSTRACT OF THESIS

THE INFLUENCE OF CLIMATE ON THE MORPHOMETRY OF GRANITIC DRAINAGE BASINS IN CALIFORNIA

Climate strongly controls landform development. One way to assess the influence of climate on the landscape is to directly compare numeric descriptors of drainage networks to those of climate. In this study 24 headwater drainage basins in the Sierra Nevada and Mojave Desert of California are described numerically. These morphometric indices are compared graphically and statistically with long-term and close proximity climate data, as well as with climatically-related variables of vegetation, soil morphology, and hydrology. All of the basins are approximately equal area, three to six square kilometers, formed on similar granitic bedrock, and distributed across a range of precipitation from 79 mm/yr to 2058 mm/yr.

Contour-crenulation drainage density and the number of tributary sources per unit area decrease, and the average length of exterior links increase, with increasing mean annual precipitation. However, contour-crenulation drainage density, or the total length of channels derived from topographic maps divided by basin area, does not correspond to the density of fluvially active, raw-channel networks. At all but the most arid sites raw channel density is nearly constant. The remaining topographic lows which are not active channels represent hollows. Therefore, the reduction in contour-crenulation drainage density with increased precipitation is an outgrowth of a reduction in the density of hollows. The definition of hollow density is contour-crenulation drainage density minus raw-channel drainage density. The reduction in hollow density relates to vegetation type and density, thickness of residual soils, precipitation variability, and weathering rates.

The patterns of morphometry observed in this study diverge from those of similar studies due to the hydrologic properties of weathered granite and its residual soils, and the mediterranean climate of California. Once soil is developed and stabilized, the majority of runoff takes place as throughflow and hollows are zones of throughflow concentration. Therefore, in the case of these granitic basins, hollows represent a significant portion of the drainage net at all but the most arid sites. The highly permeable residual soils inhibit overland flow which results in inverse relationships of mean annual precipitation, precipitation intensity, and runoff to contour-crenulation drainage density.

The results of this study imply that the effect of climate on drainage basin morphometry is strongly influenced by local factors. The role climate plays in governing drainage basin morphometry may be difficult to predict until there is a better understanding of the hydrologic characteristics of particular bedrock types and their weathering products, the influence of regional climatic patterns and temporal climate change, and the importance of regional vegetation communities. This strong dependence on local conditions partially explains the wide range of conflicting published accounts of climate and drainage basin morphometry.

Daniel R. Levish
Earth Resources Department
Colorado State University
Fort Collins, CO 80523
Spring 1992

ABSTRACT

FREQUENCY CHIRP OF A HYBRID DOPPLER LIDAR

Robert F. McCoy Jr.
Physics Department

A hybrid Doppler lidar utilizes a pulsed infrared carbon dioxide laser as the transmitter in a laser radar system for measuring wind velocity and direction. Some of the laser light is backscattered by aerosols that are carried by the wind. The scattered light is shifted by an amount proportional to the aerosols' radial velocity. If the frequency of the transmitting laser changes throughout a pulse, the velocity estimate of the wind field is affected.

The primary laser within the system is the hybrid cavity composed of two sections. The first section is a continuous-wave (cw) laser, and the second is a transverse excited atmospheric pressure (TEA) laser which is basically a high-power pulsed amplifier. In the past, CO_2 Doppler lidars used custom-built TEA sections costing between one-quarter and one-half million dollars. The lidar being built for the Center for Geosciences at Colorado State University utilizes commercial off-the-shelf components which result in an order-of-magnitude reduction in the cost of the TEA section. The commercial TEA sections do not appear to introduce more problems than a custom-built TEA; their problems and solutions are addressed in the thesis.

The TEA section is a gas laser and exhibits frequency chirping during a pulse. When the density of the gas within the TEA section changes, the frequency of the hybrid cavity radiation can also change. To minimize the uncertainty in the velocity estimate, the frequency chirp should be reduced to a minimal value and the resulting chirp must be known. Three different techniques to characterize the chirp are presented, along with methods to reduce the chirp. The chirp is measured directly and parameters that affect the chirp are identified. Two of the experiments yield the chirp toward the end of the pulse where the direct measurement techniques tend to provide poor data. They also provide information on the optical quality of the cavity before, during, and after the pulse. Suggestions for modifying parameters to optimize the hybrid cavity design, thus reducing the chirp, include increased cavity length, larger mode volumes, vibrational isolation of TEA laser and shorter pulse lengths.

ABSTRACT

AN EVALUATION OF THE FACTORS AFFECTING WINTERTIME QUANTITATIVE PRECIPITATION FORECASTS IN AN EXPLICIT CLOUD MODEL OVER MOUNTAINOUS TERRAIN

Michael P. Meyers
Atmospheric Science Department

A prolonged orographic precipitation event, in a relatively steady-state synoptic environment occurred over the Sierra Nevada Range in central California on 12-13 February 1986. This well documented case was investigated via the non-hydrostatic version of the CSU Regional Atmospheric Modeling System (RAMS). Two-dimensional, cross barrier simulations have shown the feasibility of producing a quantitative precipitation forecast (QPF) with an explicit cloud model. The simulated flow fields, microphysical structure, and precipitation distribution compared quite well with observations. The experiment, however, exhibited a profound sensitivity to the input sounding. Initializing with a sounding which is representative of the upstream environment is most critical to the success of the simulation.

The flow fields showed little sensitivity to the model microphysics. Sensitivity to microphysical parameters have shown that the removal of a precipitation process, such as graupel or secondary ice production due to riming, is compensated by the enhancement of other processes such as rain and aggregation. The sensitivity of lowering the graupel density effectively changed the graupel species to a graupel-aggregate hybrid which dominated the ice-phase precipitation budget, resulting in a broadening of the precipitation distribution on the lower half of the barrier.

The flow fields were sensitive to the absence of the Coriolis term, with the u-component winds weaker at the base of the barrier. The precipitation distribution was slightly affected with Coriolis turned off, with a more pronounced mid-mountain peak than in the control run, which resulted from enhanced vertical velocities over the barrier. The Coastal Range produced a seeder-type cloud but enhancement of precipitation was not evident. Sensitivity to the diabatic influences of melting were seen in the microphysical fields but showed little influence on the flow fields and resultant precipitation distribution. A standing 15 km wave was evident upstream of the barrier crest and its origin was not sensitive to latent heat effects or the Coastal Range.

ABSTRACT

THE EFFECTS OF SPATIAL VARIABILITY OF OVERLAND FLOW PARAMETERS ON RUNOFF HYDROGRAPHS

Glenn E. Moglen
Civil Engineering Department

The behavior of the overland flow system depends largely on the degree of equilibrium exhibited by the system. Large variations in discharge result from partial equilibrium conditions, while systems in complete equilibrium produce only small variations in discharge. The use of spatially averaged values to quantify hydrologic parameters for overland flow modeling is, therefore, insufficient information to accurately simulate discharge hydrographs when the system being modeled has not reached equilibrium. In contrast, a system at equilibrium exhibits a peak discharge independent of the spatial distribution of the watershed characteristics

Uncorrelated spatial variability in each of the input parameters causes differing relative variability in overland flow discharge. Overland flow discharge is most sensitive to spatial variations in excess rainfall intensity. Manning's "n" and width produce comparable variability in discharge. Variations in slope have the smallest effect on overland flow discharge. These results are relatively independent of the spatial distribution functions used for the perturbations.

The procedures developed to analyze effects of uncorrelated spatially varied parameters are applied using spatially correlated slope input data. This is done using the spectral distribution of terrain height values for a mountainous region near Steamboat Springs, Colorado. These spectra are used to vary the slope parameter in the Manning equation. The results corroborate the earlier findings regarding the demonstrated variability of overland flow discharge at various degrees of equilibrium. The results also indicate that spatial correlation of a parameter has an influence on the magnitude and timing of the discharge variations.

The results provide a means of determining an appropriate grid spacing for sufficiently describing variability within a watershed. For durations of rainfall greater than equilibrium, the effects of spatial variability of overland flow parameters are small. Rearrangement of the equation for the time to equilibrium yields an expression for the desired grid spacing. This grid spacing provides a means of ensuring that complete equilibrium will be achieved within all grid areas, therefore minimizing the error due to partial equilibrium variations.

ABSTRACT

INFERENCE OF HORIZONTAL TEMPERATURE GRADIENTS USING PASSIVE RADIOMETRIC METHODS

Peter Olsson
Atmospheric Science Department

There exist many situations in nature where relatively strong horizontal temperature gradients are present in the boundary layer. The purpose of this work is to investigate the impact of horizontal temperature gradients on the infrared radiance properties of the boundary layer and devise a scheme for inferring the gradient magnitude from these radiance properties.

The temperature and spectral dependence of the radiance of various atmospheric constituents are examined and the IR portion of the spectrum $500cm^{-1} \leq \nu \leq 800cm^{-1}$ is shown to be most sensitive to temperature induced radiance changes. The two important radiating gases at these wavenumbers are CO_2 and H_2O. The spectral radiative properties of these constituents are discussed. The variability of the water vapor mixing ratio is shown to be an important factor in this remote sensing application. A model is discussed which numerically estimates the radiance of the boundary layer in the presence of a horizontal temperature gradient. The results of this model demonstrate the possibility of estimating the gradient magnitude from narrow band azimuthally scanned radiance measurements.

Two parameters, the attenuation length and the centered normalized radiance, are introduced and their relationship to the gradient magnitude is explored. Using these parameters, a method is developed which permits the inference of temperature gradient magnitude from infrared radiance measurements and local pressure, temperature and mixing ratio values. The success of this technique is demonstrated by the accurate recovery of gradient magnitudes from calculated radiance data. Finally, consideration is given to sources of error and uncertainty in the measurement process and the impact of these on the inference of the gradient magnitude.

ABSTRACT OF THESIS

THE EFFECT OF CLIMATE ON DRAINAGE BASIN CHARACTERISTICS IN CENTRAL TEXAS

Many factors contribute to drainage basin morphology, such as climate, lithology, structure, and relief. In order to determine relationships between drainage basin characteristics and climate all other factors should be held constant.

In order to determine how climate alone affects drainage basin morphology, especially topographic texture, eleven drainage basis were selected along an east-west transect across central Texas with a range of mean annual precipitation from 250 mm to 1351 mm. All basins are fourth order, and are located on flat-lying shale units in proximity to weather stations. A variety of morphometric variables were obtained for each basin using topographic maps and aerial photographs. Climatic data were gathered from U.S. Weather Bureau monthly reports and technical papers.

Drainage density increases from arid to semi-arid conditions, and it reaches a maximum at about 450-500 mm. Drainage density then decreases to a minimum at about 965-1016 mm as precipitation increases. Drainage density, stream frequency, and the number of first order streams all show the same relation with precipitation.

Vincent L. Sortman
Earth Resources Department
Colorado State University
Fort Collins, CO 80523
Summer 1988

ABSTRACT

THE BROADBAND RADIATIVE PROPERTIES OF CIRRUS CLOUDS DEDUCED FROM AIRCRAFT MEASUREMENTS DURING FIRE

William L. Smith, Jr.
Atmospheric Science Department

The bulk radiative and microphysical properties of five cirrus clouds sampled via the NCAR Sabreliner on four days during the FIRE first cirrus IFO are described. These cirrus systems, which developed under a variety of synoptic weather conditions, occurred at various altitudes and ranged in geometric thickness from about 2.0 to 4.5 *km*. A broadband, infrared radiative transfer model is employed to deduce the impact of the cirrus layers on infrared radiation. This model isolates the effect of the atmospheric gases from that of the cloud ice water permitting retrieval of the cloud emittance (ϵ_{cld}) and profiles of the mass absorption coefficient (K).

For the five cirrus cloud cases, the total cloud emittance, ϵ_{cld}, ranged from about 0.4 to 0.8 and the deduced emittance profiles appear as similar functions of ice water path (IWP). Furthermore, the mass absorption coefficient, K, is found to decrease with increasing particle size ranging from about 0.48 m^2g^{-1} in the top of one layer to about 0.007 m^2g^{-1} near the base of another. This relationship is somewhat dissimilar from one cirrus system to the next suggesting the significant effect of some unmeasured microphysical property. Small particles, which have been shown by other authors to be prevalent in cirrus clouds via the spectral characteristics remotely sensed in the 8-12 μm window region, are a likely suspect. Broadband, infrared absorption coefficients (σ) are also computed and found to exhibit a similar temperature dependence as data recently presented by other authors.

The horizontal variabilities in the shortwave and infrared properties of these cirrus systems are explored. The range of variation in the shortwave properties are found to be similar to the observed range in the infrared. Good correlation was found between the shortwave albedo (ρ) and upward effective emittance ($\epsilon^* \uparrow$). A scatter plot of these two parameters agreed well with theoretical calculations assuming an asymmetry parameter of 0.7. Downward effective emittances ($\epsilon^* \downarrow$) were found to range from about 0.4 to 0.8, while the shortwave effective extinction (ζ) ranged from 0 to 0.45. $\epsilon^* \downarrow$ and ζ were not well correlated owing to cloud heterogeneities.

Finally, the current state of cirrus radiation parameterizations was briefly assessed in relation to this data set and there appears to be sufficient observational evidence to support the initial development of parameterization schemes for general circulation and climate models.

ABSTRACT

SOCIAL LOAFING AND VIGILANCE DECREMENT WHILE MONITORING DIFFERENT LEVELS OF SIMULATED AIR TRAFFIC

Paul A. Weiler
Psychology Department

Using a computerized simulation of an air traffic control display, this study examined the phenomenon of social loafing (a decrease of individual contribution in a group setting) and vigilance decrement (the decrease in monitoring performance over time). A total of 96 introductory psychology students served as subjects in a 2 X 2 X 2 X 3 split-plot design. The independent variables were the difficulty of the task (easy, hard), perceived uniqueness of an individual's contribution (unique, non-unique), and identifiability of individual performance (identifiable, non-identifiable). Additionally, three 10-minute time blocks within the simulation were examined. Groups of four subjects were instructed on, and then participated in, a 30-minute simulation of an air traffic controller radar screen. Subjects were asked to monitor the simulated traffic for a critical stimulus of '999' in the display. Subject performance was recorded as the latency of response to a critical stimulus once presented. Results showed significant main effects for task difficulty and for time block within the simulation. Additional results showed the failure of the identifiability and uniqueness manipulations hypothesized as necessary for social loafing to occur. Both failures may be related to the lack of perception of a group setting by the subjects. It is recommended that future studies increase subject perception of group membership.

4. FELLOWS AND GRADUATE STUDENTS

Table 1

Table 2

Table 1

Degree Information for ARO Geosciences Fellows

Fellow Name	Degree	Academic Department	Advisor
Raul Alvarez	Ph.D.	Physics	Dr. J. She
Deborah Anthony	M.S.	Earth Resources	Dr. S. Schumm
Bonnie Ashburn	M.S.+	Atmospheric Science	Dr. E. Reiter
Charlotte Atwater	M.S.	Atmospheric Science	Dr. T. Vonder Haar
James Bossert	Ph.D.	Atmospheric Science	Drs. W. Cotton/T. McKee
Thomas Burke	M.S.*	Civil Engineering	Dr. P. Julien
Loren Caldwell	Ph.D.*	Physics	Dr. C. She
Thaddeus Cline	M.S.	Civil Engineering	Drs. D. Simons/P. Julien
Jeff Copeland	Ph.D.*	Atmospheric Science	Drs. W. Cotton/R. Pielke
Keely Costigan	Ph.D.*	Atmospheric Science	Dr. W. Cotton
William Doe	Ph.D.	Civil Engineering	Dr. P. Julien
Jeff Fredericks	Ph.D.+	Civil Engineering	Dr. D. Simons/P. Julien
Yahya Golestani	Ph.D.	Electrical Engineering	Dr. V. Bringi
Scot Greenidge	M.S.+	Electrical Engineering	Dr. T. Brubaker
Benjamin Hayes	Ph.D.	Earth Resources	Dr. S. Schumm
J. Hubbert	Ph.D.	Electrical Engineering	Dr. V. Bringi
Russell Huonder	M.S.	Computer Science	Dr. T. Brubaker
Andrew Jones	M.S. Ph.D.*	Atmospheric Science	Dr. T. Vonder Haar
Scot Makinen	Ph.D.+	Electrical Engineering	Dr. T. Brubaker
Robert McCoy	M.S.	Physics	Dr. D. Krueger

* In progress
\+ Left program without degree

Table 1 (cont'd)

Fellow Name	Degree	Academic Department	Advisor
Michael Meyers	M.S. Ph.D.*	Atmospheric Science	Dr. W. Cotton
Glenn Moglen	M.S.	Civil Engineering	Drs. D. Simons/P. Julien
Fred Ogden	Ph.D.	Civil Engineering	Dr. P. Julien
Peter Olsson	M.S.	Atmospheric Science	Dr. S. Cox
R. Raghavan	Ph.D.	Electrical Engineering	Dr. V. Bringi
Jerry Richardson	Ph.D.	Civil Engineering	Dr. P. Julien
William Smith	M.S.	Atmospheric Science	Dr. S. Cox
Otto Stein	Ph.D.	Civil Engineering	Dr. P. Julien
Joseph Turk	Ph.D.	Electrical Engineering	Dr. V. Bringi
Paul Weiler	M.S.	Psychology	Dr. R. Loomis
Douglas Wesley	Ph.D.	Atmospheric Science	Dr. R. Pielke
Paul Wolyn	Ph.D.	Atmospheric Science	Dr. T. McKee

* In progress
\+ Left program without degree

Table 2

Graduate Degrees Supported by Center for Geosciences Research Grant

Name	Degree	Department	Advisor
Gye Woon Choi	Ph.D.	Civil Engineering	Dr. P. Julien
William Doe	Ph.D.	Civil Engineering	Dr. P. Julien
Marc Fusco	M.S.	Psychology	Dr. R. Loomis
Harold Gibson	M.S.	Atmospheric Science	Dr. T. Vonder Haar
Yahya Golestani	Ph.D.	Electrical Engineering	Dr. V. Bringi
Mark Hadfield	Ph.D.	Atmospheric Science	Dr. W. Cotton
George Howard	M.S.	Atmospheric Science	Dr. T. Vonder Haar
J. Hubbert	Ph.D.	Electrical Engineering	Dr. V. Bringi
Frank Kelly	Ph.D.	Atmospheric Science	Dr. T. Vonder Haar
Y.Q. Lan	Ph.D.	Civil Engineering	Dr. P. Julien
Daniel Levish	M.S.	Earth Resources	Dr. S. Schumm
Alan Lipton	Ph.D.	Atmospheric Science	Dr. T. Vonder Haar
Khalid Marcus	Ph.D.	Civil Engineering	Dr. P. Julien
R. Raghavan	Ph.D.	Electrical Engineering	Dr. V. Bringi
B. Saghafian	Ph.D.	Civil Engineering	Dr. P.Julien
V. Sortman	M.S.	Earth Resources	Dr. S. Schumm
Craig Tremback	Ph.D.	Atmospheric Science	Dr. W. Cotton

5. TECHNICAL TRANSFERS

Technical Transfers from Center for Geosciences

Technology or product transferred:

Microwave radiative transfer analysis techniques and software

Center for Geosciences scientist(s) involved:

Dr. Viswanathan Bringi
Dr. Joseph Turk

Government facility and scientist(s) involved:

NASA/Jet Propulsion Lab
Dr. F. Davarian

Description of product application at receiving facility:

Techniques developed under the Center for Geosciences for understanding K-band microwave radiative transfer and propagation from ground-based radars are being applied to design of earthstations and software for K-band communications satellites. Attenuation of microwaves by precipitation particles is of particular interest.

Technical Transfers from Center for Geosciences

Technology or product transferred:

Microwave radiative transfer analysis techniques and software

Center for Geosciences scientist(s) involved:

Dr. Viswanathan Bringi
Dr. Joseph Turk

Government facility and scientist(s) involved:

NASA/Marshall Space Flight Center
Dr. Roy Spencer

Description of product application at receiving facility:

Techniques developed under the Center for Geosciences for understanding K-band microwave radiative transfer and propagation from ground-based radars are being applied to understanding of ground and space-based microwave measurements.

Technical Transfers from Center for Geosciences

Technology or product transferred:

Octree encoding of volumetric data for visualization

Center for Geosciences scientist(s) involved:

Dr. Thomas Brubaker
Dr. Gerald Taylor

Government facility and scientist(s) involved:

University of Colorado, Health Sciences Center (under federal funding)
Dr. Firouz Daneshgari

Description of product application at receiving facility:

The octree encoding software package was applied to encoding and visualization of tumorous prostate glands. This application initially showed how biopsy sections relate spatially with tumors. There is the possibility that octree encoding could be used in daily practice for this purpose. This use of octree encoding is considerably different from the geosciences applications pursued previously.

Technical Transfers from Center for Geosciences

Technology or product transferred:

RAMS cloud simulation capability

Center for Geosciences scientist(s) involved:

Dr. William Cotton
Dr. Graeme Stephens

Government facility and scientist(s) involved:

Air Force Office of Scientific Research
LTC J. Stobie

Description of product application at receiving facility:

Modifications are being made to RAMS in this study to allow the parameterization of cloud physics and dynamics processes. Emphasis is placed on forecasting characteristics of middle and upper tropospheric layer clouds, particularly cirrus clouds.

Technical Transfers from Center for Geosciences

Technology or product transferred:

RAMS cloud simulation capability

Center for Geosciences scientist(s) involved:

Dr. William Cotton
Dr. Robert Walko
Dr. Craig Tremback

Government facility and scientist(s) involved:

U.S. Department of Energy/Argonne National Laboratory
C. Frazier

Description of product application at receiving facility:

RAMS cloud parameterization schemes and simulations are being used in this study to derive techniques for representing cloud processes in global climate models (GCMs). The approach is to derive the GCM parameterizations scheme from data obtained from the statistical analysis of detailed explicit RAMS simulations of deep convective clouds, mesoscale convective systems, and convectively generated cirrus clouds.

Technical Transfers from Center for Geosciences

Technology or product transferred:

Hydrologic model CASC2D

Center for Geosciences scientist(s) involved:

P. Julien
B. Saghafian

Government facility and scientist(s) involved:

U.S. Army Corps of Engineers, Waterways Experiment Station
N. Raphelt, W. Johnson

Description of product application at receiving facility:

Use of the Hydrologic model CASC2D at Waterways Experiment Station for surface runoff modeling on Goodwin Creek.

Technical Transfers from Center for Geosciences

Technology or product transferred:

Atmospheric mesoscale model (RAMS) for Mesomet intercomparison and WINDS project support.

Center for Geosciences scientist(s) involved:

Dr. Roger Pielke
Dr. Robert Walko

Government facility and scientist(s) involved:

U.S. Army Research Laboratory,
Battlefield Environment Directorate

R. Brown
R. Pierce

Description of product application at receiving facility:

The Mesomet intercomparison involves evaluation of several mesoscale models through comparison of their results with each other and with observational data. The WINDS project collected mesoscale data over complex terrain and subsequently worked to simulate the flow over the project area. RAMS participated in both simulation efforts.

Technical Transfers from Center for Geosciences

Technology or product transferred:

Report on variability of Mississippi River

Center for Geosciences scientist(s) involved:

Dr. Stanley Schumm

Government facility and scientist(s) involved:

Hydraulics Division Vicksburg District COE
Phil Combs

Description of product application at receiving facility:

Provides information on variability of Mississippi River and the influence of geologic controls on river reaches.

Provides an evaluation and analysis of Vicksburg District potamology data.

Based upon this investigation Schumm is using the rivers data as part of a geomorphic analysis of the New Madrid seismic zone for the U.S. Geological Survey.

The techniques employed will likely be utilized at Eglin AFB and at White Sands Missile Range as part of the DoD environmental program.

Technical Transfers from Center for Geosciences

Technology or product transferred:

Report - Dynamics of sending bedforms on Natural Channels Examples from the Lower Mississippi River

Center for Geosciences scientist(s) involved:

David Jorgensen
Stanley Schumm

Government facility and scientist(s) involved:

River Engineering Division, Lower Mississippi River Division, Corps of Engineers, Vicksburg, MS
Charles Elliott

Description of product application at receiving facility:

Provides information on the variability and changes of bedforms and bed roughness in Mississippi River channel. Should aid in design of river control structures.

Provides an analysis of data collected by Vicksburg District COE during 5 year period.

Technical Transfers from Center for Geosciences

Technology or product transferred:

Cloud liquid water analysis from SSM/I and GOES satellite data.

Center for Geosciences scientist(s) involved:

Dr. T. Vonder Haar
Mr. A. Jones

Government facility and scientist(s) involved:

U.S. Army Research Laboratory,
Battlefield Environment Directorate

Bruce Miers

Description of product application at receiving facility:

Research and software developed at the Center for Geosciences to analyze cloud liquid water was applied to a study of supercooled cloud liquid water for the purpose of deriving an index of aircraft icing potential.

Technical Transfers from Center for Geosciences

Technology or product transferred:

Personal computer system to ingest digital satellite data from GOES, and Area-Time Integral (ATI) method for estimating volumetric rainfall.

Center for Geosciences scientist(s) involved:

Dr. T. Vonder Haar
Mr. D. Reinke

Government facility and scientist(s) involved:

U.S. Army Corp of Engineers/Hydrologic Engineering Center
David Goldman
Arlan Feldman

Description of product application at receiving facility:

The PC system for GOES data ingest provides data for the ATI method to operate on. The ATI method allows the Corps of Engineers to estimate rainfall volume over watersheds of interest from those satellite data. Knowledge of rainfall volumes is important for the streamflow management and engineering projects conducted by the Corps.

6. CONCLUSION

Conclusion

Many of the original goals of the Center for Geosciences have been met during the nearly six years that it has existed. Considerable detail was added to those goals during the Center's lifetime as a result of the discoveries generated by the research accomplished here. A few of the objectives changed significantly as the research progressed. We have documented the important scientific publications, listed the graduates, and summarized the significance of the research results of the Center for Geosciences as indications of the Center's success.

Although there currently is no opportunity for ARO to renew its grant supporting the activities of the entire Center for Geosciences, the research directions pursued by the Center's investigators still are being followed. The interdisciplinary ties and spirit of cooperation in research fostered by the Center remain as two of its greatest assets, and these also are carried forward into current and future activities of participants in the Center for Geosciences. Thus, ARO, Colorado State University, and the Nation continue to benefit from ARO's investment in scientific research.

7. REFERENCES

References

Chesters, D., L.W. Uccellini, and W.D. Robinson, 1983: Low-level water vapor fields from the VISSR Atmospheric Sounder (VAS) "split window" channels. *J. Clim. Appl. Meteor.*, **22(5)**, 725-743.

Clark, T.L., and R.D. Farley, 1984: Severe downslope windstorm calculations two and three spatial dimensions using anelastic interactive grid nesting: A possible mechanism for gustiness. *J. Atmos. Sci.*, **41**, 329-350.

Clark T.L., T. Hauf, and J.P. Kuettner, 1986: Convectively forced internal gravity waves: Results from two-dimensional numerical experiments. *Quart. J. Roy. Meteor. Soc.*, **112**, 899-925.

Doneaud A.A., S. Ionescu-Niscov, D.L. Priegnitz, and P.L. Smith, (1984): The area-time integral as an indicator for convective rain volumes. *J. Clim. Appl. Meteor.*, **23**, 555-561.

Fletcher, N.H., 1962: Physics of Rain Clouds. Cambridge University Press, 386 pp.

Gibson, H.M., and T.H. Vonder Haar, 1990: Cloud and convection frequencies over the southeast United States as related to small-scale geographic features, *Mon. Wea. Rev.*, **118**, 2215-2227.

Golestani, Y., V. Chandrasekar, and V.N. Bringi, 1989: Intercomparison of multiparameter radar measurements. Preprints, *AMS 24th Conference on Radar Meteorology*, March 27-30, 1989, Tallahassee, FL, 309-314.

Griffith, C.G., W.L. Woodley, P.G. Grube, D.W. Martin, J. Stout, and D.N. Sikdar, 1978: Rain estimation from geosynchronous satellite imagery - visible and infrared studies. *Mon. Wea. Rev.*, **106**, 1153-1171.

Hardesty, R.M., 1984: Measurement of range-resolved water vapor concentration by coherent CO_2 differential absorption lidar. *NOAA Tech. Memo ERLWPL 118.*

Henry, S.L.G., 1991: Impact of inferred latent heating rates on predictions of convective storms. *M.S. Thesis*, Department of Atmospheric Science, Colorado State University, Ft. Collins, CO.

Hillger, D.W., and T.H. Vonder Haar, 1988: Estimating noise levels of remotely sensed measurements from satellites using spatial structure analysis. *J. Atmos. Oceanic Tech.*, **5(2)**, 206-214.

Hillger, D.W., A.S. Jones, J.F.W. Purdom, and T.H. Vonder Haar, 1988: Spatial and temporal variability of VAS radiance measurements by structure and correlation analysis. Preprints, *AMS 3rd Conf. on Sat. Meteor. and Ocean.*, Anaheim, CA, 31 January - 5 February 1988, 51-54.

Jones, A.S., and T.H. Vonder Haar, 1990: Passive microwave remote sensing of cloud liquid water over land regions. *J. Geophys. Res.*, **95(D10)**, 16673-16683.

Kelly, F.P., 1988: Spatial and temporal short range total cloud cover estimation of metric analysis of composite images. *Ph.D. Dissertation.* Department of Atmospheric Science, Colorado State University, Ft. Collins, CO.

Kelly, F.P., T.H. Vonder Haar, and P.W. Mielke, 1989: Imagery randomized block analysis (IRBA) applied to the verification of cloud edge detectors. *J. Atmos. Ocean Tech.*, **6(4)**, 671-679.

LeMone, M.A., 1990: Some observations of vertical velocity skewness in the convective boundary layer. *J. Atmos. Sci.*, **47**, 1163-1169.

Mason, J.B., 1975: Lidar measurement of temperature: A new approach. *Appl. Opt.*, **14**, 76-78.

Meyers, M.P., and W.R. Cotton, 1992a: Evaluation of the potential for wintertime quantitative precipitation forecasting over mountainous terrain with an explicit cloud model. Part I: Two-dimensional sensitivity experiments. *J. Appl. Meteor.*, **31(1)**, 26-50.

Pielke, R.A., 1974: A three-dimensional numerical model of seabreezes over south Florida. *Mon. Wea. Rev.*, **102**, 115-139.

Saghafian, B., 1992: Hydrologic analysis of watershed response to spatially varied infiltration. *Ph.D. Dissertation*, Civil Engineering Department, Colorado State University, Ft. Collins, CO.

Schneider, J.M., 1991: Dual Doppler measurement of a sheared, convective boundary layer. *Ph.D. Dissertation*, The University of Oklahoma, Norman, OK. 134 pp.

Scofield, C.A., and V.J. Oliver, 1977: A scheme for estimating convective rainfall from satellite imagery. *NOAA Tech Memo NESS 80*. 47 pp.

Tremback, C.J., G.J. Tripoli, and W.R. Cotton, 1985: A regional scale atmospheric numerical model including explicit moist physics and a hydrostatic time-split scheme. Preprints, *AMS 7th Conference on Numerical Weather Prediction*, June 17-20, 1985, Montreal, Quebec.

Tripoli, G.J., and W.R. Cotton, 1982: The Colorado State University three-dimensional cloud/mesoscale model - 1982. Part I: General theoretical framework and sensitivity experiments. *J. de Rech. Atmos.*, **16**, 185-220.

Wetzel, M.A., and T.H. Vonder Haar, 1991: Theoretical development and sensitivity tests of a stratus cloud droplet size retrieval method for AVHRR-K/L/M. *Remote Sens. Environ.*, **36**, 105-119.

Young, K.C., 1974a: The role of contact nucleation in ice phase initiation in clouds. *J. Atmos. Sci.*, **31**, 768-776.

Young, K.C., 1974b: A numerical simulation of wintertime, orographic precipitation: Part I. Description of model microphysics and numerical tehcniques. *J. Atmos. Sci.*, **31**, 1735-1748.

8. ACKNOWLEDGEMENTS

Acknowledgements

The Director and Co-Principal Investigators of the Center for Geosciences would like to thank the Army Research Office Technical Representative, Dr. Walter D. Bach Jr., and the Advisory Panel members, Dr. George Ashton, Dr. Douglas Brown, Dr. Richard Gomez, Dr. Victor LaGarde, Dr. Glen Rubel, and Dr. Felix Schwering for their expert guidance of the research accomplished at the Center. Thanks also are extended to Mr. John Caron, Administrative Officer at the Colorado State University Office of Sponsored Programs, and to Mr. Ray Garcia, Ms. Joanne DiVico, Mr. Lance Noble, Ms. Lisa Huss-Dattore, and Ms. Loretta Wilson of the Cooperative Institute for Research in the Atmosphere at CSU for their technical and administrative support.